An Experimental Examination of the Effect of Trailing Edge Thickness on the Aerodynamic Performance of Gas Turbine Blades

by

Omar Zeidan

Thesis submitted to the Faculty of the

Virginia Polytechnic Institute and State University

in partial fulfillment of the requirements for the degree of

Master of Science

in

Mechanical Engineering

APPROVED:

Dr. Hal L. Moses, Chairman

Dr. John Moore

Dr. Felix J. Pierce

June 29, 1989

Blacksburg, Virginia

An Experimental Examination of the Effect of Trailing Edge Thickness on the Aerodynamic Performance of Gas Turbine Blades

by

Omar Zeidan

Dr. Hal L. Moses, Chairman

Mechanical Engineering

(ABSTRACT)

This thesis documents the experimental research conducted on a transonic turbine cascade. The cascade was a two-dimensional model of a jet-engine turbine with an, approximately, 1.2 design, exit Mach number, and was tested in a blow-down type wind-tunnel. The primary goal of the research was to examine the effect of trailing edge thickness on aerodynamic losses. The original cascade was tested and, then, the blades were cut-back at the trailing edge to make the trailing edge thicker. The ratios of the trailing edge thickness to axial chord length for the two cascades were 1.27 and 2.00 percent; therefore, the ratio of the two trailing edge thicknesses was 1.57. To simulate the blade cooling method that involves trailing edge coolant ejection, and to examine the effect of that on aerodynamic losses, CO_2 was ejected from slots near the trailing edge in the direction of the flow. Two different blowing rates were used, in addition to tests without CO_2. A coefficient, $\bar{L}$, was used to quantify aerodynamic losses, and this was the mass-averaged total pressure drop, normalized by dividing with the total pressure upstream of the cascade. The traversing, downstream total pressure probe was stationed at one of three different locations, in order to investigate the loss development downstream of the cascade. The two cascades were tested for an exit Mach number ranging from 0.60 to 1.36. The research suggested that the main influence of the trailing edge thickness on losses is through affecting the strength of the trailing edge shock system, since $\bar{L}$ was almost the same for the two cascades in the subsonic Mach number region. The losses mainly differed (larger for the cut-back cascade) in the Mach number region of 1.0 to 1.2. In this region, the difference in loss maximized, showing a loss for the cut-back cascade 20 to 30 percent more than the original cascade. The CO_2 was found to have no significant effect for

high Mach numbers; for low Mach numbers, the high blowing rate slightly decreased the loss. Finally, the loss, nearly, stopped to increase after one axial chord length downstream of the cascade.

Acknowledgements

A research project such as the one documented in this thesis could not have been conducted if it were not for the hard work and help of many people. My greatest thanks go to my first research partner, Since his "hands-on" mechanical skills were better than mine, working with him was a learning experience for me. Also, being the older guy in the wind-tunnel facility, he went out of his way to teach me what he knew about the lab. Last but not least, his companionship lightened up a lot of the, sometimes, tedious work involved in this project. I would like to thank my new partner, , for his hard work during the past couple of months since he came aboard, and I wish him the best of luck in his future work on this project.

Thanks to General Electric Company, Aircraft Engine Company for funding this project. I would like to thank and for being kind enough to supply me with a few of the technical references that I used in my literature review.

I am especially grateful to my advisor, Dr. Hal Moses. A large part of the fluid mechanics I learned in graduate school was in his classes. He always took time to answer my questions, and he made me feel that I was working with him rather than for him.

I would also like to thank Dr. J. Moore and Dr. F. J. Pierce for serving as members of my graduate committee and providing constructive criticism of this work. I am grateful to Dr.

E. F. Brown, a former member of my committee, for his help as a committee member and for supplying me with a few references on Uncertainty Analysis in experimental research.

I am deeply grateful to all those people in the Mechanical Engineering machine shop and the Aerospace and Ocean Engineering shop, who made this project possible with their truly skillful work. I am especially indebted to Mr. Gary Stafford whose daily technical assistance we could not have managed without.

Finally, I hope a general thanks would suffice to all those whom I did not mention here, and who were supportive to me in accomplishing this work successfully.

Table of Contents

List of Illustrations

List of Tables

List of Symbols

p_b = base pressure

p_t = total pressure

Δp_t = drop in total pressure across the blade row

P_t = normalized total pressure drop

CO_2 = carbon dioxide

$\bar{L}$ = mass-averaged total pressure loss coefficient

ρ = local density

u = horizontal component of the local flow velocity

y = vertical (pitchwise) coordinate

B = blowing rate (a non-dimensional measure of coolant flow rate)

$\dot{m}$ = mass flow rate

V = local flow velocity

A = flow cross sectional area normal to the mean flow direction

A^* = throat area

M = Mach number

h_{te} = trailing edge thickness

c = axial chord length

x = horizontal distance from the leading edge

v_p = probe speed

p = static pressure

$p_{t,2,prb}$ = total pressure as read by the downstream probe

γ = constant specific heat ratio for air

$M_{2,isen}$ = exit, isentropic Mach number

R = ideal gas constant for air

T = absolute static temperature

T_t = absolute total temperature

α = angle of downstream probe misalignment with the flow

Q = volumetric flow rate

C_D = discharge coefficient for the coolant exit slots in the blades

U_{P_t} = estimated absolute error in P_t

b = absolute bias error

S = absolute precision error

t = student t value, a statistical parameter used in error calculations

$U_{\bar{L}}$ = estimated absolute error in $\bar{L}$

Subscripts

1 = position upstream of the blade row, or related to the first cascade

2 = position downstream of the blade row, or related to the second cascade

t = condition of flow stagnation

c = coolant

ex = exit from blade coolant passage

air = main flow

b,s = suction side of blade

b,p = pressure side of blade

w,f = wall, forward position

w,r = wall, rear position

isen = isentropic

x = immediately upstream of the probe bow shock

y = immediately downstream of the probe bow shock

m = condition at the CO_2 volumetric flow-meter

stp = standard temperature and pressure

i = initial, just before wind-tunnel blow-down

Superscripts

* = choked condition

Abbreviations

VPI & SU = Virginia Polytechnic Institute and State University

1.0 Introduction

The gas turbine emerged during the second world war, with its first use in aircraft propulsion. Since that time it has found rapid expansion in its applications, which included electric power generation, marine propulsion, and numerous applications in industry.

Considering this large scale dependence on gas turbines for delivering power, the demand on improving their efficiency has been very strong. Gostelow, 1981 [1] states that a one percent change in turbine efficiency of a 1000 MW machine has an estimated worth effect between 5 and 14 million dollars. Also, need has dictated lowering the weight/size to power output ratio. All this has required the development of highly loaded gas turbine blades that can operate with high inlet gas temperatures.

In a typical gas turbine, a 1 percent loss of turbine efficiency means 1.5 percent loss in power output.[1] The most obvious option to increase the efficiency is to increase the temperature of the inlet gases. In open gas turbine cycles, the inlet gases are the products of combustion. Increasing the temperature of these products is limited by the highest temperature the turbine blades can operate under without thermal failure.

The last two decades have witnessed concentrated efforts in the development of turbines that can withstand higher temperatures. These efforts concentrate on two approaches:

---

[1] Xu, 1985 [2], pp. 1.

(1) developing better heat resistant materials, and (2) cooling down the turbine blades with injected coolants. The result has been increasing the maximum operating temperatures from 1050 K in the 1950's to 1800 K in the 1980's, according to Sieverding [3].

Various methods of injecting coolants in the sides of the blades and ejecting them through holes in the blades surface have been implemented. One common method, which is of concern to us in this thesis, is referred to as *trailing edge ejection*. In this method, the coolant is exhausted through holes near the trailing edge in the direction of the main flow.

The coolant is usually extracted from the gas turbine compressor. This has the effect of decreasing the overall efficiency. Thus any gain in efficiency due to higher gas temperatures may be offset by the amount of coolant that has to be extracted.

The portion of the turbine blade near the trailing edge is the thinnest, and, thus, the most vulnerable to failure under mechanical and thermal stresses. With highly loaded blades operating at high temperatures, a finite trailing edge thickness is, therefore, unavoidable. A thick trailing edge complicates the flow in the trailing edge region, and increases the aerodynamic losses significantly. The trailing edge loss, which includes mixing and shock losses, may be more than the boundary layer loss throughout the blade passage.

The flow leaving the trailing edge separates at both sides of the blade forming two shear layers which unite further downstream. A small triangular shaped region is formed right behind the trailing edge and between the two shear layers. This region is sometimes referred to as the *dead air* region. Despite the presence of some vortices in this region, it is treated as isobaric. The pressure in it, known as the *base pressure*, is found to be lower than the pressure just downstream, and just upstream before the flow separates from the blade. The base pressure has been found, experimentally and theoretically, to have a close effect on trailing edge mixing loss, and on the strength of the trailing edge shock system.[2] The base pressure loss generating mechanism is still, however, poorly understood. One fact that re-

---

[2] Xu, 1985 [2], pp. 2.

searchers generally agree upon is that the thicker the trailing edge, the lower the base pressure, and the greater the trailing edge loss.

At the present stage of gas turbine development, an increase in efficiency by an increase in the inlet gas temperature, will be offset by the need for more coolant and thicker trailing edge.

This thesis documents the experimental results of testing the same set of transonic, two dimensional gas turbine blades with two trailing edge thicknesses [3]. The set was cut once at the trailing edge, making the chord length shorter and the trailing edge thicker. The goal was to investigate the effect of the trailing edge thickness on the aerodynamic loss. The flow in the real turbine would be three dimensional; nevertheless, two dimensional testing is adequate to show the flow characteristics; and the simplified form of the flow is very helpful in providing valuable physical insight.

Since trailing edge losses were of interest, a small amount of coolant was ejected from the trailing edge to investigate the effect of that on the aerodynamic loss. This method of coolant ejection may affect the loss through affecting the base pressure, the mixing, the boundary layer thickness, or through some unforeseeable effects.

This thesis documents the results of this experimental program. Previous work on trailing edge flow, trailing edge coolant ejection, and their effect on aerodynamic loss in turbine blades is also reviewed. The nomenclature used in quantifying the results is introduced. The experimental set-up, experimental procedure, and testing program are described. A discussion of the data reduction algorithm is included, followed by the results of the research, and conclusions and recommendations for further research. An uncertainty analysis is provided as an attempt to estimate the degree of accuracy of the results.

[3] The testing took place at the VPI & SU cascade wind-tunnel facility.

2.0 Literature Review

There is a fair amount of published work in the literature on the aerodynamics of wind-tunnel cascade testing; in particular, the aerodynamics of the flow in the trailing edge region, for transonic turbine cascades. Trailing edge flow has been the subject of extensive research in the past two decades, given the large size of losses in the trailing edge region, and the strong influence of the trailing edge shock system, in the case of supersonic exit flow, on a significant portion of the flow field. A specific concern for researchers has been the effect of trailing edge coolant ejection on the trailing edge flow, since this method of coolant ejection is widely in use, and is accepted as the ejection method that causes the least amount of losses. As in this thesis, the flow development behind the *blade row* has been another concern, because of its relevance to multi-stage machines, or those with stator rows.

This section reviews several references that are available in the literature, and presents a summary of their results and recommendations. The author also cites these references in portions of their analyses of aerodynamic features of turbine cascade flows.

2.1 General Features of Wind-Tunnel Turbine Cascade Testing

Gostelow [1] presents a description of the general features of existing cascade wind-tunnel facilities. He evaluates the role of today's high speed wind-tunnel testing, describes the different types of wind-tunnels in operation, discusses some of the main problems faced by researchers, and recommends some ways of solving them.The reference (year of publication, 1981) includes a list of known high speed cascade wind-tunnel facilities in the western hemisphere. Gostelow estimates there is an equivalent number in the Soviet block; but due to lack in translated technical papers, he does not include a listing.

The demand on turbomachines to deliver more power with limitations on volume and cost, made it clear that turbines should be designed with higher pressure ratios than those that involve subsonic flows. Turbines with subsonic inlet and supersonic exit flows (transonic turbines) have been more and more in profitable use [4]. Gostelow states that the financial rewards of attaining transonic speeds have been even more than early expectations. Considering these large savings made by transonic turbines, it is not surprising that there has been no shortage in funds for research into this area. Wind-tunnel, two dimensional testing has been the most helpful research method. Its advantages over full scale rig testing include lower cost, simpler configurations, and the ease it provides in gaining physical insight into the flow. According to Gostelow, published correlations derived from wind-tunnel research have been in use by manufacturers all over the world.

---

[4] According to Gostelow, typical design exit Mach numbers do not exceed 1.2; but up to 1.8 has been reached.

2.1.1 Types of Wind-Tunnel Facilities

Gostelow [1] speaks of three types of wind-tunnels: (1) blow-down tunnels, (2) tunnels that utilize suction downstream of the test section, and (3) closed circuit variable density tunnels. The first, and most common, type, of which the VPI & SU cascade wind-tunnel is an example, utilizes an external source of high pressure air and discharges that through the wind-tunnel, into the atmosphere. The second type is self-explanatory; and the third type recycles the air in a closed loop. The advantage of the latter lies mainly in the fact that the air density is more controllable, and thus the Mach number and the Reynolds number can be varied more independently. The main advantages of the second type are less power requirement, and the absence of compressor leakage oil on the windows of the test section. Oil becomes a problem when it is desired to take pictures of the flow.

2.1.2 Main Concerns in Wind-Tunnel Design

Gostelow [1] discusses three important flow conditions that a wind-tunnel design should meet: (1) good periodicity in a *pitchwise* direction (see Figure 1), (2) good uniformity in a *spanwise* direction, and (3) repeatability.

Periodicity in a pitchwise direction: pitchwise periodic behavior enforces the assumption that the cascade flow simulates the flow in the real turbine; since aperiodicity would be due to non-uniformities or interferences that would not be present in the real turbine. Gostelow states that achieving this periodicity is the most difficult condition to meet in transonic turbine cascade flows; the overwhelming reason for that being the reflected waves from the back boundary of the test section.

Gostelow reports that some researchers use a solid or a perforated tailboard to guide the exit flow by closing the gap between it and the backwall of the test section, while others prefer not to use a tailboard. Obviously, waves would be reflected off the tailboard, or off the free shear layer.Gostelow explains that the shear layer would be highly turbulent and, thus, would reflect waves in a spurious manner. The solid tailboard, on the other hand, would reflect waves in a more steady manner, but the reflections would be stronger. The method that Gostelow recommends, is the use of a perforated tailboard with pores of controllable size. He argues that the reflected waves of opposite nature (compression and expansion) interfere, and cancel each other out, a certain short distance from the tailboard. Zaccaria [4] reports the results of tests done on the VPI & SU cascade wind-tunnel using a solid tailboard, a perforated tailboard, and no tailboard. He reports good periodic behavior for the central blades (the ones that are tested in the research documented by this thesis) for all three cases. However, for considerations concerning better exit Mach number and flow angle control, and for attaining flows with Mach numbers and shock angles independent of the total pressure upstream of the blade row, Zaccaria recommends the use of a solid tailboard [5].

Another problem which affects the flow periodicity is the boundary layers at the top and bottom walls of the test section. According to Gostelow, some researchers use boundary layer suction to fix this problem. In addition, all researchers concede that increasing the number of blades reduces the boundary layer and wave reflection effects on the central blades' periodicity. Seven blades is accepted as the minimum.

Uniformity in a spanwise direction: the two dimensionality of the flow is a basic assumption in all wind-tunnel research. Assuming that inlet flow uniformity is achieved, the problem threatening two-dimensionality is secondary flow, that is, the disturbance in the flow due to the boundary layers at the side walls. Gostelow speaks of boundary layer suction as a corrective

[5] The cascade tested by Zaccaria has the same number of blades, the same pitch, the same turning angle, and blades of the same order of thickness as the cascade tested in this research.

measure used by some researchers. Another effective measure would be increasing the blade span, thereby, decreasing the relative significance of the boundary layer thickness.

Repeatability: a poor ability to regenerate a flow field is an indication of significant, random flow disturbances. Obviously, the credibility of any research depends on how well these disturbances are kept below an acceptable level, therefore, on how well repeatability is achieved.

Gostelow discusses one possible source of irrepeatability, the sporadic shocks in supersonic flow regions due to condensate particles forming on the blades, in case of humid, cold air. Air driers are often necessary to relieve this problem.

MacMartin, et al. [5] report having some problems with repeatability. They, also, cite various supersonic cascade testers in reporting problems of this nature.

Zaccaria [4] reports achieving acceptable repeatability for the range of upstream total pressure from 140 kPa (21 psia) to 190 kPa (28 psia).

2.2 Trailing Edge Flow Research

As mentioned earlier, trailing edge flow in transonic turbines has been the subject of extensive research over the past two decades. A large amount of experimental results have been accumulated, and many correlations have been derived. Due to the complexity of transonic turbine flow, the usability of an experimental correlation is typically restricted by many conditions. The most prominent limitation on experimental research is the difficulty in installing enough instrumentation in the trailing edge region, due to the small dimensions of test turbine blades. This problem is particularly restrictive in the case of *base flow* research; where base flow refers to the flow in the immediate vicinity of the trailing edge, specifically, the small *dead air* region behind it. Some researchers, like Sieverding [3], Sieverding, et al.

[6], Amana, et al. [7], and Sieverding, et al. [8], use models that simulate cascade flow; yet, they have larger dimensions allowing for more instrumentation.

The prime motivation behind trailing edge research has been that most attempts to model transonic turbine flows theoretically, have failed because of inaccurate modeling of the trailing edge flow, in particular, the base flow. Gostelow [1] asserts that the role of high speed cascade testing today is seen as one of securing improved understanding of the physics of the base flow. The reason why the knowledge of the base flow is so important, is that (1) the mixing losses in that region are high, (2) the base flow sets the *trailing edge shock system*, which has a major influence on the flow field, and (3) understanding of the base flow is essential for predicting the optimum coolant flow rate to be ejected from slots close to the trailing edge. The optimum flow rate would minimize mixing and shock losses.

Another problem facing theoretical modeling is poor understanding of shock-boundary layer interaction, which typically takes place in transonic turbine flows on the blades' suction side.

2.2.1 Description of the Trailing Edge Flow Field

References [3], [6], [7], and [8] include thorough descriptions of the trailing edge flow field in the case of supersonic exit flow. Their descriptions agree, and this section includes a summary of them. The discussion presented is for rounded trailing edges, of the type used in this research. Amana, et al. [7] states that a rounded trailing edge reduces the effective thickness of the trailing edge, and,therefore, reduces the losses. In this section, refer to Figure 2 for a schematic of the flow field.

When the flow reaches the rounded trailing edge from both sides, and before it separates, it follows the rounded contour while undergoing a Prandtl-Meyer expansion (lines 1 in Figure 2). Eventually the slope gets too steep, and the flow separates. A *separation shock* (lines 2 in Figure 2) is required, because the Prandtl-Meyer expansion overexpands the air, and, therefore, there is a need for a fast compression to meet the base pressure (p_b) boundary condition. Incidentally, the base pressure is always lower than the pressure just upstream of the Prandtl-Meyer expansion. The separated *shear layers* (lines 3 in Figure 2) reattach a certain distance downstream, and undergo compression through *reattachment shocks* (lines 4 in Figure 2). The latter shocks are stronger than the separation shocks, and are typically referred to as *wake shocks*, or, more commonly, *trailing edge shocks*. Sieverding, et al. [8] speak of a *reattachment region* rather than a *reattachment point*, and support this by Schlieren photographs that clearly show the reattachment taking place over a region of significant size.They also calculate the strength of the separation shocks through various methods, and conclude that the different methods yield disagreeing results. It is their belief, however, that the shocks are of moderate strength. Sieverding, et al. [6] claim that the separation shock strength, measured by the static pressure ratio across the shock, is constant for varying flow conditions.

In most cases of transonic turbine flows, a trailing edge shock intersects the suction side of an adjacent blade (as shown in Figure 2), creating the very poorly understood situation of shock-boundary layer interaction. Amana, et al. [7] states that one of the most important goals of better understanding trailing edge flow, is to enable the prediction of whether and where trailing edge shocks will hit neighboring blades. Sieverding, et al. [8] conclude that the shock-boundary layer interaction affects the trailing edge flow significantly, in particular, the separation shocks. One of the effects was seen as an increase in the base pressure for the same exit Mach number, when a shock-boundary layer interaction existed.

2.2.2 Base Pressure

It is widely accepted that knowledge of the base pressure, or the ability to predict it, is essential for modeling transonic flows. After comparisons between experimental data and theoretical solutions, MacMartin, et al. [5] conclude that proper prediction of the base pressure in a theoretical model is essential for getting good results. Sieverding, et al. [6] state that, at present, base pressure prediction methods are very poor. Xu, et al. [9] make a similar statement, and add that many failing attempts to predict the base pressure have been made in the past thirty years.

According to Sieverding, et al. [6], the information in the literature on base pressure measurements is extremely scarce. They add that the standard method of reading the base pressure through a single tap at the trailing edge is inadequate for a study of the base region pressure distribution. They report the results of research done on a large scale model, simulating cascade flow, yet allowing for detailed instrumentation. For instance, they managed to install 19 pressure taps along the rounded trailing edge. Amana, et al. [7], Sieverding [3], and Sieverding, et al. [8] conducted similar model experiments. Some of the results obtained from such model experiments are briefly discussed below.

One of the main goals of the model experiments was to determine the validity of the assumption of an *isobaric mixing region* behind the trailing edge; because if this assumption is validated, then measuring the base pressure via a single tap at the trailing edge would be sufficient. Sieverding [3] reports that the base pressure at the trailing edge is basically uniform (uniform over the central 70 percent of the trailing edge's rounded end). If a coolant ejection slot exists, however, there might be two uniform pressure regions on each side of the slot. In that case, a pressure tap on each side would be sufficient.

Sieverding, et al. [8] measured how far downstream the isobaric region extends, and found that its length is only 60 to 80 percent of the trailing edge thickness. They also found that the *pressure recovery region* (or reattachment region) is twice as long as the isobaric region. Therefore, they conclude that the assumption of an isobaric mixing region was not confirmed.

Researchers work diligently trying to understand what influences the base pressure. Xu, et al. [9] report that thinner trailing edges result in higher base pressure, for the flow conditions that are otherwise the same. This, incidentally, happens to be a widely accepted. Sieverding, et al. [8] found that the shape factor of the boundary layer just upstream of the trailing edge plays a significant role in setting the base pressure. Xu, et al. [9] conducted tests on two types of blades that only differ slightly in the suction side's profile near the trailing edge. The ones more prone to separation showed lower base pressures. It is concluded, therefore, that separated flow causes a drop in base pressure.

As mentioned earlier, base flow research aims primarily at gaining the ability to predict the base pressure theoretically. Xu, et al. [9] found their theoretical predictions of the base pressure inaccurate, because they failed to properly include the detailed state of the boundary layer upstream of the trailing edge. Amana, et al. [7], who conducted model and cascade tests, propose a theoretical model for the base flow around a round trailing edge, which, among other things, predicts the base pressure. The theoretical model worked well for flat plate experiments, but not so well for cascade experiments. Sieverding, et al. [6] used a theoretical method, extracted from the literature, to calculate the base pressure. The method works well when the flow conditions just upstream of the trailing edge are known. Since the research conducted by Sieverding, et al. [6] was on an extensively instrumented model, they had enough knowledge of the flow upstream of the trailing edge to enable them to predict the base pressure successfully. They point out, however, that it would be very difficult in a cascade to accurately predict the flow conditions upstream of the trailing edge.

2.3 Aerodynamic Loss

The two main contributors to aerodynamic loss in transonic turbine cascades are the loss due to the boundary layers throughout the blade passages, and the *trailing edge loss*. The latter consists of mixing losses behind the trailing edge, and the losses caused by the trailing edge shock system. Naturally, the loss keeps increasing downstream of the blade row, until the flow gets *fully mixed*. Xu, et al. [9] asserts that for typical, transonic turbine trailing edge thicknesses, and in the typical range of exit Mach number (from 0.8 to 1.2), the trailing edge losses are dominant.

2.3.1 Development of the Loss Downstream of the Blade Row

Xu, et al. [9] report that, for the cascades they tested, 70 percent of the loss occurs downstream of the blade row. By taking traverse readings at several downstream planes, they managed to gain some detailed information on how fast the loss develops. The main conclusions they make are:

- in the immediate vicinity of the blade row (down to 10 percent chord length downstream of it [6]) as much as 20 percent of the total loss occurs. Considering that little of the shock loss has yet occurred there (see Figure 2 on page 63), this indicates intense viscous mixing in that region.

- at 80 percent chord length downstream of the blade row, only 80 percent of the total loss had occurred, suggesting significant shock and mixing losses still further downstream.

Prust, et al. [10] report that the flow was almost fully mixed one blade pitch downstream of the blade row.

2.3.2 Factors Affecting the Aerodynamic Loss

Flow speed: Xu, et al. [9] report that loss increased with exit Mach number (in the Mach number range from 0.8 to 1.2), with a sharp rise around unity Mach number. Singer [11] reports similar results for transonic turbine cascade tests done in the VPI & SU wind-tunnel. He indicates that the loss versus exit Mach number curves suggest a quadratic relationship.

---

[6] See Figure 7 for an illustration of blade *chord length*.

Trailing edge thickness: Xu, et al. [9] conducted tests on a family of four, similar turbine cascades, that differ only in trailing edge thickness. They concluded that at all speeds the trailing edge loss (not the total loss) is directly proportional to the trailing edge thickness, with the constant of proportionality being greater at supersonic exit speeds. They add that the trailing edge loss was, on the average, 70 percent of the total loss, with the percentage being higher for higher speeds. At high speeds, the trailing edge loss dominated, and the total loss variation with trailing edge thickness was closely linear.

Prust, et al. [10] conducted tests on similar blades with three different trailing edge thicknesses. They report that thicker trailing edges gave lower base pressures and higher losses. They also noticed that there was more flow angle non-uniformity for thicker trailing edges.

Trailing edge geometry: Prust, et al. [10] ran tests on cascades with round and square trailing edges. The flow was generally the same, except that the loss in the region very close to the trailing edge was higher for the square trailing edge blades.

Lokai [12] tested cascades with different types of trailing edge accommodations for coolant ejection slots. The different geometries were:

1. trailing edge with a continuous coolant slot along the blade's span.

2. trailing edge with individual slots, separated along the span by webs.

3. trailing edge with a continuous constricted slot (nozzle shaped trailing edge).

4. trailing edge of the type in item 2 above, with grooves on the pressure side, at positions where the webs are.

5. trailing edge of the type in item 2, with grooves on both sides of the blade, at positions where the webs are.

Lokai found that there was no difference in aerodynamic loss between types 1 and 2. Type 3, which reduced the effective trailing edge thickness, showed 0.5 percent increase in the dynamic pressure at the wake (immediately behind the blade). Types 4 and 5 increased the dynamic pressure by 0.5 and 1 percent, respectively.

2.4 Effect of Trailing Edge Coolant Ejection

MacMartin [5] and Sieverding [3] investigated the effect of trailing edge coolant ejection on the blade surface pressure distribution, and on the strength and location of shocks. They agree in their findings that the effects were negligible. In general, the main influence, if any, of coolant ejection is its effect on the aerodynamic loss.

Effect on the aerodynamic loss: Singer [11] conducted tests on a transonic turbine cascade in the VPI & SU wind-tunnel, using CO_2 as the coolant. He could not detect any significant or consistent influence on the aerodynamic loss. He concludes that the effect of the coolant must have been smaller than the error involved in the calculated value of the loss [7].

Xu, et al. [9] give similar conclusions. They report that the effect of coolant flow on the loss was not clear. They noticed that the coolant increased the base pressure, which should have decreased the loss. However, the coolant also induced significant mixing losses; and it was not obvious which of the two effects was dominant.

MacMartin, et al. [5] measured an increase in the base pressure with coolant flow, although there was no substantial difference in the loss. The slight difference they obtained, was an irregular increase with increasing coolant flow rates.

---

[7] Note that Singer tested a cascade with the same number of blades, the same pitch, the same turning angle, and blades of the same order of thickness as the cascade tested in this research. The coolant and its flow rates were also the same.

Sieverding [3] proposes an involved explanation of the effects of coolant flow on the base flow. From his detailed experiments, he found that the base pressure first increased with increasing coolant flow rates, and then started to decrease again.

Prust, et al. [13] report significant and approximately linear increase in loss with coolant flow rate. Different ejection slot geometries had significant influence only for low flow rates.

Effect of the coolant-to-main-flow density ratio: Sieverding [3] states that, in actual engines, the density ratios of coolant to main flow vary from 1.5 to 2, due to temperature differences.In his experiments, he used air, CO_2, and air-freon mixtures as coolants. He concludes that the choice of coolant has no significant effect on the base pressure, for coolant flow rates less than that at which the base pressure reaches a maximum. For higher flow rates, higher density ratios keep the base pressure slightly higher.

3.0 Discussion

3.1 Introduction to Nomenclature

This section introduces a few of the terms and quantities that will be referred to in this thesis. Specifically, a coefficient is defined which will be used as the measure of aerodynamic losses; and a way will be presented on how to non-dimensionally quantify the amount of CO_2 injected.

3.1.1 Mass-Averaged Total Pressure Loss Coefficient

The research documented in this thesis investigates the aerodynamic performance of gas turbine blades. It is, therefore, essential to define a quantity to be used as the measure of aerodynamic performance. The aerodynamic performance is improved if losses are reduced. The second law of thermodynamics indicates that losses increase the entropy and decrease the total pressure. In this thesis the drop in total pressure is taken as the measure of loss.

Let the total pressure upstream of the blade row be $p_{t,1}$, and that at a point downstream of the blade row be $p_{t,2}$. The total pressure drop is:

$$\Delta p_t = p_{t,1} - p_{t,2} \qquad [3.1]$$

Divide by $p_{t,1}$ to get a non-dimensional quantity, P_t :

$$P_t = \frac{p_{t,1} - p_{t,2}}{p_{t,1}} = \frac{\Delta p_t}{p_{t,1}} \qquad [3.2]$$

This represents the loss between the flow upstream of the blade row (assumed uniform) and just one point downstream of it. Following Oates [14], to quantify the overall losses, average P_t over two blade spacings. Velocity gradients across the blade spacing are accounted for by taking the average weighted by mass flow rate. That is,the localities where there is more flow contribute more to the average total pressure drop. The averaged quantity is referred to as the *mass-averaged total pressure loss coefficient*

$$\bar{L} = \frac{\int_0^2 \rho_2 u_2 P_t dy}{\int_0^2 \rho_2 u_2 dy} \qquad [3.3]$$

y is the vertical direction, u is the horizontal component of velocity, and the averaging is done at station 2, which is one of three vertical planes downstream of the blade row, where the downstream total pressure probe traverses.

Note that in the definition of P_t (Eqn. 3.2), the total pressure drop, Δp_t, was non-dimensionalized by dividing it with $p_{t,1}$. Some researchers prefer to divide by $p_{t,1} - \bar{p}_2$, where $\bar{p}_2$ is the pitchwise averaged, downstream static pressure. Since an increase or decrease in $p_{t,1}$, typically, causes a respective increase or decrease in $\bar{p}_2$, fluctuations in $p_{t,1}$ have less of an effect on the dimensionless coefficient, with the latter method.

3.1.2 Coolant Blowing Rate

To quantify the amount of injected CO_2, a non-dimensional quantity, the *blowing rate*, is defined as follows:

$$B = \frac{\rho_{c,ex} V_{c,ex}}{\rho_{air} V_{air}} \qquad [3.4]$$

where the subscript "air" refers to the main flow, and "c,ex" refers to the coolant flow at the exit from the blades. The density and velocity of air are the pitchwise averages right behind the blade row. Note that the quantity ρV represents flow rate per unit area.

In this research, the blades are tested with two absolute amounts of coolant injection, in addition to no injection. The two injection rates are assumed independent of the main flow Mach number [8]; therefore, strictly speaking, two constant values of $\rho_{c,ex} V_{c,ex}$ result while $\rho_{air} V_{air}$ varies in Eqn. 3.4. In this thesis, however, only two nominal values for B, approximated for an exit Mach number of 1.15 (the design exit Mach number of the blades is, approximately, 1.2), are referred to, and they are $B_{low} = 0.47$ and $B_{high} = 1.33$, which correspond to total coolant mass flow rates of $\dot{m}_{c,low} = 0.0261$ kg/sec (0.0575 lb/sec), and $\dot{m}_{c,high} = 0.0732$ kg/sec (0.161 lb/sec). Since the estimated mass flow rate for air at a Mach number of 1.15 is $\dot{m}_{air} =$ 8.07 kg/sec (17.80 lb/sec), the flow rate ratios by mass of coolant to air are 0.32 and 0.91 percent.

The blowing rate was calculated, also, for exit Mach numbers of 0.60 and 1.36, which are the lower and upper boundaries of the Mach number range in this research. The Mach number was found to have a significant influence on the value of the blowing rate. For these results and a full discussion of the blowing rate calculation method, refer to Appendix C.

---

[8] this is a good assumption if the coolant flow at the exit from the blades is choked. Preliminary calculations reveal that the flow is choked for the high injection rate only. For the low injection rate, therefore, effects of air flow variations are neglected.

3.2 Description of the Apparatus

This section describes in detail the experimental set-up used in this research [9]. The wind-tunnel and the coolant injection system are detailed. Subsequent sections include descriptions of the data acquisition systems, the experimental procedure, and the testing program followed.

3.2.1 Wind-Tunnel

The wind-tunnel used in this research is shown in Figure 3 and Figure 4. As mentioned earlier, it is of the blowdown type. External storage tanks are pumped up to a desired pressure by two reciprocating compressors. The air is then released via a pneumatic control valve, and discharged through the wind-tunnel into the atmosphere. Excluding a round to rectangular cross-section converter just upstream of the test section, the wind-tunnel upstream of the test section is composed of 14 in, Schedule 30 (35.56 cm OD/33.65 cm ID) carbon steel pipe. The test section and the above mentioned cross-section converter are made of the same material.

To reduce the amount of compressor leakage oil and water, the air leaving the compressors is passed through two desiccant filled cylinders before it enters the storage tanks. Unfortunately, the oil leakage in the compressors is, at present, more than can be handled by this drying procedure, and, consequently, the presence of oil in the test section is a cause for concern.

---

[9] The author is indebted to Singer [11] for the valuable information included in his thesis, which was helpful in putting together this section.

Control valve operating system: A photograph of the control valve is shown in Figure 5. The control valve operating system consists of an electronic circuit, an electro-pneumatic converter, a valve actuating air supply, and a source of constant reference pressure. The function of the operating system is to vary the valve opening during the run to maintain air flow in the tunnel, as closely to steady as possible, while the pressure in the storage tanks drops.

The storage tanks are equipped with a pressure transducer whose voltage output is fed into the valve electronic circuit. The circuit produces a proportionate output voltage which is fed into the electro-pneumatic converter, which is just a pressure regulator controlled by a voltage. The input pressure to the converter is the constant reference pressure (close to 20 psig/137.9 kPa,gage), and the output pressure is applied to the valve actuator. When the latter pressure equals the reference pressure, the valve is fully open. This takes place near the end of the run. The valve opening is less for lower converter output pressures.

The electronic circuit has two adjustable knobs. One of them controls an offset applied to the input voltage, and the other controls the output voltage change as a function of the input voltage change. By systematically adjusting these two knobs, it has been possible to achieve a situation where the voltage fed into the electro-pneumatic converter caused the valve opening to increase at a desirable rate during the run so as to keep the total pressure just upstream of the cascade ($p_{t,1}$) nearly close to a desired value, for a long enough period. In this research, the run duration, over which steadiness was essential, was nominally 17 seconds. The unsteadiness that had to be tolerated during this time was typically 15 percent deviation from an average of the gage total pressure upstream of the blade row. This unsteadiness is considered to be of a sizeable magnitude, and may be significantly responsible for some *scatter* noticed in the reduced data.

Flow straightener: uniform inlet flow to the test section is essential for achieving pitchwise periodicity. To make sure that this uniformity exists, a flow straightener is installed starting at a position 1.041 m upstream of the test section inlet and extending downstream. It consists of a group of long (approximately 10.0 in/ 25.4 cm), thin walled pipes (0.875 in/ 2.22 cm in diameter) welded side by side to fill the inside of that round wind-tunnel section. Uniformity was tested by Zaccaria [4] via a vertical (the pitchwise direction), spanwise centered traverse just upstream of the blade row. The traverse was displaced by 2.54 cm steps, and Zaccaria reports that the uniformity was excellent over the central part of the test section, covering the region where the test blades are mounted in this research. Non-uniformities closer to the upper and lower walls were attributed to boundary layers.

Test section: a photograph of the test section is shown in Figure 6. The cross section is rectangular, 15.24 cm wide and 37.26 cm high. The movable total pressure probe upstream of the blade row, that is used to test uniformity, is fully retracted through the upper wall hole it goes through during normal operation. This avoids probe interference with the flow.

The blade row consists of eleven blades with rounded trailing edges and identical geometry [10]. Some geometric features are shown in Figure 7and Figure 8. The main difference between the uncut and the cut blades, from hereon referred to as the *first cascade* and the *second cascade*, respectively, is the trailing edge thickness. The trailing edge thickness (measured with a micrometer) of the first cascade is $h_{te,1}$ = 0.483 mm (0.019 in), and of the second cascade $h_{te,2}$ = 0.762 mm (0.030 in); the trailing edge thickness ratio is, therefore, $\frac{h_{te,2}}{h_{te,1}} = 1.57$. The axial chord length changes slightly, but the change is negligible for most our purposes, and the axial chord length for both cascades is taken as c = 38.1 mm (1.50 in); the trailing edge thickness to axial chord length ratios are, therefore: $\frac{h_{te,1}}{c} = 0.0127$, and $\frac{h_{te,2}}{c} = 0.0200$. For the cooled blades, the amount by which the very short distance between the coolant slots and the trailing edge is changed, due to the cut-back, is of significance. The cut-back involves shortening the blades by Δd = 1.016 mm (0.040 in), measuring along the blades, and "d" being the distance from the tip of the trailing edge to the downstream end of the coolant ejection slot (see Figure 8). For the first cascade, d_1 = 2.032 mm (0.080 in), and for the second cascade, d_2 = 1.016 mm (0.040 in). Notice that the distance d is cut in half,

[10] The blade profile specifications are withheld, because permission for publishing them was not granted by the manufacturer.

which substantially changes the position of the coolant slots with respect to the critical base region. Note, also, that no more than one further cut-back of the cooled blades would be practical, without cutting into the coolant slots (d_2 is already very small).

The inlet flow is horizontal, and this is taken as the reference angle. The design exit flow is assumed to be 68° below the horizontal. Of course, even with design conditions met, the latter assumption ignores the two dimensionality of the flow; because there is always some pitchwise variation in the flow angle.

In all the theoretical quantifications in this thesis, relations for air, derived for one dimensional flow, are used. This means that flow uniformity is assumed in the direction normal to the flow as the flow turns. Implicit in this simplification is the assumption of a nominal flow angle that changes only with downstream motion.The throat section of the blade passage lies close to the exit, and the entire throat area for the whole cascade (A^*) is 275.02 cm², where the throat area is the area normal to the flow at sonic speed. With an inlet flow area (A_1) of 567.84 cm², the one dimensional, isentropic relations for air indicate an inlet Mach number (M_1) of 0.295 , for choked flow.

The blades are mounted between two pieces of plexiglas. The transparency of the plexiglas allows visual access into the test section, which is especially important for taking pictures of the flow. The blades and plexiglas form a removable unit (Figure 9), which is referred to as the *cascade*. The cascade also includes two *end pieces* of aluminum at the top and bottom (see Figure 10) that form part of the boundaries of the flow. Figure 10 shows the numbering and lettering system used in referring to the blades and passages. Blades are numbered from one to eleven, and passages are lettered from A to J. The blades are identical in geometry, except for the CO_2 passages in the *cooled* ones (blades 4, 5, and 6), and the static pressure taps (0.254 mm D) in the *instrumented* ones (blades 7 and 8). The static pressure taps are distributed along the spanwise centerline. Blade number 7 has nine taps drilled into the suction surface, and blade number 8 has five taps drilled into the pressure surface and one in its trailing edge. The latter pressure tap is used to read the nominal base pressure. Stainless steel tubings (1.067 mm OD/0.635 mm ID) are connected to the pressure taps, and are routed inside the blades and through the cascade's plexiglas to allow connection to a pressure measuring system. Each cooled blade (see Figure 11) is hollow with 0.794 cm holes in each side to allow CO_2 injection, and 40, 2.381 mm by 0.635 mm holes very close to the trailing edge to allow CO_2 ejection into the main flow. Holes are made in the plexiglas, and special fittings are used (Figure 12) to connect CO_2 plastic tubings to the side holes of the blades.The trailing edge holes are drilled close to the trailing edge but not at it, in order to allow for some cutback on the blades.

Static pressures downstream of the blade row are read via two groups of pressure taps. In the right-hand side (facing in the flow direction) plexiglas, holes are drilled in at two horizontal positions (see Figure 13). With x defined as the horizontal distance downstream of the blades' leading edges, the two groups of pressure taps are at x= 42.86 mm (referred to as the *forward* position), and x= 114.3 mm (referred to as the *rear* position). Short (1.905 cm) pieces of stainless steel tubing (1.588 mm OD/0.794 mm ID) are epoxied into the drilled holes, and plastic tubing connects those to a pressure measuring system. The forward position consists of eleven vertical taps, 3.73 mm apart, such that the middle one is directly behind the trailing edge of blade number 6 at the design exit angle, and a whole blade pitch is covered. The rear position consists of three taps, 18.63 mm apart, such that the lower tap is behind the trailing edge of blade number 6, and the upper tap is behind the trailing edge of blade number 7, both at the design exit angle. Again, a whole blade pitch is covered.

An opening (10.16 cm by 15.24 cm) is located in the floor of the test section (Figure 14), through which the downstream total pressure probe and probe support fixture (Figure 15) are inserted. The total pressure probe is movable through the fixture, and is used for vertical traverses at three horizontal locations downstream of the blade row: *forward*: x= 42.86 mm, *middle*: x= 63.51 mm, and *rear*: x= 114.3 mm, where x defines the position of the probe's tip. The forward and the rear locations are in the same vertical plane as the two groups of static pressure taps that are drilled in the plexiglas. Positioning of the probe at one of the three locations is done by using one of three different support fixtures. The purpose of the flange on the support fixture is to prevent bending of the probe, since the probe has to quite long in order to reach the test blades (the distance between the floor of the test section and the uppermost traversed passage is approximately 52 cm at the blade row). The probe itself is a 61.0 cm (24.0 in) long, 6.35 mm (0.250 in) OD, stainless steel, hollow tube, with a 1.65 mm (0.065 in) OD, hollow tube extending inside it and protruding from both ends. The thin inside tube is the pitot tube, while the outside tube is its fixture. The bottom protrusion of the inside tube is connected to plastic tubing extending to a transducer, while the top protrusion is straight, 2.3 cm (0.91 in) long, and angled such that it faces the design, exit flow (68° below the horizontal). The tip of this thin, round section is slightly flattened.

Two aluminum doors enclose the test section (Figure 16). Slots are milled into the inner surfaces of the doors so that they support the cascade rigidly in place. 10.80 cm by 15.24 cm openings are cut into both doors at the same location, offering visual access into blade passages D, E, and F. A total pressure probe (1.588 mm OD/0.794 mm ID) penetrates the left-hand door at a location upstream of the blade row. The total pressure reading takes place 3.81 cm from the inside of the door.

The back wall of the test section is designed at an angle parallel to the design exit flow. A solid tailboard is attached to the back wall via six adjustable bolts, and this assembly is a removable unit (Figure 17 shows the back wall with the tailboard removed). The tailboard's angle is varied by adjusting the bolts, while its upper end is always made to hinge around one position, such that the exit flow from the uppermost passage is immediately guided by the tailboard. In other words, the presence of the tailboard prevents the exit flow from being a free jet.

3.2.2 Carbon Dioxide Supply System

CO_2 is uniformly supplied to the three cooled blades at constant rates [11]. The supply system is shown schematically in Figure 18. CO_2 is emptied from commercial, high pressure tanks (10.34 MPa,gage , 1500 psig) into a large low pressure tank (275-350 kPa,gage , 40-50 psig). A mechanical ball valve and a solenoid valve control the exhaust from the tank, and 4.88 m of copper tubing (1.905 cm ID) connect the tank to a distribution manifold equipped with a pressure gage. A pressure regulator and a float-type flowmeter are installed in series upstream of the manifold, with the flowmeter between the regulator and the manifold. The pressure regulator determines a constant flow rate which depends on the control pressure applied to the regulator. The manifold distributes CO_2 evenly to the three blades via six tubes of flexible plastic (76.20 cm long, each), with a tube going to each end of each blade.It is assumed that the CO_2 ejection at the trailing edges of the blades is spanwise uniform, although no direct measurement has been taken. Finally, as mentioned earlier in section 3.1.2, the coolant flow at the ejection slots is choked for the high blowing rate (B = 1.33), and not choked for the low one (B = 0.47).

3.3 Experimental Procedure

Two types of data are collected in this research: pressure data and visual data. The latter consist of still pictures that are taken using the shadowgraph technique for selected runs.

---

[11] CO_2 was chosen because the density ratio of CO_2 to air (1.5) closely simulates the density ratio of the coolant air to the main flow air in the actual turbine.

As mentioned in section 3.2.1, the duration of a run is about 17 seconds. The control valve operating system is previously adjusted to produce a blowdown with a total pressure upstream of the blade row as closely constant as possible over at least 17 seconds. It is also important that this total pressure be at an appropriate level, so as to choke the cascade or not, whichever the goal may be.

Seventeen seconds is the time required for the downstream total pressure probe to traverse two blade passages. It is driven by a traversing mechanism (Figure 19) which consists of a stepper motor, a reduction gear, and a rack and pinion arrangement, which converts the driving rotational motion into linear motion of the probe. The speed of the probe was $v_p = 0.47$ cm/s. It was adopted because it was found to be the fastest speed at which the transient response of the probe, transducer system was still fast enough. It was found that when the probe was driven at a lower speed, no apparent difference was observed in the measured total pressure; while when the probe was driven faster, differences were noticed. The two traversed passages start in the middle of passage C below the lowest cooled blade (blade number 4), and end in the middle of passage E below the highest cooled blade (blade number 6). Two blade passages are traversed instead of one, as an attempt to account for some possible aperiodicity by averaging the two passages.

Pressure data: the pressure data collected is of two types: digital data that is read by an IBM PC and stored on disk, and analog data that is recorded on stripcharts. The pressures that are read are the following [12]:

1. Total pressure upstream of the blade row, $p_{t,1}$, via a fixed total pressure tube described in "Wind-Tunnel".

---

[12] The pressures described below are all gage pressures. Later in this thesis, the same symbols will be used to represent these pressures in absolute form, after the daily measured atmospheric pressure is taken into account.

2. Total pressure downstream of the blade row, $p_{t,2}$, via the traversing probe [13].

3. Blade suction surface static pressure (9 locations), $p_{b,s,1-9}$.

4. Blade pressure surface static pressure (6 locations), $p_{b,p,1-6}$.

5. Wall static pressure, forward position (11 locations), $p_{w,f,1-11}$, via the taps drilled in the plexiglas at the forward horizontal position (see "Wind-Tunnel").

6. Wall static pressure, rear position (3 locations), $p_{w,r,1-3}$.

In this thesis, the subscript 2 for the probe station *downstream of the blade row* (for an example, see item 2 in the above list) refers to any of three stations the probe may occupy, forward, middle, or rear (see "Wind-Tunnel"). Therefore, *downstream of the blade row* does not necessarily mean immediately behind it.

A pressure measuring system[14] utilizes a multi-channel sensor (with a transducer per channel) to read $p_{t,1}$, $p_{b,s,1-9}$, $p_{b,p,1-6}$, $p_{w,f,1-11}$, and $p_{w,r,1-3}$. It electronically scans these pressures successively at a very fast rate. Each read value is stored in memory, and when the entire scan is accomplished, all the values are downloaded to the computer. The scanning rate is fast enough to safely assume that the readings are taken at the same instant in time. This pressure measuring system calibrates its transducers using an internal, digital, quartz, reference transducer, which corrects for all thermal zero and sensitivity shifts, including nonlinearity of the transducers, amplifiers and built in A/D converter. The final output is pressures in psig.

---

[13] For the first cascade, a differential transducer was used to read the total pressure drop between upstream and downstream of the blade row, Δp_t, with connections to the two, above mentioned probes. For the second cascade, the total pressure drop typically exceeded the operation range of the differential transducer; therefore, $p_{t,1}$ and $p_{t,2}$ were read via two transducers. In this thesis, only the case of reading $p_{t,1}$ and $p_{t,2}$ separately is referred to in the presentation of the computational methods, with the simple modification for the other case omitted.

[14] *Digital Pressure Measurement System - Model 780 B*, manufactured by Pressure Systems Incorporated.

A separate pressure measuring system consists of an Analog/Digital converter board added to the basic computer, and two pressure transducers that read $p_{t,1}$ and $p_{t,2}$. The output of the transducers is fed into the A/D converter, and a corresponding digital reading is stored on disk. Note that the first pressure measuring system also reads $p_{t,1}$, directly and not through the pressure transducer used with the A/D converter. Figure 20, Figure 21, and Figure 22 are example plots of the A/D converter data for first cascade runs taken at the forward, middle, and rear positions, respectively, at an isentropic exit Mach number of 1.25. Figure 23, Figure 24, and Figure 25 are similar plots for second cascade runs at an isentropic exit Mach number of 1.26. Note how the drop in total pressure, particularly behind the blades, is notably higher for the second cascade.

A computer program controls the entire data acquisition procedure. The operation of the program is summarized as follows:

- At the instant the program is initiated (shortly after the wind-tunnel control valve is switched open), the first pressure measuring system takes all its pressure readings, assumed simultaneous, and those are all the readings it takes throughout the run.

- At the instant the program is initiated, the downstream probe, initially at its lowest position, starts moving upwards at a constant speed of $v_p = 0.47$ cm/s.

- At the instant the program is initiated, the second pressure measuring system starts reading simultaneous values of $p_{t,1}$ and $p_{t,2}$, repeatedly at the rate of 40 times per second, until 800 readings of each are read. As mentioned earlier, it takes the probe close to 17 seconds to traverse the two designated passages. It turns out that 657 readings are taken during this time period by the pressure measuring system. Thus, the rest of the 800 readings are taken afterwards.This is done to gain the advantage of extra data points, in case the probe was initially positioned lower than it should have been; in that case, the first portion of the data set will not be used in the data reduction procedure.

- After the probe traverses the two passages and a short distance more, it is driven back down to its initial position, to be ready for the next run.

The output of the two transducers reading $p_{t,1}$ and $p_{t,2}$ is also plotted to a stripchart. Although the computer stored data can easily be plotted, having an immediate plot is helpful in monitoring the experiment, and gaining some insight into the flow.

Visual data: flow patterns in gas flows can be observed by means of optical techniques that make use of density variations in the flow field. Light is passed through the flow and gets refracted differently due to the variation in the density dependent refraction index. The result is light rays leaving the flow field in different directions; and when they are intercepted by a screen to form an image, the difference in direction causes a variation in the light intensity across the image, or even dark regions or *shadows* where light has been completely diverted. With the more sensitive techniques, quantitative information on the flow field can be obtained. Even in subsonic flows, patterns can possibly be visualized. Of course, as velocities go higher optical visualization becomes easier because of the larger density gradients. With less sensitive techniques, only visualization of sharp density gradients like shocks may be possible.

The three common optical techniques of flow visualization utilize the *Interferometer* system, the *Schlieren* system, and the *Shadowgraph* system. The first two are the more sensitive ones with the Schlieren system being the simpler to implement. They are both sensitive to small density gradients. The last technique is the one implemented in this research. It is the simplest, the least expensive, and the easiest to operate; it is not, however, sensitive to small density variations, and is used only when qualitative visualization of large density gradients, such as shocks, is sufficient. The technique works as follows: a parallel beam of light is passed through the flow. Some of the rays get deflected due to density gradients, and the result is bright and dark regions on the screen corresponding to ray convergence and divergence, respectively. In practice, regions of slight density variations result in a homogeneous image, and shocks create a sharp dark shadow. Boundary layers may also produce a dark image. For a thorough treatment of the three above mentioned optical techniques refer to Saad, [15].

In this research, considering the large presence of compressor leakage oil in the flow, it would have been a waste of effort to use an optical technique that is supposed to be more sensitive than the Shadowgraph technique. Therefore, the photographs taken served almost entirely to visualize shocks, with the exception of occasional boundary layer visualization near the trailing edge in the clearer pictures. Since shocks were the target of observation, pictures were taken for runs with supersonic exit velocities, for a variety of Mach numbers and coolant injection rates. Figure 26 is an example of such a picture.

Shock visualization was of interest in order to (1) verify the pitchwise periodicity (parallel shocks indicate periodicity), (2) qualitatively investigate the relative strength of the reflected shocks from the tailboard or the backwall (it is desirable to have them as weak as possible compared to the shocks originating from the trailing edges), and (3) obtain qualitative insight into the trailing edge shock system.

The Shadowgraph system employed in this research consists of a high speed light source (a strobotac), a partially focusing lens, two concave mirrors, a plane mirror and a camera (Figure 27). The strobotac is set to emit one short, high intensity pulse of light upon external triggering. The cone of emitted light rays goes through the partially focusing lens with a resulting refraction and impinges upon the first concave mirror. The focal lengths of the lens and mirror, and the relative positions of the light source, lens, and mirror are such that the beam of light is reflected off the mirror forming a parallel beam. The light passes then through the plexiglas windows of the test section parallel to the spanwise direction of the blades. The light is reflected off a second concave mirror, a plane mirror, and focuses on the film of the camera. To get a focused image on the film, the distance from the center of the test section to the second concave mirror is treated as the object distance with respect to the mirror, and the cumulative distance from this concave mirror to the plane mirror and to the film is treated as the image distance. From the known focal length of the concave mirror and a basic optics relationship, the object and image distances are adjusted to produce a focused image on the film. The implied assumption in this method is that the rays of light which "form" the shadows, or, rather, the boundaries of the shadows, are rays significantly deflected from their original direction, and hence no longer appear like they are originating from infinity, but, rather, from a luminous source in the test section.

With everything set up properly, the lights in the laboratory are turned off and the film is exposed. The wind-tunnel valve is opened, and after allowing sufficient time for the flow to reach steady state, the strobotac is triggered.

3.4 Testing Program

The two cascades have been tested under a variety of conditions: (1) the exit Mach number varied from 0.60 to 1.36, (2) two coolant blowing rates were used, B = 0.47 and 1.33, in addition to runs with no coolant injection, (3) the downstream total pressure probe was positioned at three different stations: forward ($\frac{x}{c}$ = 1.125), middle ($\frac{x}{c}$ = 1.667), and rear ($\frac{x}{c}$ = 3), and (4) some runs were taken with the tailboard installed, and some with the tailboard removed.

Tables 1 - 4 present all the runs with all the information on them included. The runs are grouped by downstream station, blowing rate, and by increasing Mach number. Separate tables were made for the runs with and without the tailboard. Inspection of the tables easily reveals the testing program that was followed.

3.5 Data Reduction

The experimental set-up, the experimental procedure, and the testing program followed have been detailed in previous sections. This section discusses the numerical algorithm that is implemented in processing the raw data,which calculates the total pressure loss coefficient, and the assumptions within this algorithm are presented [15]. "Uncertainty Analysis", a later section in this chapter, provides an attempt at estimating errors involved in the calculated value of the total pressure loss coefficient.

3.5.1 Data Reduction Algorithm

Conversion of Raw Data into Absolute Pressure Units: As discussed in "Experimental Procedure", the digital data collected consists of two types of pressure measurements. One type, which is recorded 657 times during the time it takes the downstream total pressure probe to traverse two blade passages, is collected via an analog/digital converter, and it consists of the gage total pressure upstream of the blade row (station 1), and downstream of the blade row (station 2). The A/D converter can be set to operate in different voltage ranges; the one that was used ranges from zero to ten volts, with the corresponding digital reading ranging from zero to 4095. Thus, the recorded data is divided by 409.5 to convert it into the measured value in volts. Then, the gage pressure values are calculated from the known calibrations of the two transducers used. Finally, the atmospheric pressure, recorded on each testing day, is added to get the absolute upstream total pressure, $p_{t,1}$, and the absolute downstream total pressure as measured by the probe, $p_{t,2,prb}$. The latter is later corrected to account for the ef-

[15] The FORTRAN program is listed in Appendices D and E.

fect of the shock in front of the probe's tip, in case of supersonic exit flow. This correction is described in detail in the next section.

The second type of pressure data is collected through an independent pressure measurement system. This data is taken only at one instant in the run. The system is self-calibrating, and the recorded data is already in gage pressure units. Thus, all that is needed is converting it to absolute pressure units. The pressures that are measured through the above mentioned system are the following: $p_{t,1}$, $p_{bl,s,1-9}$, $p_{bl,p,1-6}$, $p_{w,f,1-11}$,and $p_{w,r,1-3}$.

Correction for the Bow Shock Effect: For the case of supersonic exit flow, a *bow shock* is expected to form in front of the downstream total pressure probe. The total pressure that is read is downstream of this shock and, therefore, lower than the true value. This is corrected for by treating the bow shock as a normal shock. The method of correction differs slightly depending on whether the tailboard is installed or not. The method for the case of running with the tailboard is discussed first.

The case of running with the tailboard installed: Earlier experimental work done on this wind-tunnel (for more detail, refer to Zaccaria [4]) demonstrates that the isentropic, exit Mach number remains fairly constant throughout a run when the tailboard is installed. For the case of no tailboard, however, this is no longer true.This phenomenon is due to the fact that with no tailboard, the flow leaving the blade row is a free jet, and is, therefore, affected by the total pressure upstream of the blade row, which varies significantly during the run. With the tailboard installed, it is fair to expect the exit flow to be parallel to the tailboard; and a constant exit flow angle means a constant exit flow area, A. By reference to Schreier [16], the following isentropic, one-dimensional relationship holds for choked flow:

$$\frac{A}{A^*} = \frac{1}{M}\left[\frac{\frac{(\gamma+1)}{2}}{1+\frac{(\gamma-1)}{2}M^2}\right]^{\frac{(\gamma+1)}{2(1-\gamma)}} \qquad [3.5]$$

where A^* is the throat area, M the Mach number, and γ (=1.4) the constant specific heat ratio for air. Using Eqn. 3.5 as an approximate guide, we see that a constant exit flow area should yield an approximately constant exit Mach number; as we assume, essentially, the case to be with the tailboard installed. The isentropic, exit Mach number is taken to fulfill the following relationship:

$$\frac{p_{t,1}}{p_2} = \left[1 + \frac{(\gamma - 1)}{2} M_{2,isen}^2\right]^{\frac{\gamma}{(\gamma-1)}} \qquad [3.6]$$

Assuming $M_{2,isen}$ to be constant is, therefore, equivalent to assuming $\frac{p_{t,1}}{p_2}$ constant. Note that the above Mach number is referred to as isentropic because if the flow were isentropic, $p_{t,1}$ and $p_{t,2}$ would be the same, and the isentropic Mach number would be the actual one.

In order to calculate p_2, the measured values of $p_{w,f,1-11}$, $p_{w,r,1-3}$, and $p_{t,1}$ are used. The first two are measured at only one instant during the run. The average value of $p_{w,f,1-11}$ is taken as the value of p_2 when station 2 is at the forward position, and the average value of $p_{w,r,1-3}$ as the value of p_2 at the rear position, both at that instant in time when the measurements are taken. For the sake of calculating the value of p_2 at the middle position, p_2 is assumed to vary linearly from the forward to the rear position. Of course, one of the inputs to the data reduction program is the position of the downstream probe.

The same pressure measurement system that does the one instant measurements, reads the value of $p_{t,1}$ in addition to $p_{w,f,1-11}$ and $p_{w,r,1-3}$. This value of $p_{t,1}$ together with the calculated value for p_2 , as described in the last paragraph, are used to calculate the value of the constant ratio $\frac{p_{t,1}}{p_2}$. This value and the repeatedly measured value of $p_{t,1}$ are used to calculate p_2 throughout the run.

As mentioned earlier, the bow shock is treated as a normal shock. Denoting the state upstream of the shock by the subscript x, and downstream by the subscript y, the following equation (by reference to Schreier [16]) gives the total pressure drop across the shock:

$$\frac{p_{t,x}}{p_{t,y}} = \left[\frac{\frac{\gamma+1}{2} M_x^2}{1 + \frac{\gamma-1}{2} M_x^2} \right]^{\frac{\gamma}{\gamma-1}} \left[\frac{1}{\frac{2\gamma}{\gamma+1} M_x^2 - \frac{\gamma-1}{\gamma+1}} \right]^{\frac{1}{\gamma-1}} \qquad [3.7]$$

$p_{t,y}$ is the value measured, and $p_{t,x}$ the true value of the total pressure downstream of the blade row, $p_{t,2}$. The gap between the wall static pressure taps and the probe's tip is large enough to safely assume that the taps will always be upstream of the bow shock. Therefore,p_2 and $p_{t,x}$ (or $p_{t,2}$) are for the same state, and are related by the following relation:

$$\frac{p_{t,x}}{p_2} = \left[1 + \frac{\gamma - 1}{2} M_x^2 \right]^{\frac{\gamma}{\gamma-1}} \qquad [3.8]$$

$p_{t,y}$ and p_2 are already known. By eliminating $p_{t,x}$ from Eqns. 3.7 and 3.8, the value of M_x is calculated by iteration. Then the known value of M_x is substituted in Eqn. 3.7 to find $p_{t,x}$.

The case of running with no tailboard: For this case the assumption of constant $\frac{p_{t,1}}{p_2}$ is no longer valid. An empirically derived equation relating $p_{t,1}$ to $M_{2,isen}$ is used, instead, to calculate $M_{2,isen}$ for each of the 657 measured values of $p_{t,1}$. This value is used as M_x in Eqn. 3.7 to find $p_{t,x}$. Then p_2 is calculated from Eqn. 3.8. Note that, for lack of a better method, the value of the isentropic Mach number is used for the real Mach number in Eqn. 3.7.

It was mentioned in the above paragraph that an empirical equation was used to relate $p_{t,1}$ to $M_{2,isen}$. A separate equation was derived for each of the two cascades tested. The pressure readings that were taken at only one instant during the run were used, from the runs that had been taken with no tailboard installed. From each run a value for $p_{t,1}$ was obtained, and, also, a corresponding value for $M_{2,isen}$. A linear fit was created for the set of points obtained; and it turned out that the fit had a very good correlation coefficient.

Subsonic exit flow: The section of the algorithm that corrects for the bow shock effect is bypassed in the case of local subsonic flow. Some runs are entirely subsonic; or it is possible to have runs where some regions downstream of the blade row are subsonic although others are supersonic. For example, the flow behind a blade might be subsonic due to boundary layer effects or trailing edge shocks. For this reason, the algorithm tests for subsonic flow at each point. For the case of no tailboard installed, if the calculated value of $M_{2,isen}$ is less than unity, the flow is considered locally subsonic. For the case of the tailboard installed, a value of $\frac{p_2}{p_{t,2,prb}}$ greater than 0.528 is taken to indicate subsonic flow, since $\frac{p}{p_t} = 0.528$ is characteristic of sonic flow for air. Actually, $\frac{p_2}{p_{t,2}}$ should be compared with 0.528, if the value for $p_{t,2}$ were known. The error involved, however, is negligibly small. $p_{t,2,prb}$ is smaller than $p_{t,2}$, and the error introduced, therefore, is not correcting for the effect of a bow shock at a Mach number very close to unity. Such a shock will be very weak, and its effect negligible. Figure 28 is a sample plot of the mass-averaged total pressure loss coefficient, $\bar{L}$, versus exit, isentropic Mach number. The two curves represent results with and without correction for the bow shock effect, with the uncorrected case giving higher losses. Note how the curves overlap for Mach numbers less than or equal to unity. Around design Mach number ($\sim$ 1.2), the difference is, approximately, 10 percent, and at the high end of the Mach number range, it is 20 percent.

Calculation of the Mass-Averaged Total Pressure Loss Coefficient: The mass-averaged total pressure loss coefficient, $\bar{L}$, has already been defined in "Introduction to Nomenclature". Here is a description of how it is calculated in the algorithm. Recall Eqn. 3.3:

$$\bar{L} = \frac{\int_0^2 \rho_2 u_2 P_t dy}{\int_0^2 \rho_2 u_2 dy} \qquad [3.3]$$

where P_t was given by Eqn. 3.2:

$$P_t = \frac{p_{t,1} - p_{t,2}}{p_{t,1}} \qquad [3.2]$$

The integration in Eqn. 3.3 is done over two blade passages in order to include effects of possible defects in flow periodicity. The integration is taken over, roughly, the two adjacent cooled passages, between the three cooled blades (blades 4, 5, and 6). Of course, the integration is done between subsequent data points. Over the time it takes the downstream probe to traverse the two blade passages, about 657 values of $p_{t,1}$ and $p_{t,2,prb}$ are read. For each value of $p_{t,2,prb}$, the algorithm calculates $p_{t,2}$, as described in the previous section. Eqn. 3.2 is used to calculate P_t corresponding to each measurement point.

The exit density, ρ_2, and the exit velocity, u_2, are still needed to compute $\bar{L}$. Neglecting the effect of CO_2, the ideal gas equation of state for air is used:

$$\frac{p_2}{\rho_2} = RT_2 \qquad [3.9]$$

where R is the ideal gas constant for air (287 $\frac{\mathrm{N\,m}}{\mathrm{kg\,K}}$), and the adiabatic relation:

$$\frac{T_{t,2}}{T_2} = \left[1 + \frac{\gamma - 1}{2} M_2^2\right] \qquad [3.10]$$

and the expression for Mach number for a perfect gas:

$$M_2 = \frac{u_2}{\sqrt{\gamma R T_2}} \qquad [3.11]$$

The flow in the wind-tunnel is assumed adiabatic, and, therefore, the total temperature would be expected to remain uniform and constant for steady inlet flow to the wind-tunnel. It is found, however, that the total temperature drops during the run due to the air expanding in the storage tanks. During a typical run, the total temperature was monitored at a station upstream of the test section with a thermocouple. The average value of these readings is taken as the uniform and constant value of the total temperature for all runs. This value is 283 K (10 °C).

The error introduced by this simplifying assumption, in the computed value of $\bar{L}$, is expected to be negligibly small. The relative error in T_t is of the same order as a few degrees out of 283. Moreover, in the calculation of $\bar{L}$, only ρ_2 and u_2 depend on $T_{t,2}$; and both of them appear as multiplying factors in both the numerator and the denominator of Eqn. 3.3.

In Eqns. 3.10 and 3.11, the empirically computed value of $M_{2,isen}$ is used for the value of M_2, for the case of no tailboard installed, and the computed value of M_x in Eqn. 3.7, for the case of the tailboard installed. Enough information ia available, now, to calculate T_2 from Eqn. 3.10, and, then u_2 from Eqn. 3.11. At this point, the algorithm has already calculated the value of p_2 corresponding to each measurement point. With p_2 and T_2 known, ρ_2 is calculated from Eqn. 3.9.

Integration: Now that the integrands of Eqn. 3.3 are known for each measurement point, the integration can be carried out. From the known speed of the downstream probe, and the known rate of data collection, *dy* in Eqn. 3.3 is calculated, which is the vertical distance the probe traverses between two successive data collections. Finally, the integration is done using the simple *trapezoidal rule.* [18]

It was mentioned that the integration is carried out over the two passages between the three cooled blades. A practical problem is specifying to the algorithm where to carry out the integration. During the experiment, the data starts being collected just as the data collection computer program is initiated; and, at that same instant, the probe starts moving. Where the data starts being collected, therefore, depends on where the probe is initially positioned. In practice, it is hard to position the probe exactly where it should be. The second consideration is that, near the end of the run, $p_{t,1}$, sometimes, drops too fast. If it drops too much, the flow may go from supersonic to subsonic. This is an undesirable situation; since it does not make any sense, from a physical point of view, to average the loss over a run that mixes supersonic and subsonic flows.The reason is that the physical nature of the loss in supersonic flow is

[18] The trapezoidal rule of numerical integration assumes that the dependent variables vary linearly between two successive points of integration.

different from that in subsonic flow. The problem is overcome by making the algorithm plot $p_{t,1}$ and Δp_t to the screen, and allow the user to specify two regions of integration. Each region is, automatically, set to span a distance equal to one blade pitch. The first point of the first region and the last point of the second region are specified to the program. By looking at the screen plot, it is possible to know where, with respect to the blades, the data begins to be collected, and to detect subsonic regions. In a subsonic region, Δp_t is practically zero in regions not too close to blades. Care is taken to integrate over two separate and adjacent regions; although, sometimes, the two have to be made to overlap a little.

3.5.2 Summary of the Assumptions in the Data Reduction Algorithm

In the previous section, the assumptions that had to be made in developing the data reduction algorithm were pointed out. This section offers a summary of these assumptions to help in providing a clear assessment of the reliability of the results. The assumptions were:

1. For the case of the tailboard installed, $M_{2,isen}$ (or $\frac{p_{t,1}}{p_2}$) was considered constant throughout the run. This assumption was justified by previous testing of the wind-tunnel, and by the theoretical argument that was proposed. Recall that the premise for that argument was that the tailboard fixes the exit flow angle and, thus, the exit flow area. In reality, however, the tailboard is expected to vibrate and provide for a, somewhat, fluctuating exit angle. The assumption is, nevertheless, a strong one, as the older experimental results indicate.

2. For the case of no tailboard, the value of $M_{2,isen}$ was used for M_2 for lack of better means. In addition to the error involved in this approximation, this method is slightly inconsistent with the method used for no tailboard; the indiscrepancy introduced, however, is expected to be small.

3. For the case of no tailboard, $M_{2,isen}$ and $p_{t,1}$ were assumed to obey a linear, empirical relationship derived for each tested cascade. This is a safe assumption, since the data points that were taken to derive the linear relations had correlation coefficients of the order of 0.99.

4. The static pressures downstream of the blade row were based on readings from wall pressure taps. The implied assumption, here, was that the static pressure at the wall equals the static pressure at the flow centerline. This assumption was made for the lack of means to measure centerline pressures.

5. The static pressure downstream of the blade row was assumed to vary linearly with distance. This assumption neglected the discontinuities that may result from shocks. The shocks may be directly from the trailing edges, or may be reflected at the tailboard (or the back wall).

6. The total temperature was assumed uniform throughout the wind-tunnel, constant throughout the run, and the same for all runs. The value used was the average of thermocouple readings taken upstream of the test section for a *typical run*. The typical Mach number in the pipe upstream of the test section is low enough (approximately 0.13) to make the total temperature measurement by the thermocouple reliable. It was argued that the effect of this assumption on the computed value for $\bar{L}$ was negligible.

7. A group of relations were used that apply only to air as an ideal gas, with $\gamma = 1.4$ and $R = 287 \frac{N\,m}{kg\,K}$. This neglected the effect of the injected CO_2.

8. An implicit assumption was that the downstream probe points directly into the on coming flow. This assumed that the probe was correctly positioned, and that the exit flow was at the design angle of 68° below the horizontal. The actual exit angle would be affected, however, by the shock system, by the presence or absence of the tailboard, and by the

angle at which the tailboard is installed. It is generally accepted that the error caused by probe misalignment is proportional to (1 - cos α), where α is the misalignment angle. Thus, for a misalignment of 5°, the error is approximately 0.4 percent. An error of this magnitude is insignificant.

3.6 Results and Analysis

The complete results of this research are presented in tabular form (Tables 1 - 4), and graphical form (Figure 29 to Figure 53). Figure 54 to Figure 58 are sample plots of the isentropic Mach number distribution over the blades, and Figure 59 to Figure 62 are sample shadowgraph pictures of various runs with supersonic exit velocities. The tabular results are separated between tailboard and no tailboard runs. The reason is that the Mach numbers for the no tailboard runs are reported as they are computed for each run individually; while for the tailboard runs, each run is represented by a Mach number, $M_{2,isen,avg}$, which is the average of the calculated Mach numbers for all the runs taken with that same tailboard setting. Recall that the key assumption in the data reduction procedure for the case of tailboard installed was that the exit Mach number is determined by the angle of the tailboard. It is found, however, that the Mach numbers calculated for runs with the same tailboard setting vary between 1 percent to 3 percent from their average value. Since the assumption of a constant Mach number is made, it is, therefore, more logical to choose this constant as the average of all the runs. Note that in all the graphical results, tailboard runs are represented by $M_{2,isen,avg}$.

Effect of trailing edge thickness on aerodynamic loss: the primary goal of the research documented in this thesis was to study the effect of trailing edge thickness on aerodynamic performance; therefore the plots of primary concern are Figure 29 to Figure 37, which are plots of $\bar{L}$ versus exit isentropic Mach number; each plot shows the results for both cascades for a specific blowing rate and downstream probe station. The effects of blowing rate and downstream station are not meant to be for display here; there is, however, a detectable change in pattern between the plots for the different downstream stations. For all stations, $\bar{L}$ is steadily and significantly larger for the second cascade, as is expected, except for a very few occurrences where the second cascade's loss is slightly lower than the first cascade's. Considering the magnitude of the *scatter* in the results, these occurrences are considered attributable to scatter and insignificant exceptions to the strong, general pattern. The following other observations are made:

- For the forward and middle stations, the results for the two cascades, practically, coincide in the subsonic region for the case of no coolant injection and depart, only slightly, for the injection cases.

- For the rear station in the subsonic region, the loss for the second cascade is drastically higher; but the large scatter in the results for this position seriously questions their reliability.

- For all cases, the loss for the first cascade decreases sharply at a Mach number of 1.36. It was found, however, that all the runs which produce this decrease were taken on the same day. It seems likely, therefore, that an error was involved in the experimental procedure on that testing day.

- In the supersonic range for all cases, the two sets of results depart the most in the Mach number range of 1 to 1.2.

- In the 1 to 1.2 Mach number region, the region of high departure, the second cascade losses are higher by 20 to 30 percent of the first cascade losses.

- For the forward position, the results are acceptably smooth with the exception of the first cascade's sudden drop in $\bar{L}$ higher than Mach number of 1.3.

- For the middle position, the cases with injection show acceptable smoothness with the same exception mentioned above. Note that a loss decrease in the proximity of Mach=1.2 is not necessarily due to scatter, since this is the approximate design Mach number of the blades. The plot for the middle station with no coolant injection shows significant scatter.

- For the rear position, the results are seriously scattered.

Effect of coolant injection on aerodynamic loss: Figure 38 to Figure 43 display the effect of coolant injection on $\bar{L}$. Each plot is for a specific cascade and a specific downstream station with a different symbol for each of the three values of the blowing rate: B=0, B=0.47, and B=1.33. The same observations on scatter that were made earlier in this section still apply here. The following other observations are made:

- For Mach numbers higher than 1.2, the results for the three injection rates practically coincide for all cases.

- For Mach numbers less than 1.1, the loss with high injection rate tends to be significantly lower than with the other two cases, with the exception of the plot for the second cascade's rear station, where, as was noted earlier, the scatter is too large to treat the results as reliable.

Loss development downstream of the blade row: Figure 44 to Figure 53 display the development of the loss downstream of the blade row. Each plot is for a specific cascade at a specific Mach number, with individual curves for each blowing rate. A variety of Mach numbers are represented. All the tailboard runs are included, with the exception of a few for the lack of a comprehensible set of runs having their Mach number. For no tailboard runs, the Mach number is dependent on the upstream total pressure profile, and, thus, it is very hard to find a set of runs with the same Mach number. The majority of the no tailboard data is, therefore, not represented in this type of plots.

From these plots, no apparent trend exists for the effect of coolant injection. About the only observation to be made is that the loss nearly stops to increase after one axial chord length behind the blade row for most cases, or at least the loss increase is sharper within the one axial chord length region. The exceptions to this generalization are the following:

- Figure 53 shows a high increase in $\bar{L}$ between the middle and rear stations for a Mach number of 0.78. This disagrees with the accepted fact that a subsonic flow in a cascade should have a shorter mixing length than a supersonic flow in the same cascade. Note, however, that the results in this figure are for the second cascade, and it has been noted earlier that the rear position results for this cascade are far from reliable.

- Figure 46, Figure 47, and Figure 52 have individual curves in them (for a certain injection rate) which indicate a decrease in $\bar{L}$ between the middle and rear stations. This, of course, consists a violation of the second law of thermodynamics, and, therefore, attributable to scatter.

Blade surface Mach number distribution: Figure 54 to Figure 58 are sample plots of the isentropic Mach number distribution over the pressure and suction sides of the blades, as calculated from the static pressure readings from the *instrumented* blades (with no coolant passages), and the upstream total pressure. Figure 54 and Figure 56 are for an isentropic, exit Mach number of 0.90 for the first and second cascades, respectively. They show identical distributions; even the reading of the base region tap results in the same calculated isentropic Mach number (this means $\frac{p_b}{p_{t,1}}$ is the same). Another, very interesting aspect of Figure 54 and Figure 56 is the obvious presence of a strong shock which impinges on the suction side, although the exit flow is subsonic. It appears that since the wall static pressure taps which are used to calculate the exit Mach number would be downstream of the trailing edge shocks, a supersonic flow shocked to subsonic in the blade passages would produce a calculated value of exit Mach number less than unity. Figure 55 and Figure 57 are for $M_{2,isen}$ = 1.20 for the first cascade, and $M_{2,isen}$ = 1.23 for the second cascade, respectively. The exit Mach numbers are, therefore, very close, and this results in identical blade distributions, with exceptions for the last suction side location and the base region. The latter two show markedly higher Mach numbers for the second cascade, which is equivalent to lower base pressure. This agrees with expectations, since the thicker the trailing edge the lower the base pressure is supposed to be.

Since the goal in this thesis is to study the differences between the two cascades, only a small sample of blade surface Mach number distributions is included, because of the evident independence of these distributions of the trailing edge thickness (except for a slight difference in the trailing 10 percent of the blades' axial chord length).

Visual data: Figure 59 to Figure 62 are samples of shadowgraph pictures taken for supersonic exit Mach numbers. Figure 59 shows a first cascade picture at $M_{2,isen}$ = 1.31, and a second cascade picture at $M_{2,isen}$ = 1.33, almost the same Mach number, and both with no coolant injection. The two apparently exhibit the same shock structure, except, perhaps, for a slight difference in the angle of the trailing edge shocks impinging on the adjacent suction side. The same applies for Figure 60 which compares two pictures at $M_{2,isen}$ = 1.25 and 1.27. Figure 61 presents pictures of runs identical in every aspect to those of Figure 60 except for being with high coolant injection rate. No differences are detectable. The picture in Figure 62 is of a run identical in every aspect to that of the top picture in Figure 60, except that it is with no tailboard. The trailing edge shocks seem less straight and less parallel with no tailboard. This suggests that the pitchwise periodicity with the tailboard installed may be better.

Note that the pictures vary in luminosity due to different intensity settings of the light source. They also vary in the amount of oil present on the windows. The dark lines that are parallel to the flow direction are just streaks of oil blown off the blades' surfaces. Notice how these lines disappear in the clearer pictures.

3.7 Uncertainty Analysis

The results were presented and analyzed in the previous section. It was pointed out that the scatter in the values of $\bar{L}$ was, in some cases, significant; in particular, for the case of the second cascade's rear position, it was serious. In this section, an attempt is made to estimate the amount of error that is expected to exist in the calculated value of $\bar{L}$. Recall the defining equation:

$$\bar{L} = \frac{\int_0^2 \rho_2 u_2 P_t dy}{\int_0^2 \rho_2 u_2 dy} \qquad [3.3]$$

where P_t is defined as:

$$P_t = \frac{p_{t,1} - p_{t,2}}{p_{t,1}} \qquad [3.2]$$

in Eqn. 3.3, since the weighting term $\rho_2 u_2$ appears as a multiplying factor in both the numerator and the denominator, it is assumed that an error involved in it has a negligible effect on $\bar{L}$. The error in $\bar{L}$ is, consequently, taken as the error in P_t.

Following Abernethy, et al. [17], the absolute error in P_t is divided into *bias* and *precision* errors, and combined as follows:

$$U_{P_t} = [b^2 + (tS)^2]^{0.5} \qquad [3.12]$$

where b represents systematic, or bias, error which is considered to remain constant. There is no statistical equation to evaluate b; it is only based on judgement. S represents the error due to irrepeatability, and is the familiar *standard deviation* of a set of values of the quantity whose error is in question. In this case, a set of values of P_t, that ideally should be equal, are used to calculate their standard deviation, the result is the value of S. The *student t value* is a statistical parameter, and is taken as 2.

The possible sources of bias error are the non-uniformity of the upstream total pressure which is measured at only one location by a stationary pitot tube, and transducer calibration error. The former was estimated by Zaccaria, [4] as 0.5 percent. From the calibration points and the least square fit, linear calibration equations of the two transducers used to read $p_{t,1}$ and $p_{t,2}$, the maximum error the calibration equations produce is estimated at 0.25 percent.

The repeatability of P_t is evaluated as follows: during a run, two vertical locations separated by a distance of one pitch and having the same Δp_t ($= p_{t,1} - p_{t,2}$), should have the same $p_{t,1}$ value for the repeatability requirement of P_t ($= \frac{\Delta p_t}{p_{t,1}}$) to be fulfilled. For several representative runs, the recorded values of $p_{t,1}$ and the computed values of Δp_t (after correction for the bow shock had been made) were plotted, and for points separated by one pitch and having the same Δp_t, $p_{t,1}$ was read off the plot. It was found that many such points existed, having the same Δp_t value and significantly different $p_{t,1}$ values. Of course, each of the set of points compared consisted of only two points, and the standard deviation of P_t was calculated for these two points. The maximum standard deviation was found to be approximately 10 percent of the average value of P_t for the two points.

Notice that Eqn. 3.12 gives the absolute and not the relative error in P_t. The estimates given above for bias and precision errors represent relative errors. Since the components of the relative bias error were found to be of the order of 0.5 and 0.25 percent, the bias error is negligible compared to the relative precision error of 20 percent ($\sim tS = 2\text{x}10 = 20$ percent), and is, therefore, neglected. The final result is: the error in P_t, or $\overline{L}$, is a random error of:

$$(\text{Error})_{\overline{L}} = (\text{Random Error})_{\overline{L}} \sim 20 \text{ percent}$$

Note that the above estimate is conservative, and extracted from points on the sample plots that show extreme irrepeatability.

The above discussion shows that the 20 percent irrepeatability in $\overline{L}$ is not due to a physical problem, but to the way $\overline{L}$ is defined. If $\overline{L}$ were calculated from Δp_t and not $\frac{\Delta p_t}{p_{t,1}}$, less scatter would be observed. However, since this research tests a simplified model of a jet-engine turbine, non-dimensionalizing the results is a must. The most obvious way to improve the repeatability of the results is to utilize better valve controls to achieve steadier runs. Improvement is also possible, however, through alternative definitions of the loss coefficient. An example was briefly discussed in section 3.1.1, and it involved non-dimensionalizing Δp_t by dividing it with $p_{t,1} - \bar{p}_2$, where $\bar{p}_2$ is the pitchwise averaged downstream static pressure. As mentioned in in section 3.1.1, since $p_{t,1}$ and $\bar{p}_2$, typically, fluctuate in the same direction (e.g. an increase in the former causes an increase in the latter), such fluctuations should have less of an effect on the loss coefficient than in the case of using $\bar{L}$.

Comparison of estimated error to observed scatter: the estimated maximum error in $\bar{L}$ of 20 percent appears to be too conservative for most cases. The exceptions are the following:

- The sudden drop in $\bar{L}$ for all cases for Mach numbers higher than 1.3. The scatter, here, is larger than 20 percent; but as it was noted in the last section, all the runs that show this drop were taken on the same day, which suggests that some error was introduced in the testing conducted on that day.

- For the middle position with no injection, the scatter suggests error of the order of 20 percent (see Figure 32).

- For the rear position of the second cascade, the scatter is much larger than 20 percent (see Figure 35 to Figure 37, or Figure 43). Not only that, but the losses are much too high to be reasonable; for instance, the loss increases drastically between the middle position and the rear position (see Figure 53). Both observations, above, are true in the subsonic region. The supersonic region behaves acceptably well. Apparently, some special phenomenon of an unstable nature is taking place. By examining the raw data (plots of $p_{t,1}$ and $\Delta p_{t,prb} = p_{t,1} - p_{t,2,prb}$) of the runs in this region, it is obvious that the flow is far from the expected (see, for an example, Figure 63). The two wakes seem to merge, which would explain the high losses due to severe mixing. As to why the flow converges instead of staying parallel, and why this happens only for the second cascade in the subsonic region, no explanation presents itself. It is important to point out, here, that taking measurements two axial chord lengths behind the blade row (rear position) is a daring attempt as far as typical turbine cascade testing goes. Most researchers consider it unwarranted to go beyond one axial chord length, due to flow distortions.

4.0 Conclusions and Recommendations

In the last two sections of the previous chapter, the results of this research were presented and analyzed, and a maximum value for the expected error in $\bar{L}$ was estimated, with its nature and sources discussed in detail. In this chapter, conclusions are drawn based on that previous discussion, and recommendations are made for improvements and further research.

4.1 Conclusions

Note that all the proposed conclusions that include the second cascade do not apply for the case of the subsonic Mach number region with the rear downstream probe station. The unreliability of the data for the second cascade in this case prohibits drawing any conclusions.

Effect of trailing edge thickness: For the first cascade, the ratio of the trailing edge thickness to axial chord length is $\frac{h_{te,1}}{c}$ = 1.27 percent, and for the second cascade $\frac{h_{te,2}}{c}$ = 2.00 percent; therefore, $\frac{h_{te,2}}{h_{te,1}}$ = 1.57. For the second cascade, the loss is greater or almost equal to that of the first cascade, depending on the case involved. The following further conclusions are made:

- The difference in the total aerodynamic losses due to different trailing edge thicknesses is mainly due to the difference in the strength of the trailing edge shocks. This conclusion is drawn from the fact that the $\bar{L}$ values for the two cascades, practically, match in the subsonic region, where there are no shocks, for the cases of no coolant injection. For the cases of injection, the second cascade's losses are slightly higher. The difference in the effect of injection between the two cascades is, probably, due to the fact that the cut-back blades have the coolant injection slots closer to the trailing edge; therefore, the coolant is expected to have a stronger effect on the base flow.

- The losses differ mainly in the Mach number region of 1 to 1.2. The maximum increase in loss (in percentage of first cascade loss) due to thicker trailing edge is approximately 20 to 30 percent, with slightly higher values in the middle and rear positions. The increase in the difference in $\bar{L}$ in the downstream direction is explained as follows: as concluded earlier, the difference in losses is mainly due to the difference in trailing edge shock strengths. The forward station is upstream of, almost, the entire trailing edge shock system. This situation changes, of course, as the probe station is moved downstream, and, thus, the shock losses show up. Moreover, the effect of the reflected waves, from the tailboard or free shear layer, is stronger with the downstream stations, because those are closer to the reflection boundary.

- The trailing edge thickness has no noticeable effect on the blade surface Mach number distribution, except in the trailing 10 percent of the axial chord length, where the Mach number increases slightly with the thicker trailing edge.

- The two trailing edge thicknesses show only a slight difference in shock location in the shadowgraph pictures taken at the same Mach number.

Effect of coolant injection: the following two conclusions are made:

- For high air flow momentum (exit Mach numbers greater than 1.2), the effect of coolant injection (blowing rate of B=0.47 and B=1.33) on loss is negligible.

- For low air flow momentum (exit Mach numbers less than 1.1), the high coolant injection rate (B=1.33) has the effect of reducing the loss. The momentum of the coolant in this case, apparently, adds to the momentum of the air flow.

- Coolant Injection has no noticeable effect on the shock structure as appears from shadowgraph pictures.

Loss development downstream of the blade row: in most cases, the loss nearly stops to increase after one axial chord length behind the blade row.

Error Evaluation: in the section "Uncertainty Analysis" in the previous chapter, the maximum random error in $\bar{L}$ was estimated at 20 percent. One dominant source of error was involved in this estimation, and this was the unsteadiness in the upstream total pressure during a run. As it was explained earlier, the error caused by this unsteadiness is largely not because of unsteadiness in the loss generating mechanisms, in particular, the trailing edge shock system, but due to including $p_{t,1}$ in the definition of $\bar{L}$ for the purpose of non-dimensionalizing the results. For all cases, except two, the scatter in the results indicates that the estimated 20 percent error is too large. The two exceptions are: (1) the case of the middle station with no injection, and (2) the case for the second cascade with the rear station. For the former, the scatter indicates around 20 percent error. For the latter, the error is much more than 20 percent, and, as discussed earlier, the reason for this is that the flow converges and the wakes merge causing severe mixing losses. The cause of this phenomenon is unknown.

When investigating the error in $\bar{L}$, one important thing should be kept in mind, and this is that $\bar{L}$ is a measure of "a small drop in a big quantity". The upstream total pressure, $p_{t,1}$, goes as high as 206.85 kPa,abs (30 psia). The drop in total pressure, Δp_t , goes only as high as 6.89 kPa (1 psi) between the wakes, which is the majority of the vertical distance behind the blades, and 55.16 kPa (8 psi) at the wakes. Since the instrumentation used is that which has to handle large pressures, an error in reading Δp_t which is small relative to the kind of pressures the instruments read, may result in a significant error in $\bar{L}$.

4.2 Recommendations

The author would like to propose a few recommendations for future, similar research conducted in the VPI & SU cascade wind-tunnel facility:

- Since it was found that because of the way aerodynamic loss ($\bar{L}$) is defined, steadiness of the upstream total pressure, $p_{t,1}$, is essential for the repeatability in results, it is advisable to purchase a new wind-tunnel control valve capable of handling feedback controls, i.e. capable of adjusting its opening in response to continuous readings of the total pressure upstream of the blade row. This will much improve the ability to achieve steady runs.

- For the purpose of reducing the effect of upstream total pressure unsteadiness on the repeatability of the loss coefficient, it is warranted to investigate the benefit of using the alternative loss coefficient discussed in sections 3.1.1 and 3.7, which non-dimensionalizes the total pressure drop, Δp_t, by dividing it with $p_{t,1} - \bar{p}_2$.

- Since new compressors will be installed shortly, and, thus, the oil leakage problem will be eliminated, more advanced optical flow visualization methods, like interferometry, are worth implementing, for more detailed insight into the flow. For instance, strength of waves, in particular those reflected from the tailboard or the free shear layer, can then be well investigated.

- Video taping of the flow, instead of taking still pictures only, may be beneficial in investigating the effects of any unsteadiness in the blow-down.

- Further testing of the cascade tested in this research is recommended, with further cut-back of the trailing edge.

References

1. Gostelow, J. P., "The Present Role of High Speed Cascade Testing", ASME paper no. 81-GT-95, 1981.

2. Xu, Liping,"The Base Pressure and Trailing Edge Loss of Transonic Turbine Blades", Doctor of Philosophy Dissertation, Corpus Christi College, University of Cambridge, 1985.

3. Sieverding, C. H., "The Influence of Trailing Edge Ejection on the Base Pressure in Transonic Turbine Cascades", Journal of Engineering for Power, Vol. 105, pp. 215-222, April 1983.

4. Zaccaria, M. A.,"Development of a Transonic Turbine Cascade Facility", M. S. Thesis, Virginia Polytechnic Institute and State University, 1988.

5. MacMartin, I. P., and Norbury, J. F., "The Aerodynamics of a Turbine Cascade with Supersonic Discharge and Trailing Edge Blowing", ASME paper no. 74-GT-120, 1974.

6. Sieverding, C. H., Stanislas, M., and Snoeck, J., "The Base Pressure Problem in Transonic Turbine Cascades", Journal of Engineering for Power, Vol. 102, pp. 711-718, July 1980.

7. Amana, O. M., Demuren, H. O., Louis, J. F., Sieverding, C., and Chauvin, J., "Aerodynamics and Heat Transfer at the Trailing Edge of Transonic Blades", ASME paper no. 76-GT-95, 1976.

8. Sieverding, C., Decuyper, M., Colpin, J., and Amana, O., "Model Tests for the Detailed Investigation of the Trailing Edge Flow in Convergent Transonic Turbine Cascades", ASME paper no. 76-GT-30, 1976.

9. Xu, L., and Denton, J. D., "The Base Pressure and Loss of a Family of Four Turbine Blades", ASME paper no. 87-GT-202, 1987.

10. Prust, H. W., Jr. and Helon, R. M., "Flow Conditions Around the Exit and Downstream of Certain Stator Blading with Various Trailing-Edge Thicknesses and Geometries", NASA Technical Memorandum no. X-2659, 1972.

11. Singer, R. T.,"An Experimental Examination of the Effect of Trailing Edge Injection on the Aerodynamic Performance of Gas Turbine Blades", M. S. Thesis, Virginia Polytechnic Institute and State University, 1988.

12. Lokai, V. I. and Kumirov, B. A., "Losses in Turbine Cascades with Cooling Air Discharge and Various Trailing Edge Geometry", Izvestiya VUZ, Aviatsionnaya Tekhnika (Soviet Aeronautics), Vol. 16, No. 3, pp. 79-83, 1973.

13. Prust, H. W., Jr. and Bartlett, W. M., "Cold-Air Study of the Effect on Turbine Stator Blade Aerodynamic Performance of Coolant Ejection from Various Trailing-Edge Slot Geometries", NASA Technical Memorandum no. X-3000, 1974.

14. Oates, G. C., Chapter 12 - Cascade Flows, *The Aerothermodynamics of Gas Turbine Aircraft Engines*, Oates, G. C., Editor, Air Force Aero Propulsion Laboratory Report Number AFAPL TR-78-52, 1978.

15. Saad, M. A., *Compressible Fluid Flow*, Pentice-Hall, Inc., 1985, pp. 501-515.

16. Schreier, S., Chapter 2 - Elementary One Dimensional Flow, *Compressible Flow*, John Wiley & Sons, Inc., 1982.

17. Abernethy, R. B., Benedict, R. P., and Dowdell, R. B., "ASME Measurement Uncertainty", ASME paper no. 83-WA/FM-3, 1983.

Appendix A. Figures

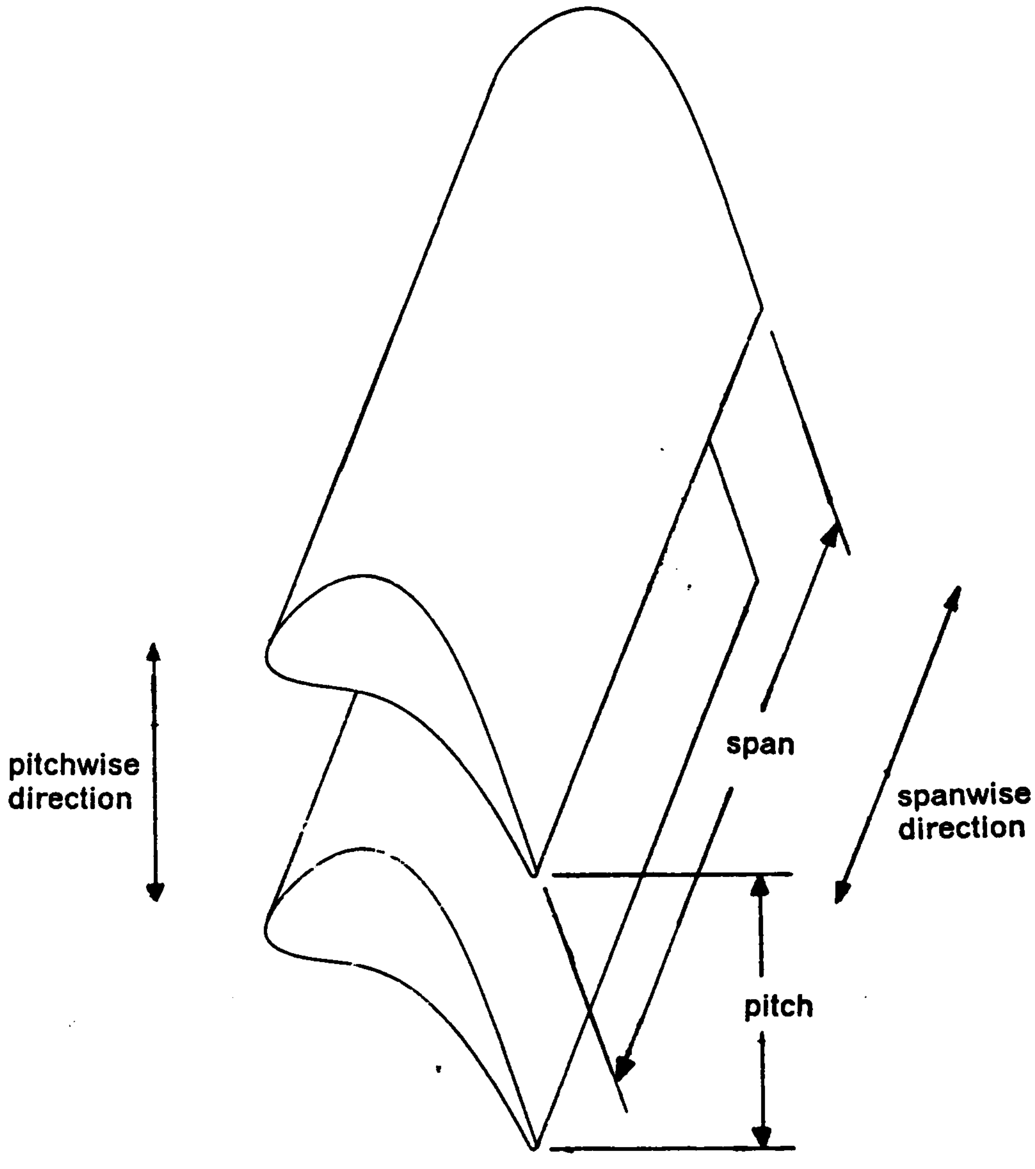

Figure 1. Definition of Blade Pitch and Span

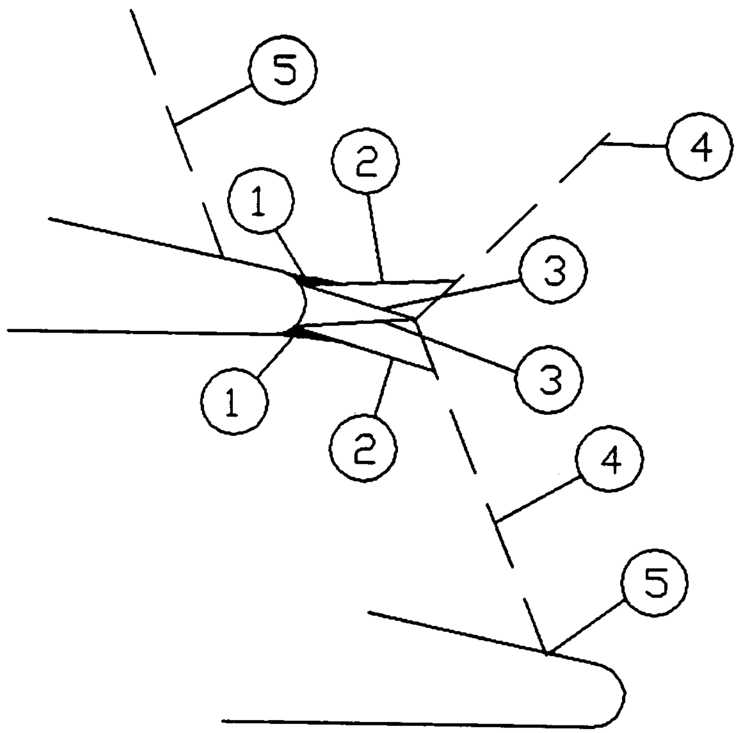

KEY:

1 Prantl-Meyer Expansion
2 Separation Shocks
3 Free Shear Layer
4 Reattachment Shocks
5 Shock-Boundary Layer Interaction

Figure 2. Model of Supersonic Trailing Edge Flow

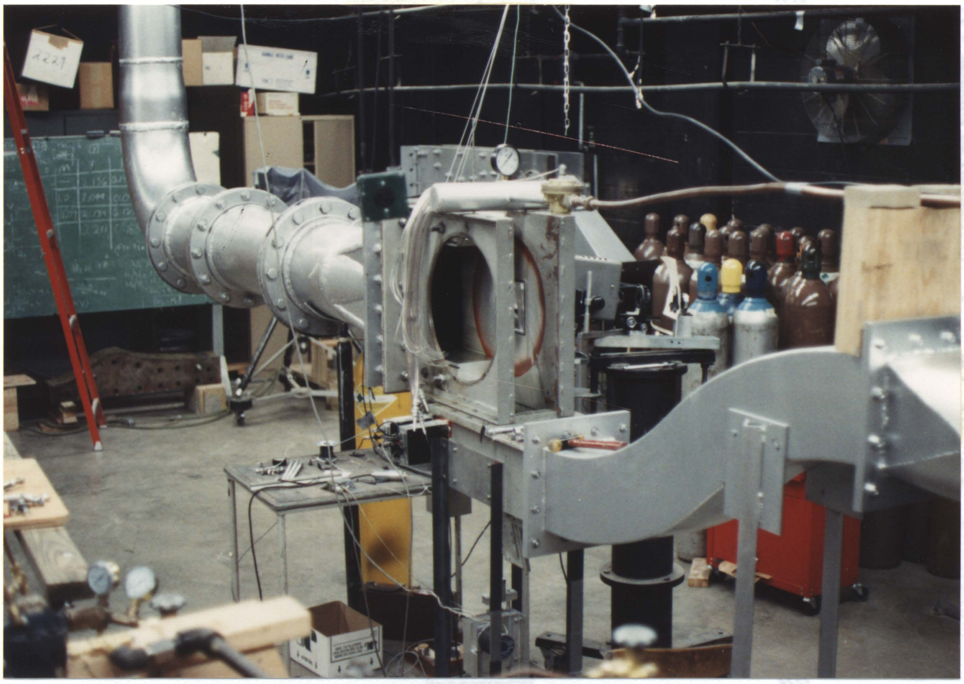

Figure 3. Photograph of the Wind-Tunnel

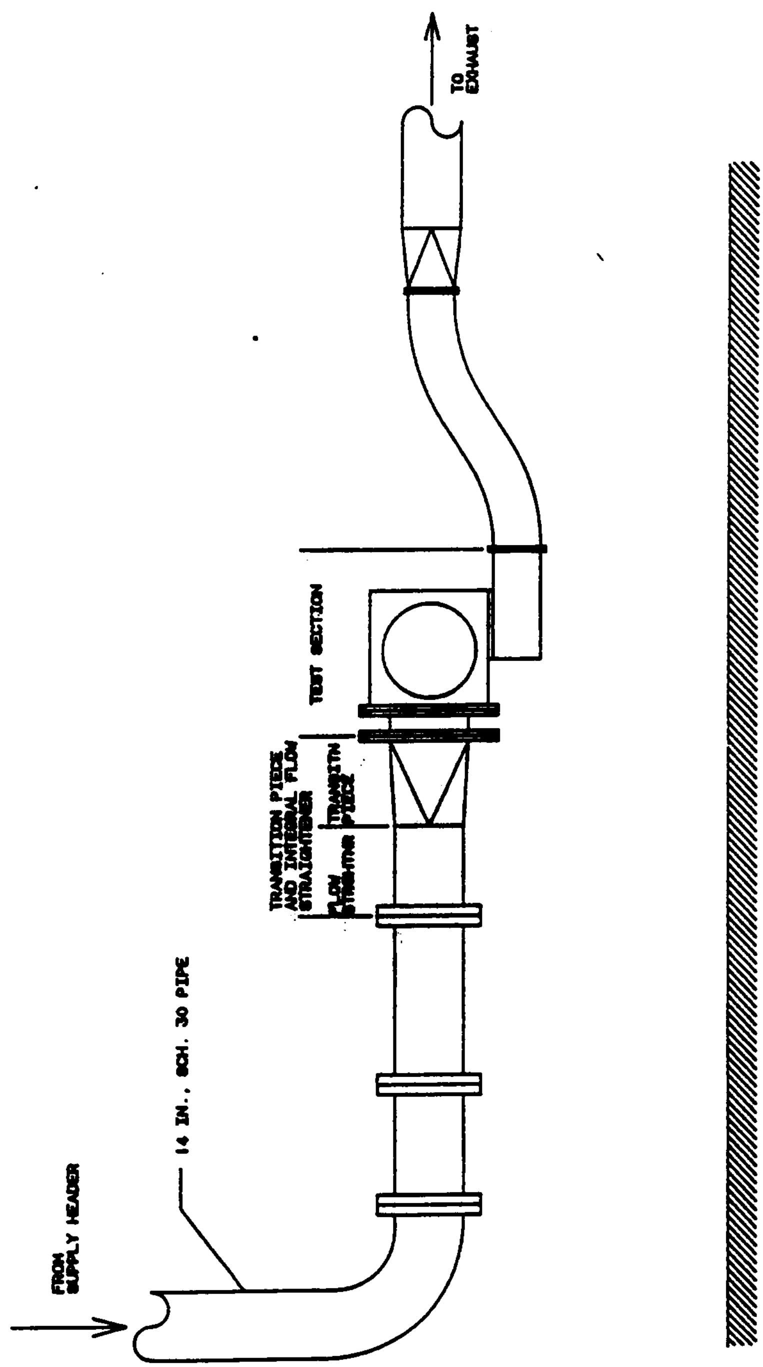

Figure 4. Schematic of the Wind-Tunnel: (courtesy of Singer, [11])

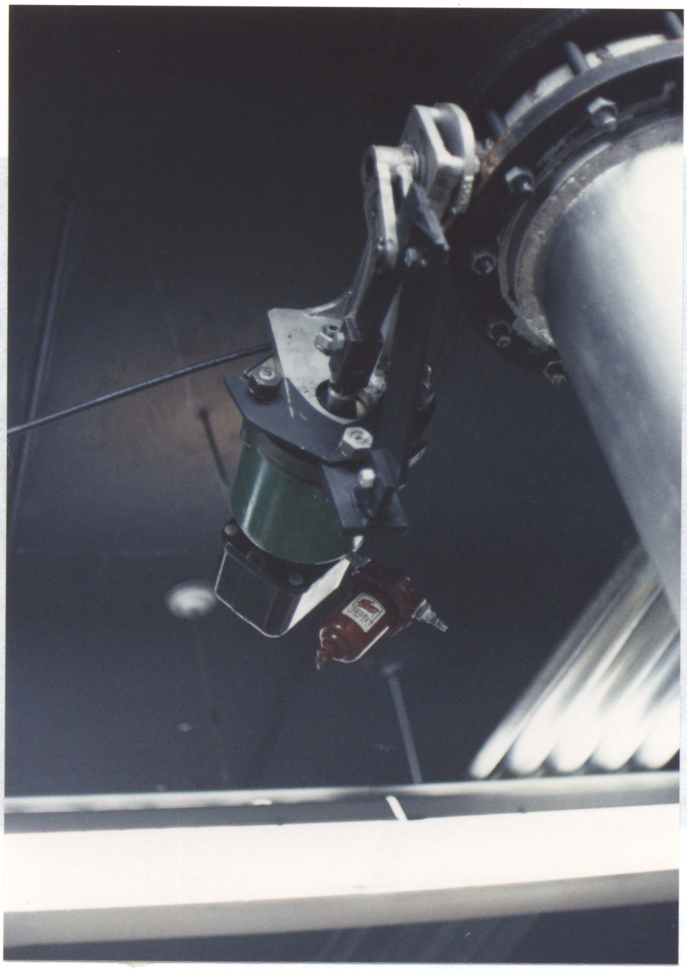

Figure 5. Photograph of the Wind-Tunnel Control Valve

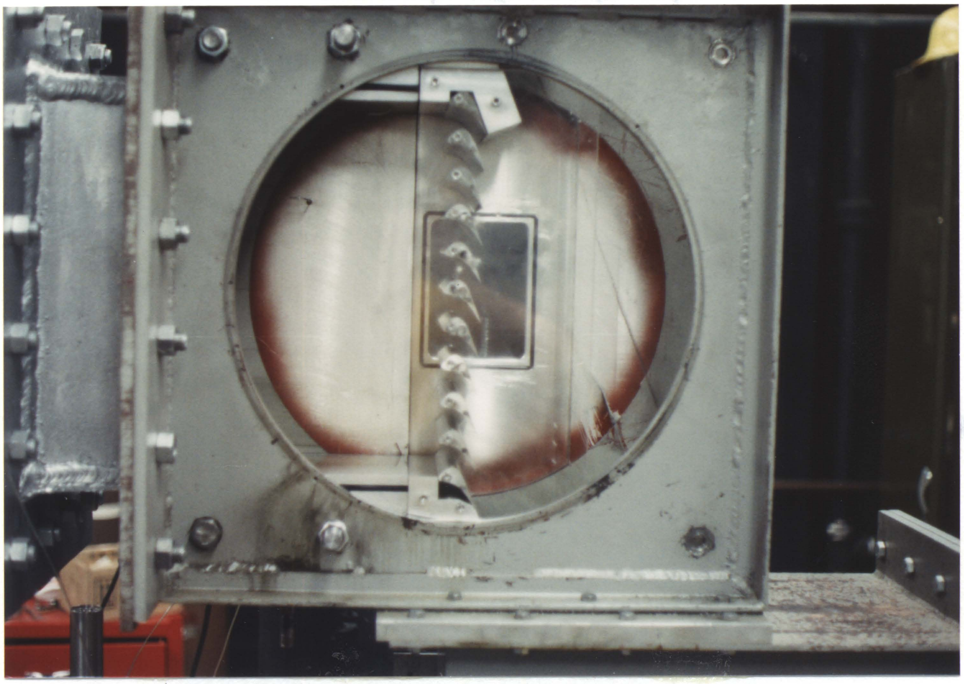

Figure 6. Photograph of the Test Section with the Doors Removed

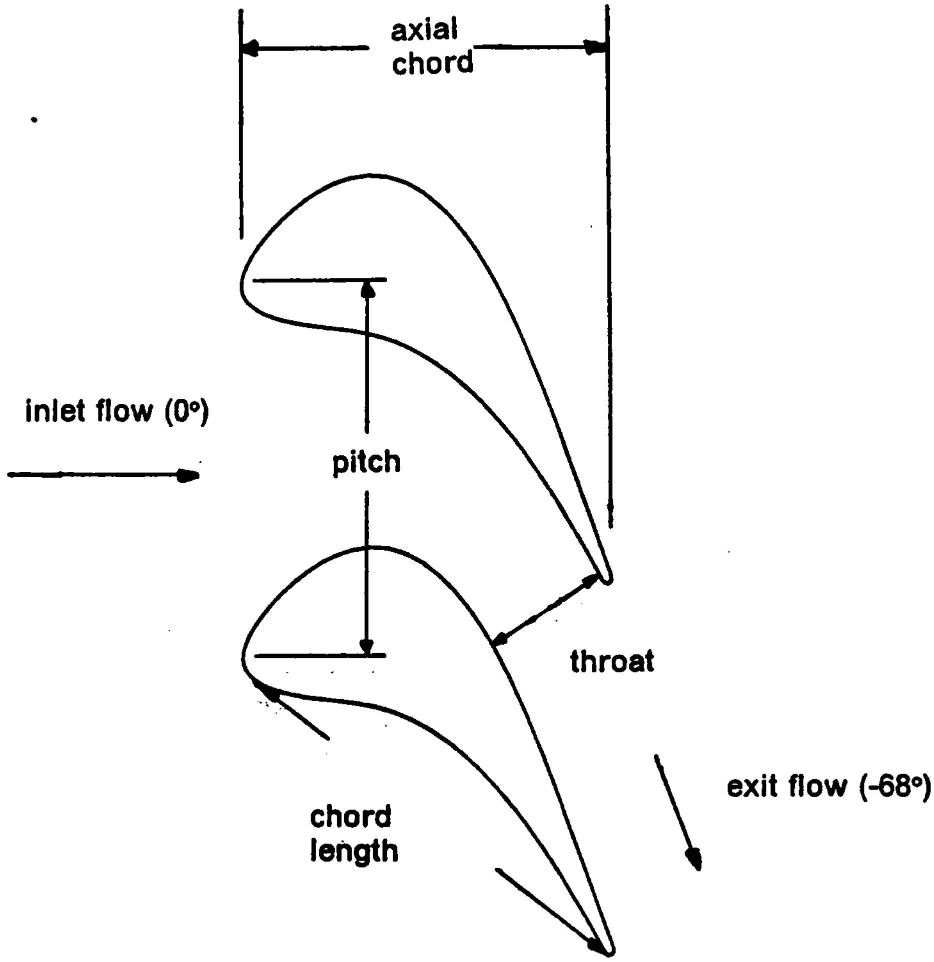

axial chord = 38.1 mm
trailing edge thickness = 0.483 mm, for uncut blades
0.762 mm, for cut-back blades
pitch = 37.262 mm
throat = 18.05 mm
inlet flow angle = 0 degrees
design exit flow angle = -68 degrees

Figure 7. Description of Some Blade and Flow Parameters

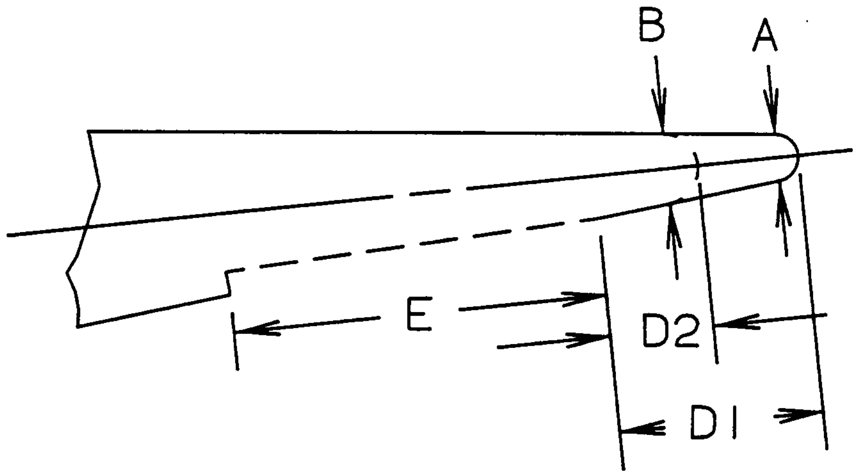

A = 0.483 mm (0.019 in)

B = 0.762 mm (0.030 in)

D1 = 2.032 mm (0.080 in)

D2 = 1.016 mm (0.040 in)

E = 4.064 mm (0.160 in)

Figure 8. Sketch Showing Trailing Edge Geometry of a Cooled Blade: the dashed straight line is part of the coolant ejection slot; the dashed circle is the cut-back trailing edge

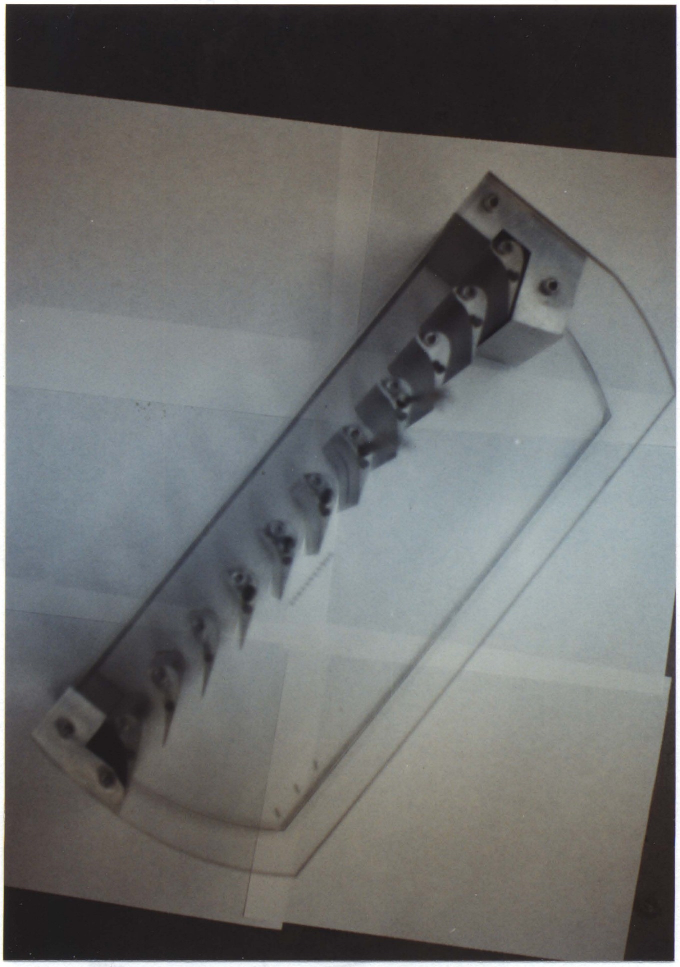

Figure 9. Photograph of the Cascade

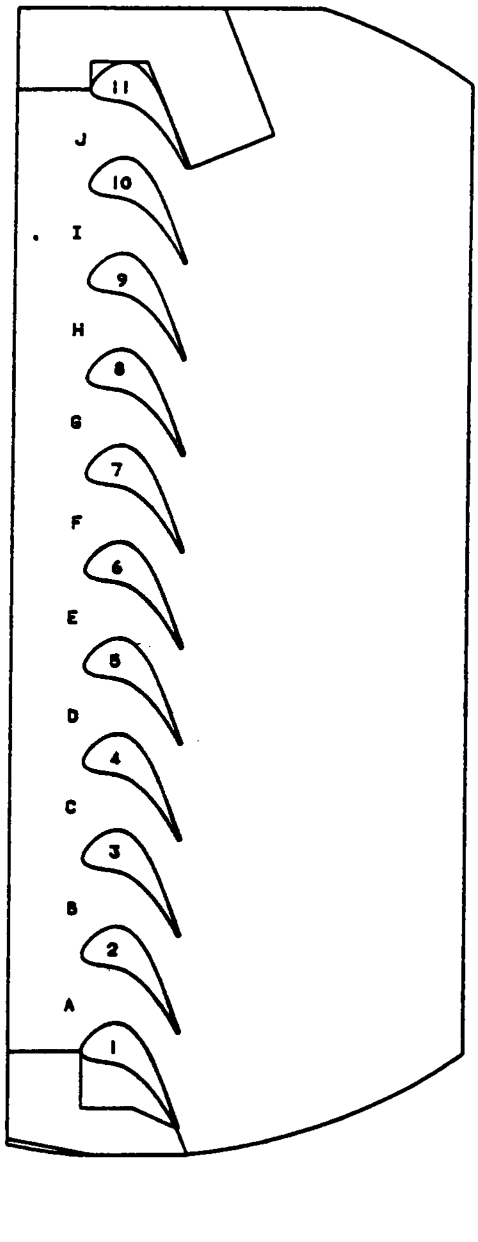

Figure 10. Schematic of the Cascade - Not Instrumented: (courtesy of Singer, [11])

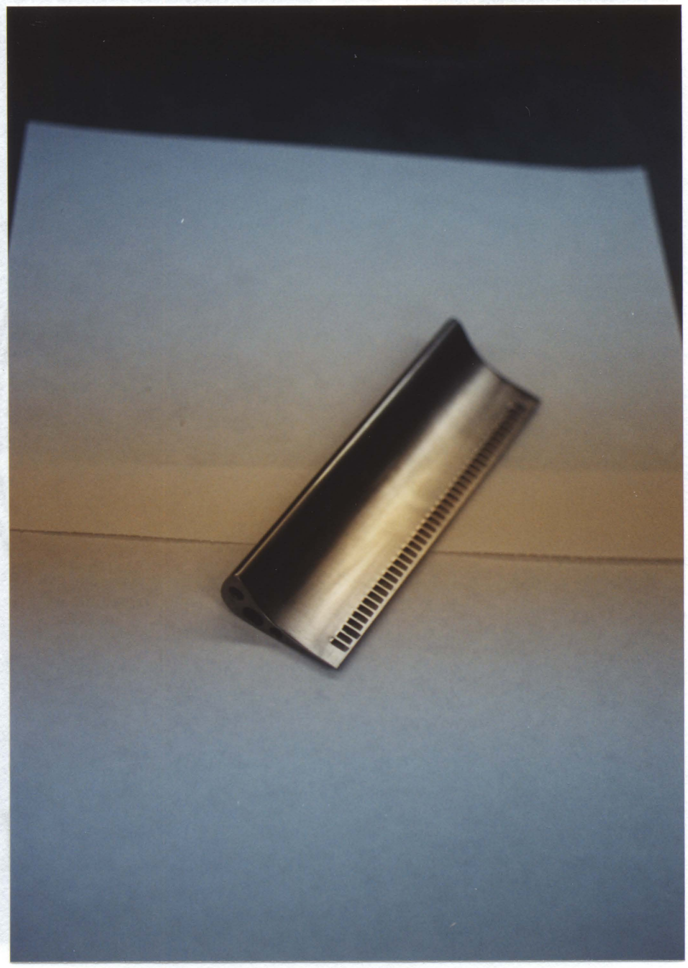

Figure 11. Photograph of a Cooled Blade: note the side and trailing edge slots

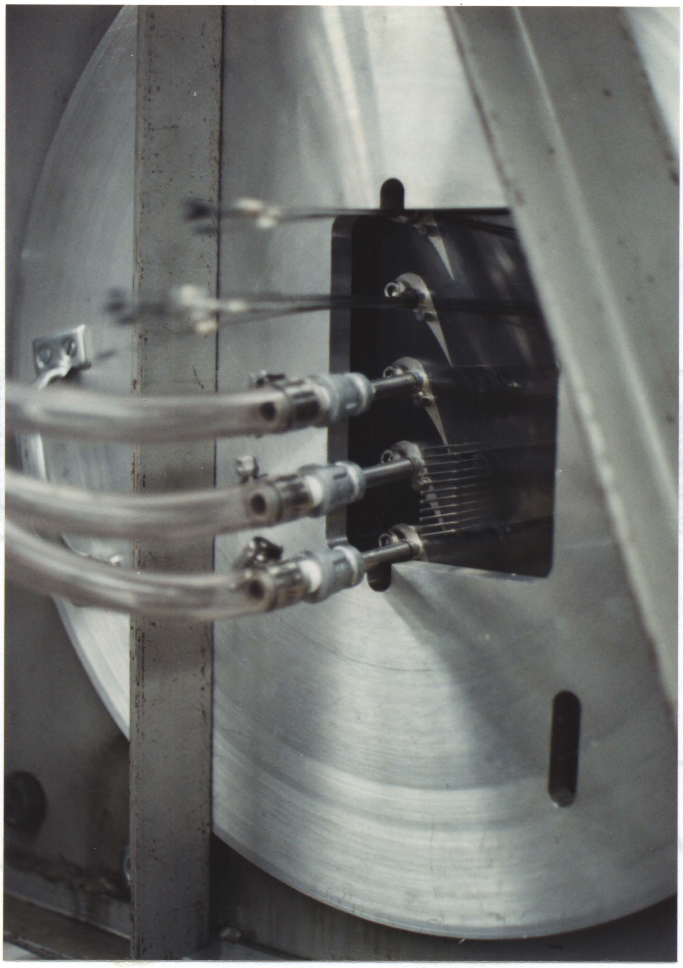

Figure 12. Photograph of the Cooled Blades: note the CO_2 fittings

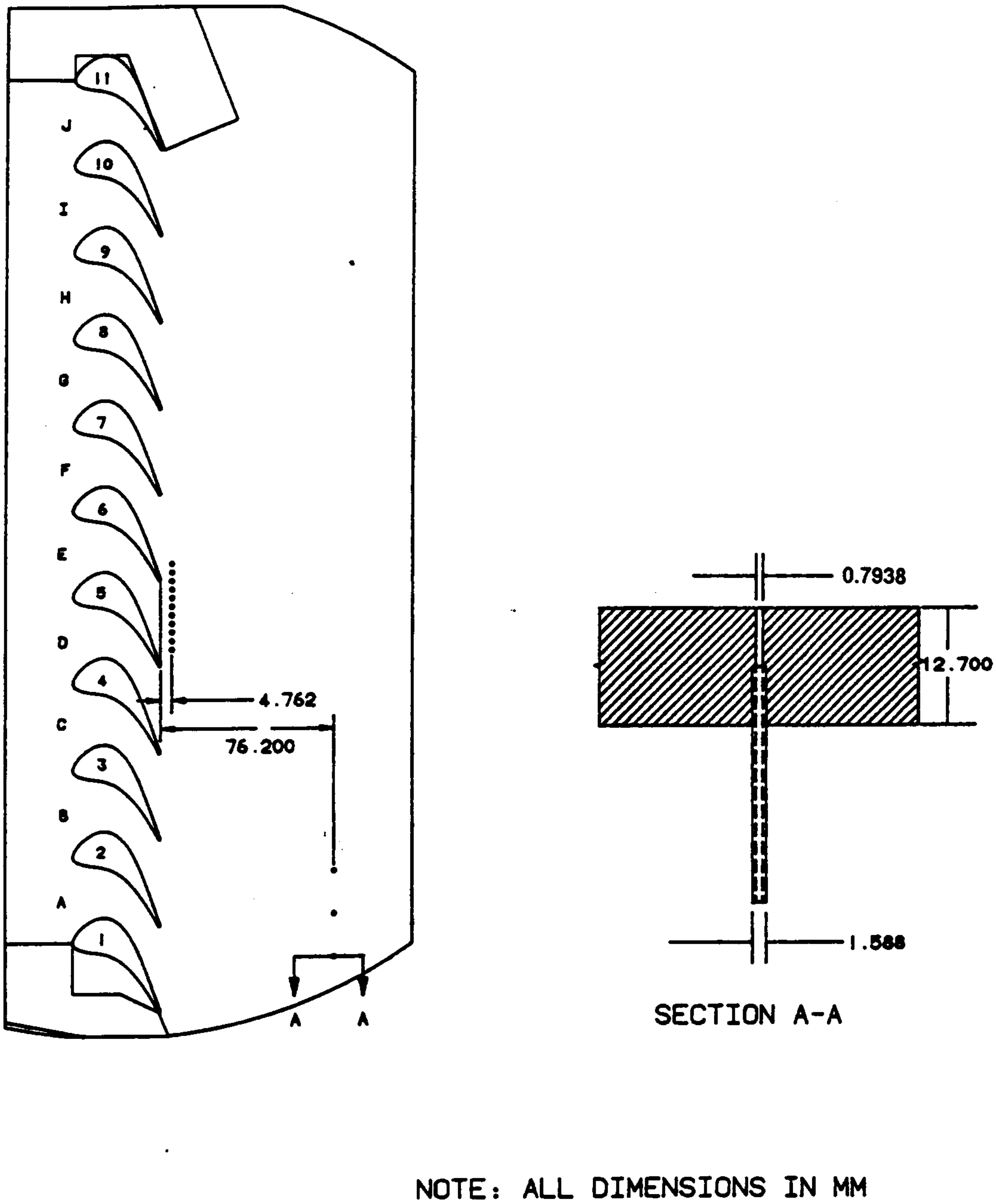

Figure 13. Schematic of the Cascade - Instrumented: note the static pressure taps in the plexiglass (courtesy of Singer, [11])

Figure 14. Photograph of the Opening in the Floor of the Test Section: the probe and the probe support fixture are inserted through this access opening

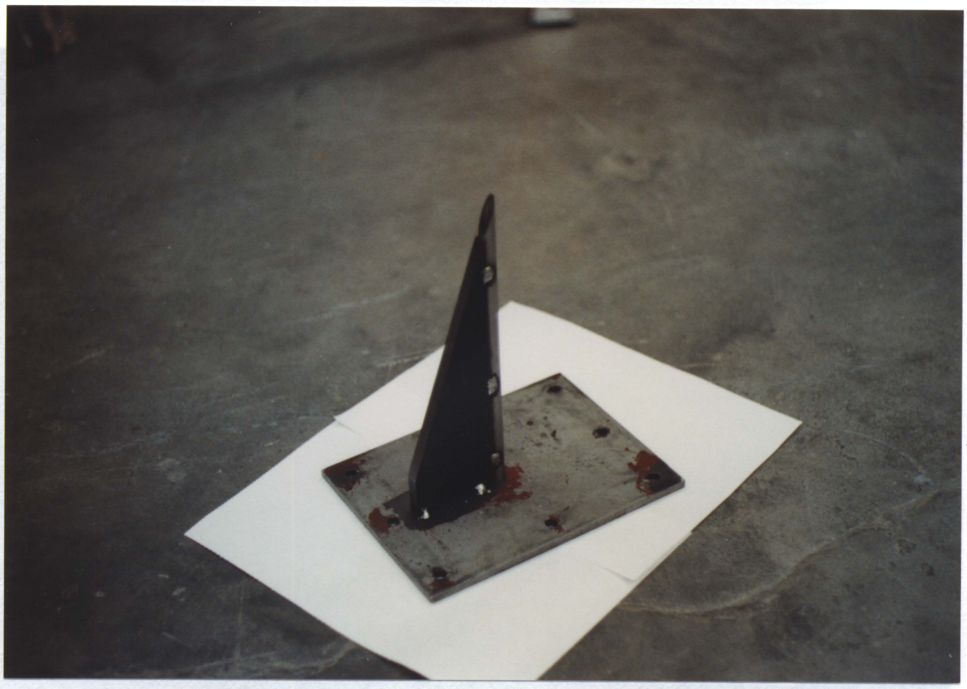

Figure 15. Photograph of the Probe Support Fixture: this is one of three similar fixtures used to position the probe at one of three locations downstream of the blade row

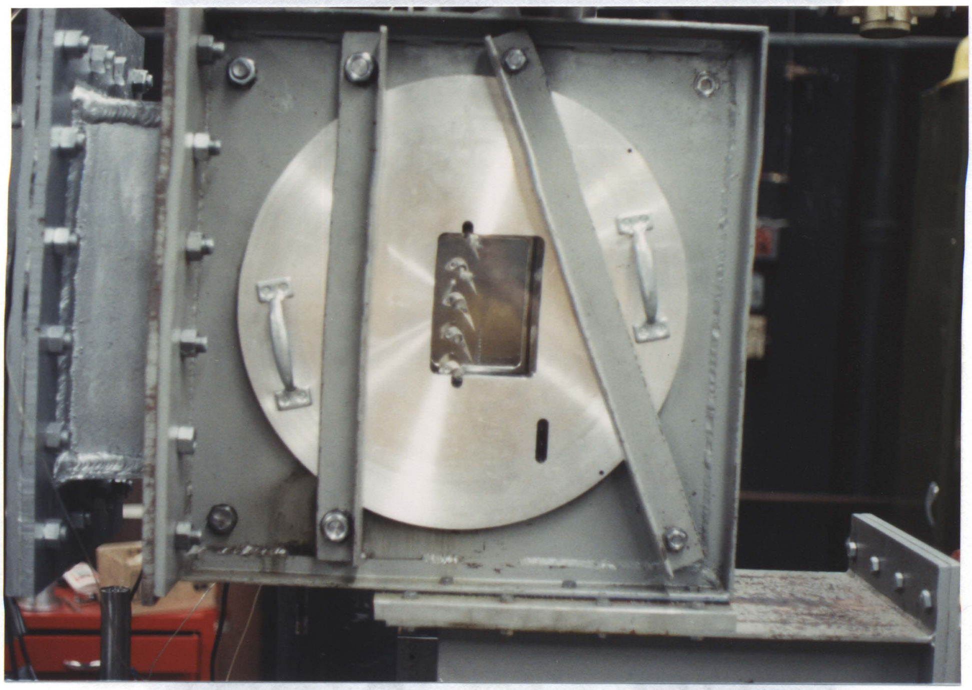

Figure 16. Photograph of the Test Section with the Doors Mounted

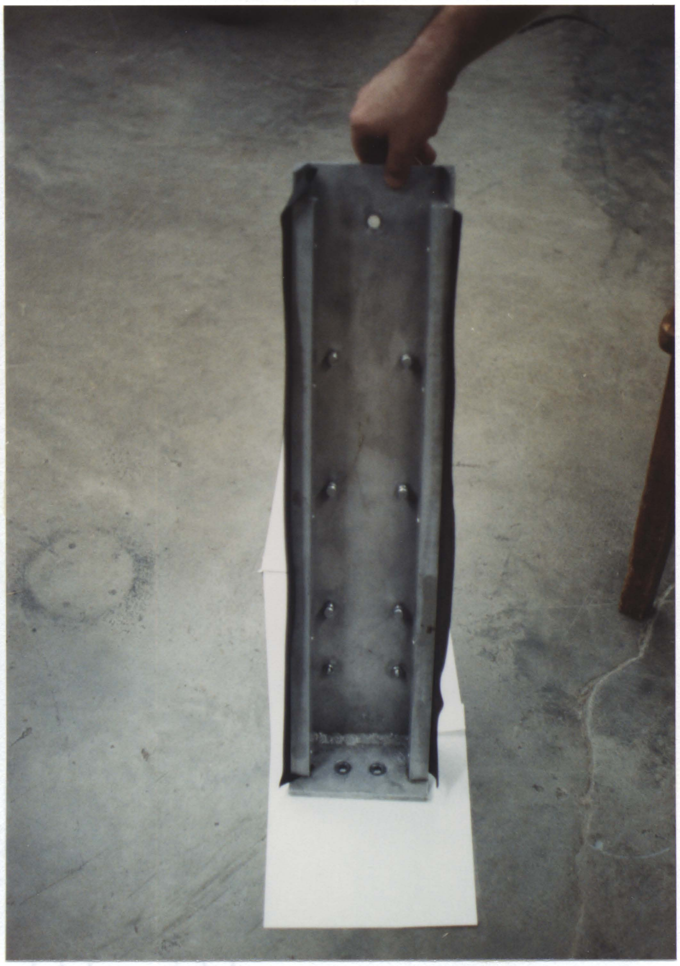

Figure 17. Photograph of the Back Wall

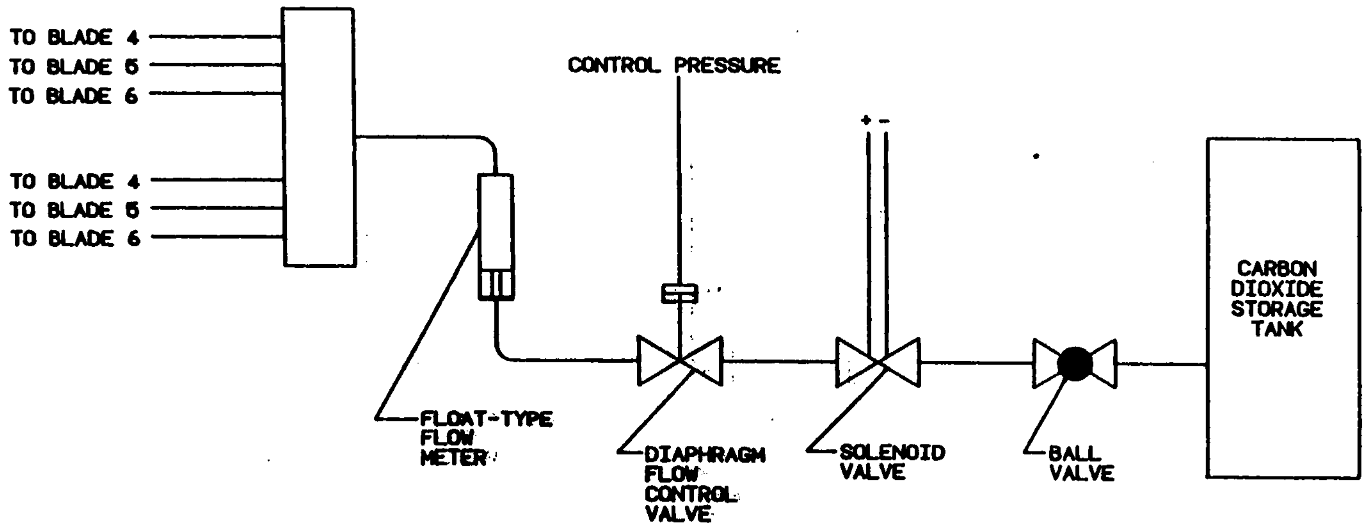

Figure 18. Schematic of the carbon dioxide supply system: (courtesy of Singer, [11])

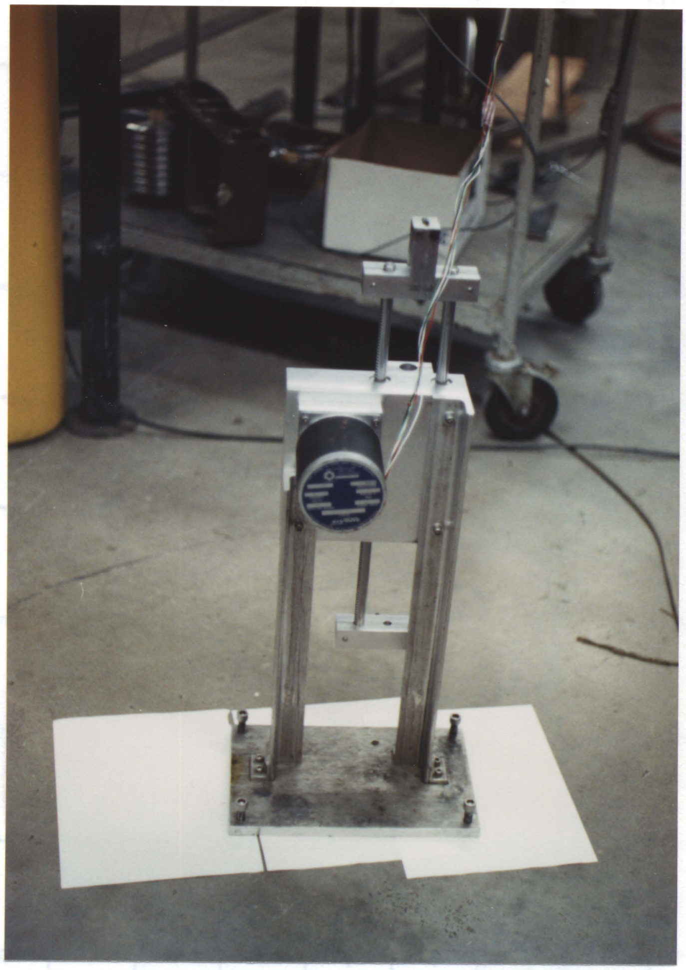

Figure 19. **Photograph of the Probe Traversing Mechanism:** this stepper motor, reduction gear, and rack and pinion assembly is the traversing mechanism for the downstream total pressure probe

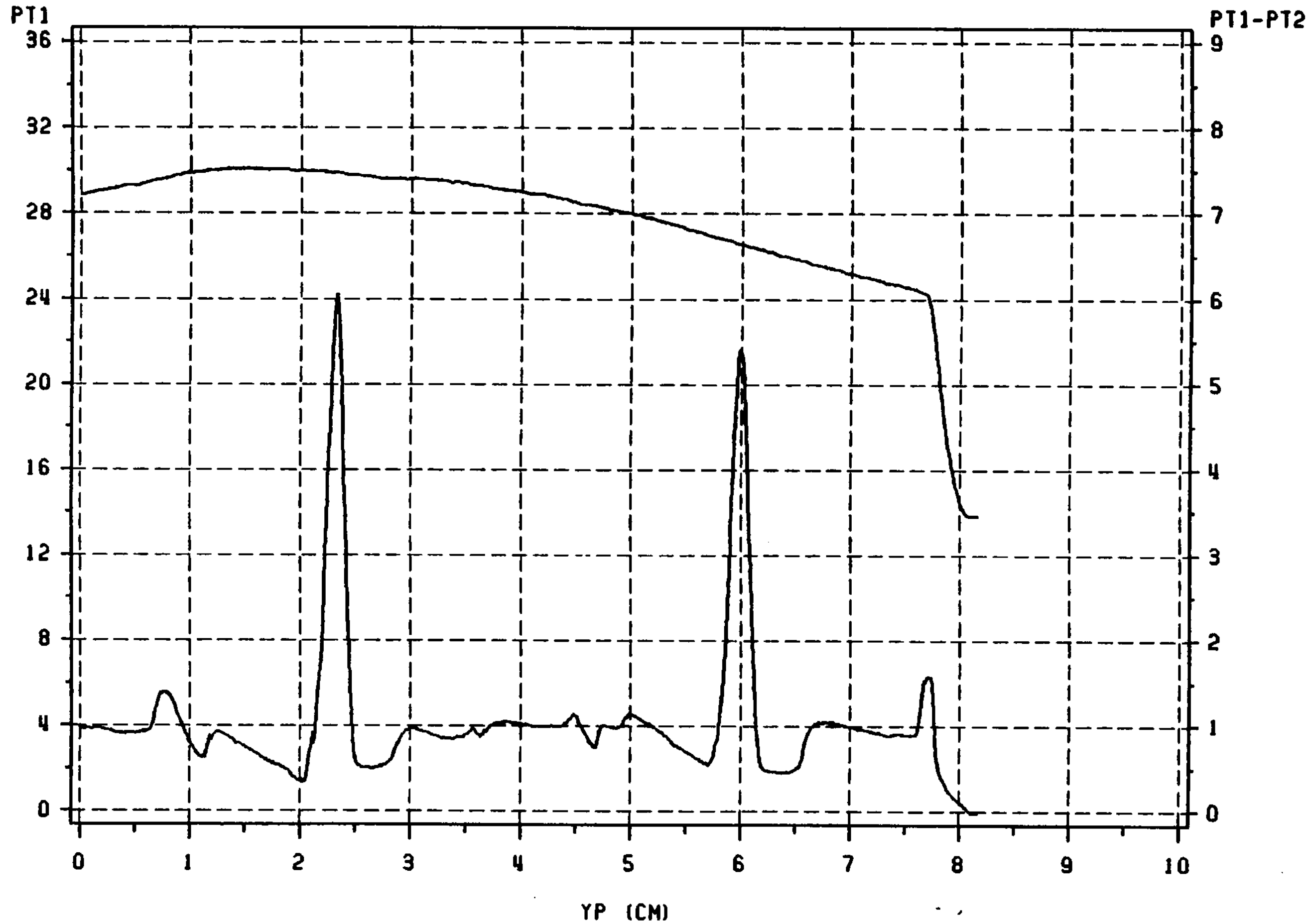

Figure 20. Example of A/D Converter Data: a first cascade run, forward station ($x/c = 1.125$), no coolant injection, $M_{2,isen} = 1.25$. YP is the probe's vertical position. $p_{t,1}$ is in psia.

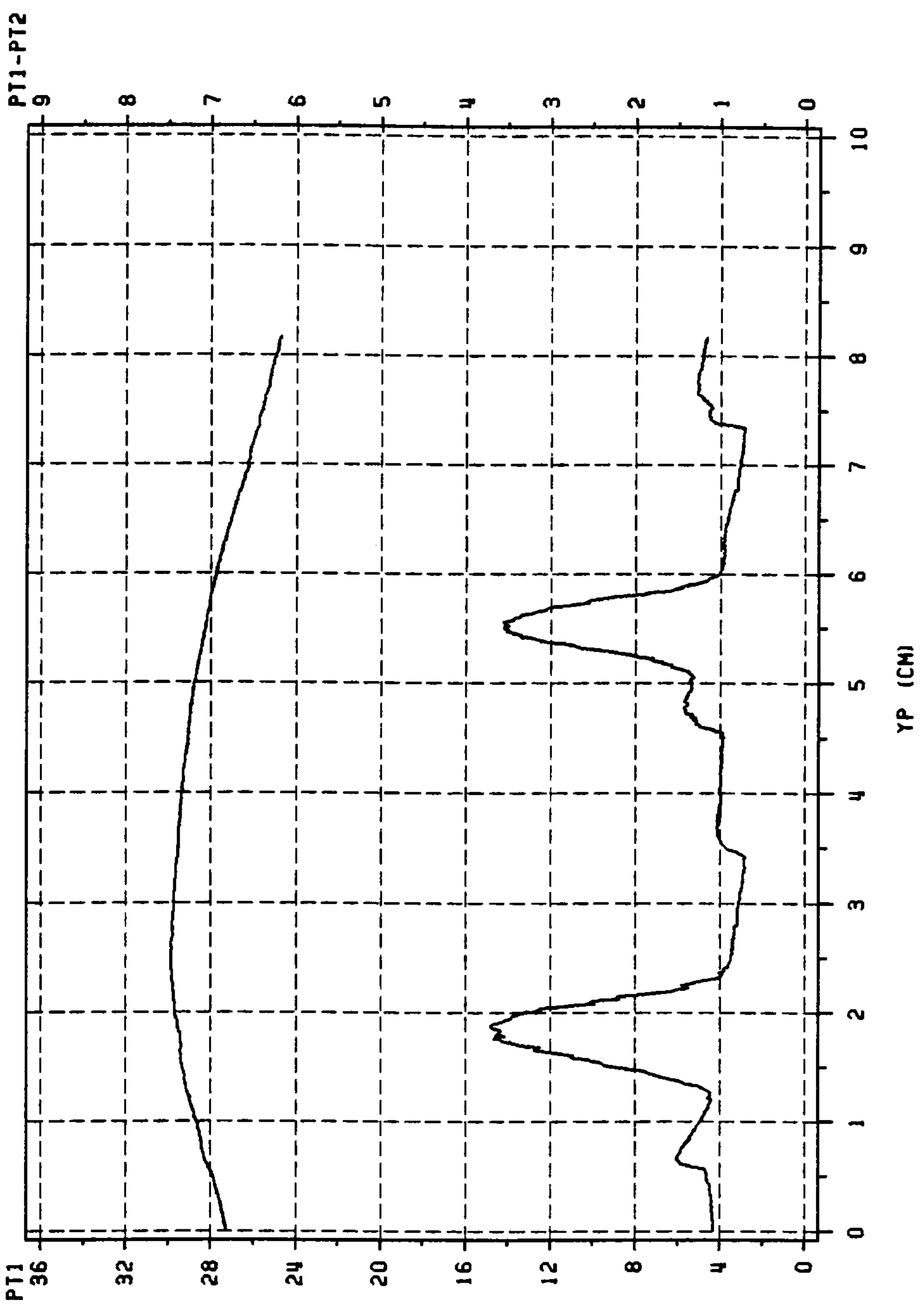

Figure 21. **Example of A/D Converter Data:** a first cascade run, middle station ($x/c = 1.667$), no coolant injection, $M_{2,isen} = 1.25$. YP is the probe's vertical position. $p_{t,1}$ is in psia.

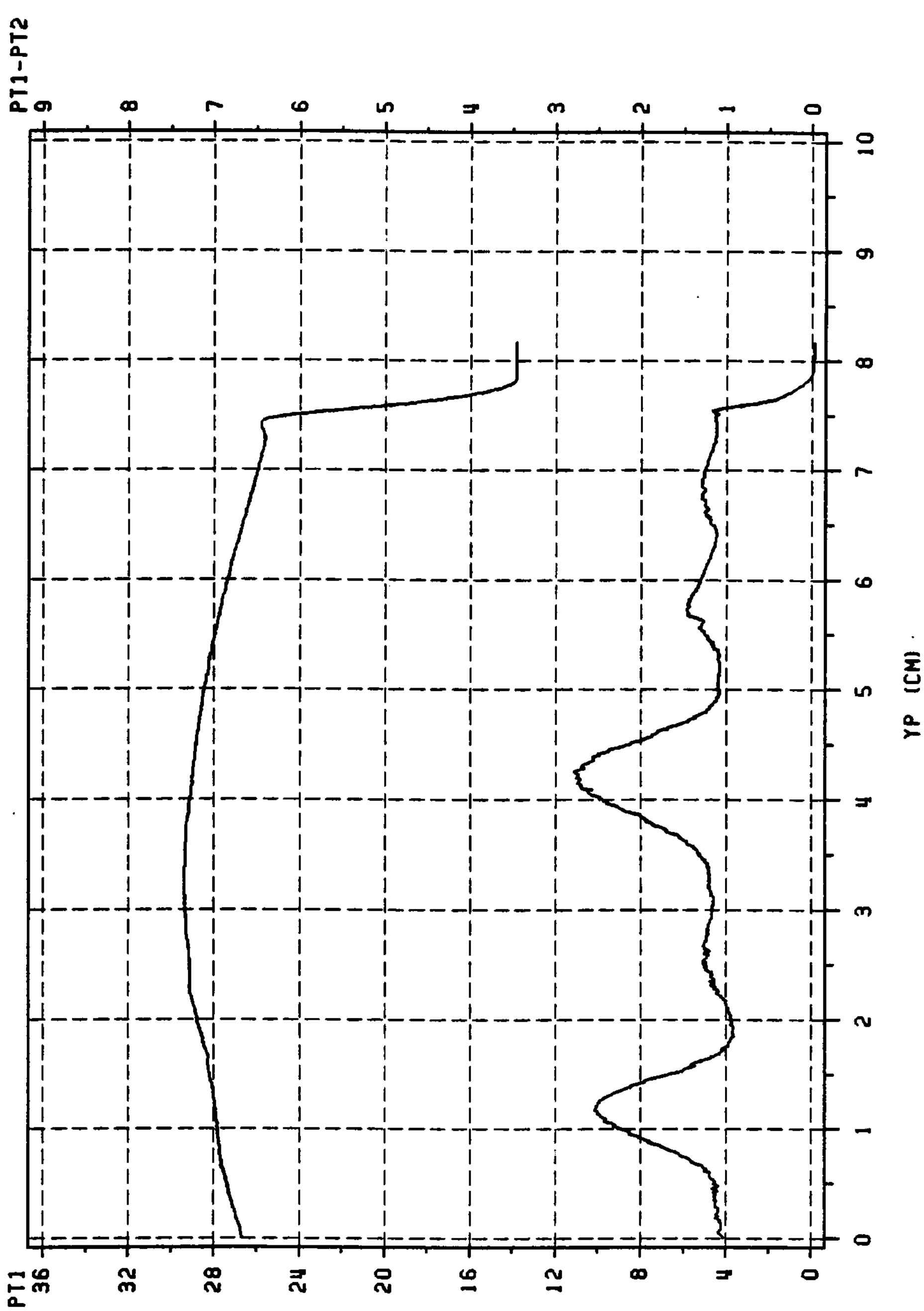

Figure 22. Example of A/D Converter Data: a first cascade run, rear station (x/c = 3.000), no coolant injection, $M_{2,isen}$ = 1.25. YP is the probe's vertical position. $p_{t,1}$ is in psia.

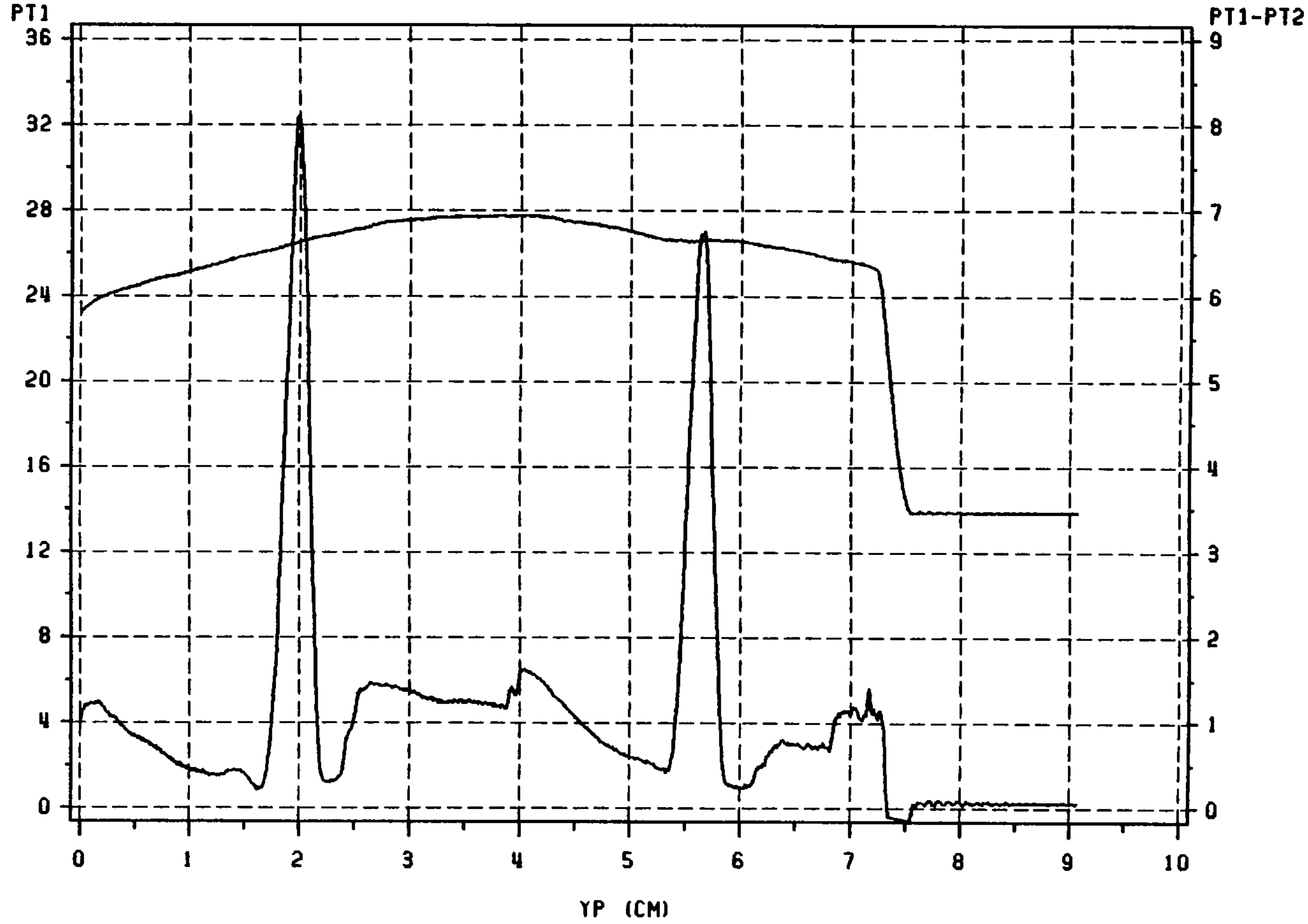

Figure 23. Example of A/D Converter Data: a second cascade run, forward station (x/c = 1.125), no coolant injection, $M_{2,isen}$ = 1.26. YP is the probe's vertical position. $p_{t,1}$ is in psia.

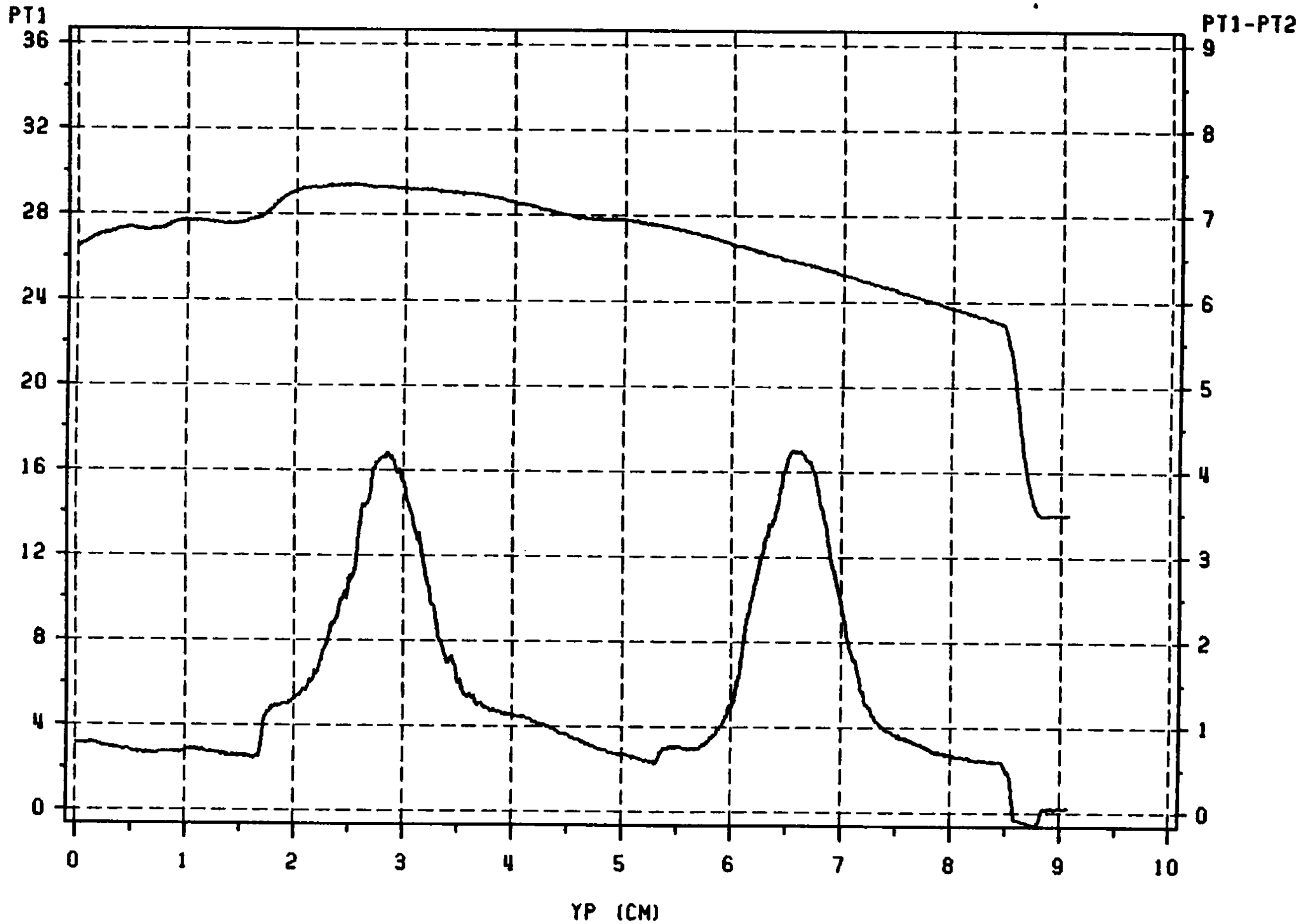

Figure 24. Example of A/D Converter Data: a second cascade run, middle station ($x/c = 1.667$), no coolant injection, $M_{2,isen} = 1.26$. YP is the probe's vertical position. $p_{t,1}$ is in psia.

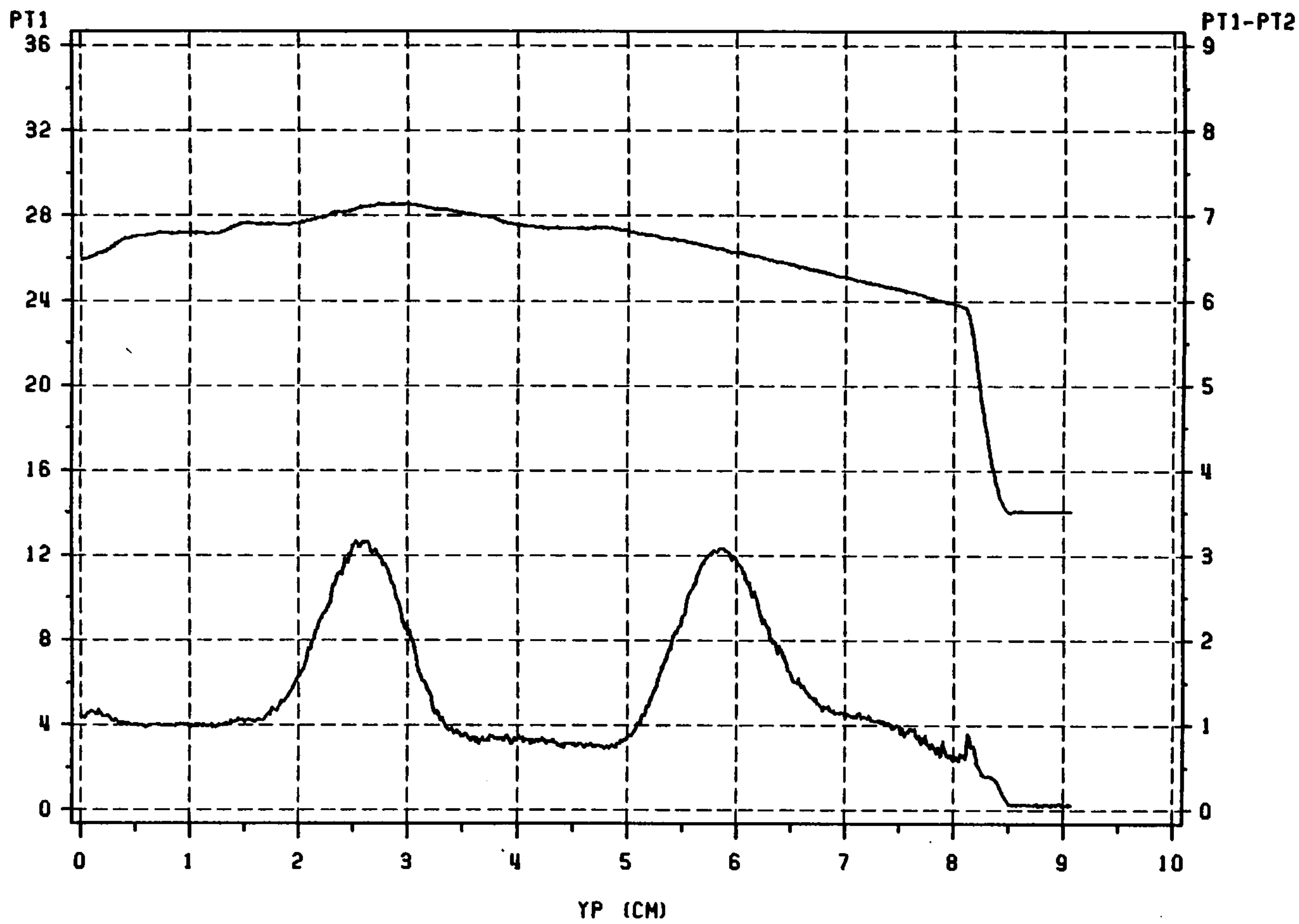

Figure 25. **Example of A/D Converter Data:** a second cascade run, rear station (x/c = 3.000), no coolant injection, $M_{2,isen}$ = 1.26. YP is the probe's vertical position. $p_{t,1}$ is in psia.

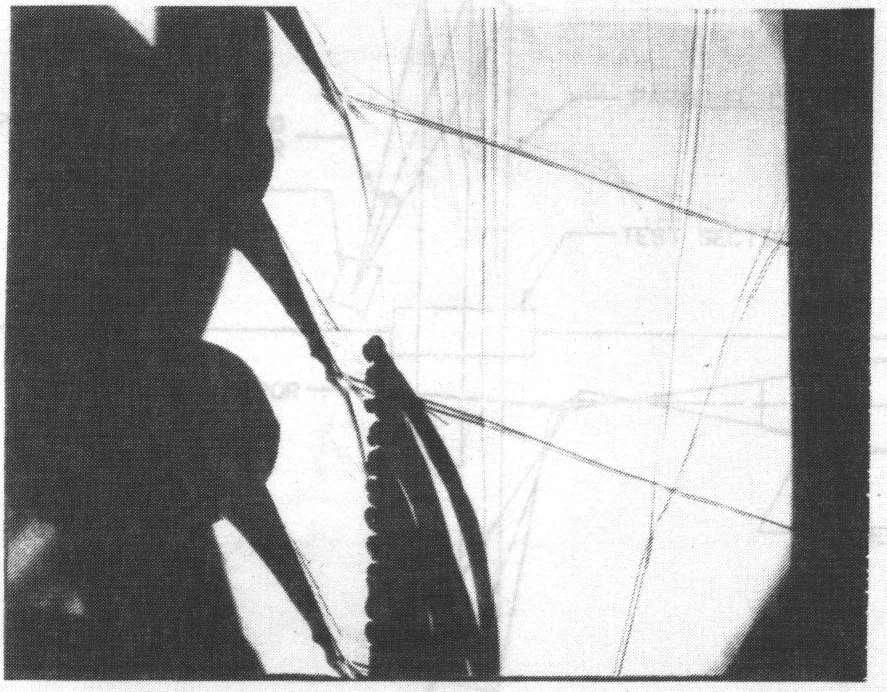

Figure 26. Example of a Shadowgraph Picture

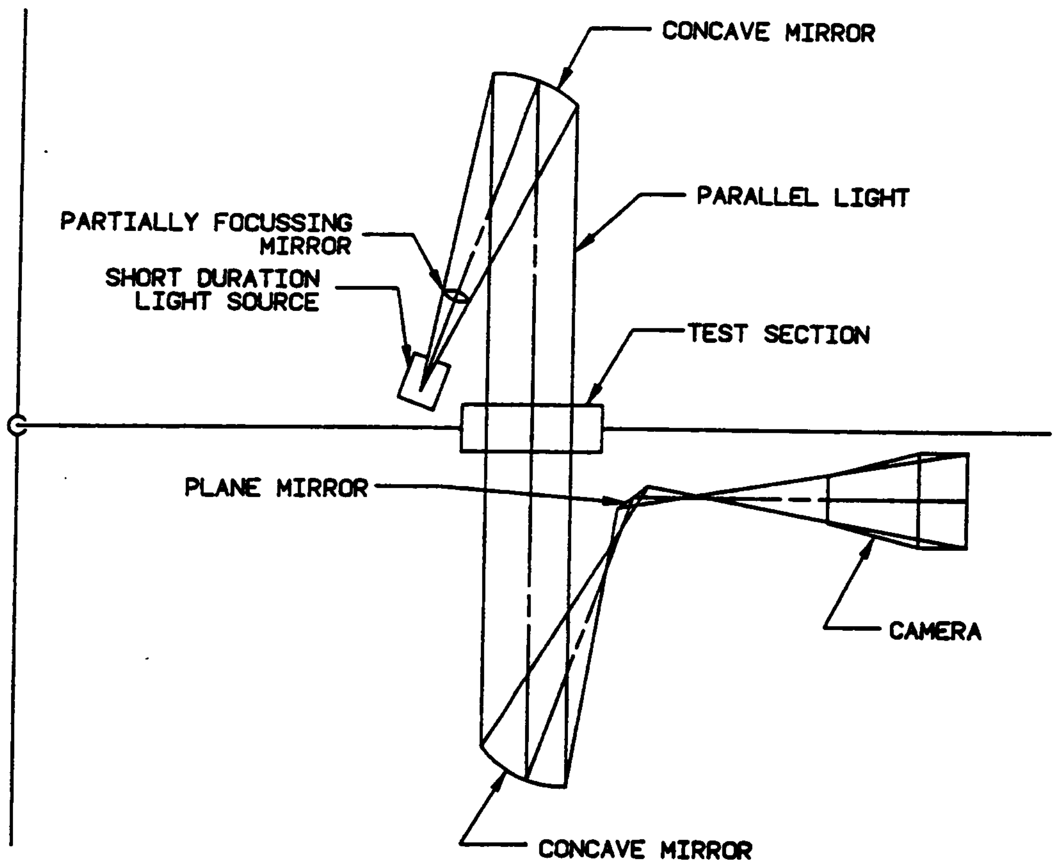

Figure 27. Schematic of the Shadowgraph System: an optical technique for flow visualization (courtesy of Singer, [11])

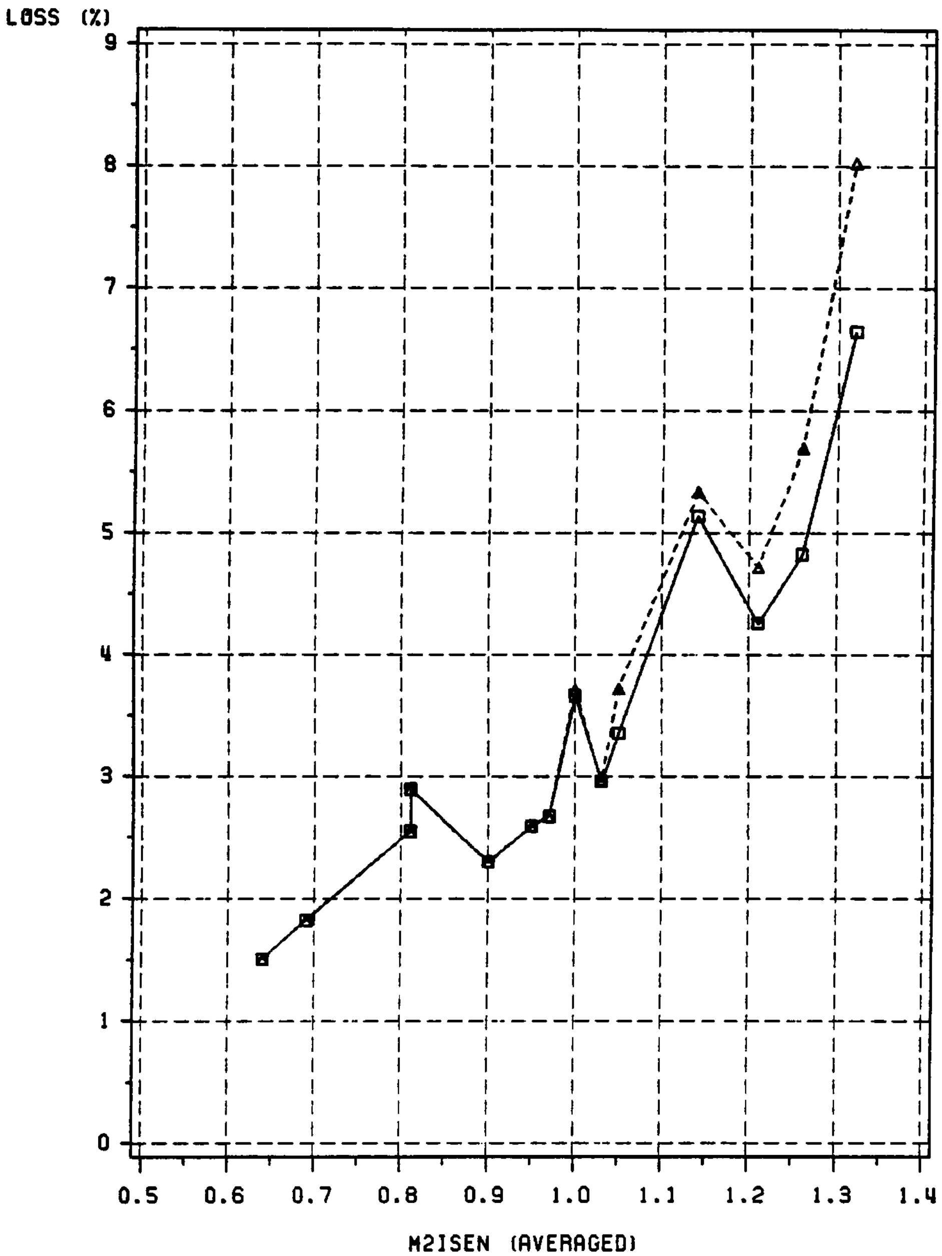

Figure 28. Plot Showing the Magnitude of the Bow Shock Correction: a sample plot of $\bar{L}$ versus exit Mach number (second cascade, middle station (x/c = 1.667), no coolant), the solid line represents the corrected results.

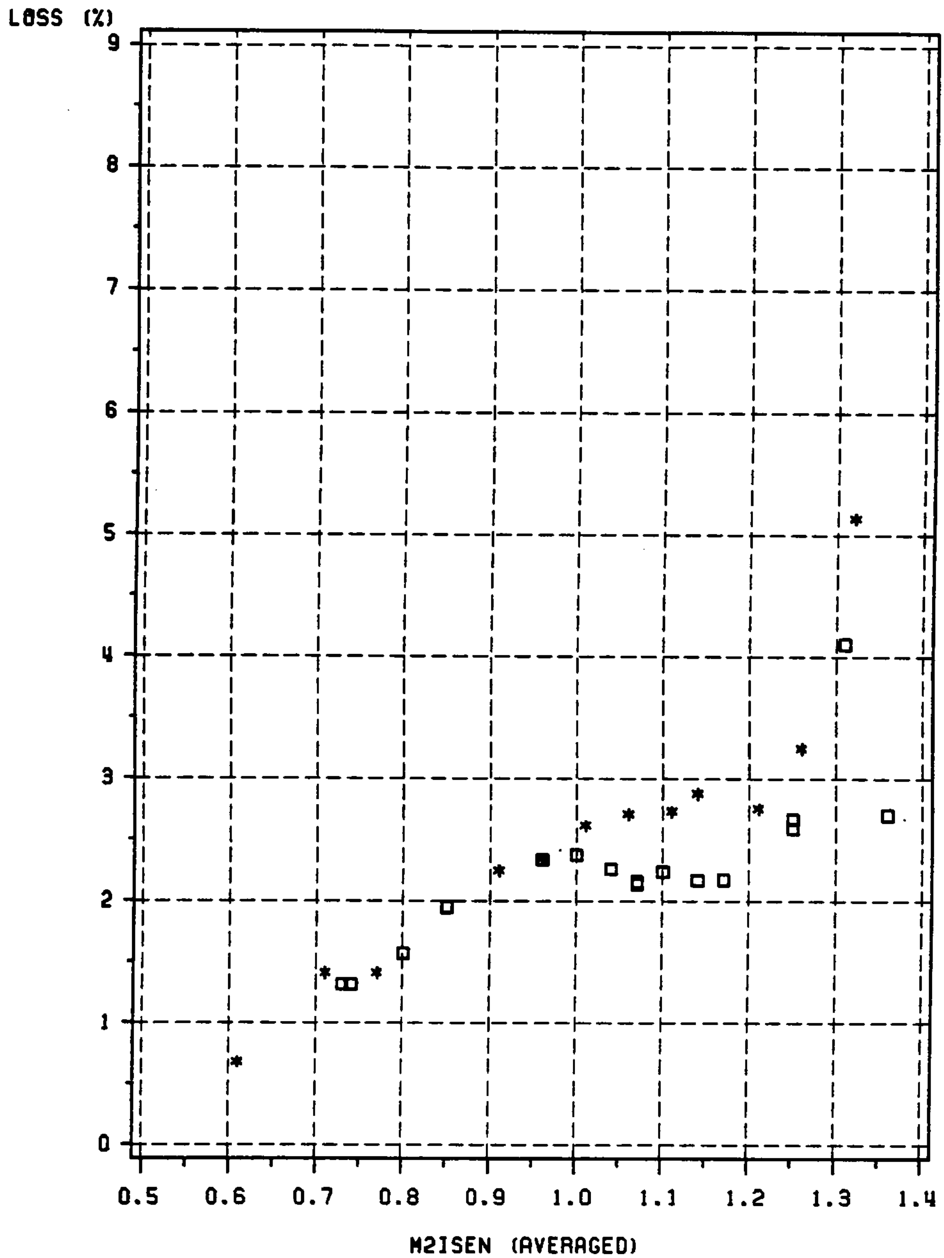

Figure 29. Loss Versus Isentropic Exit Mach Number: forward position (x/c = 1.125) - no coolant injection. □ - first cascade, * - second cascade.

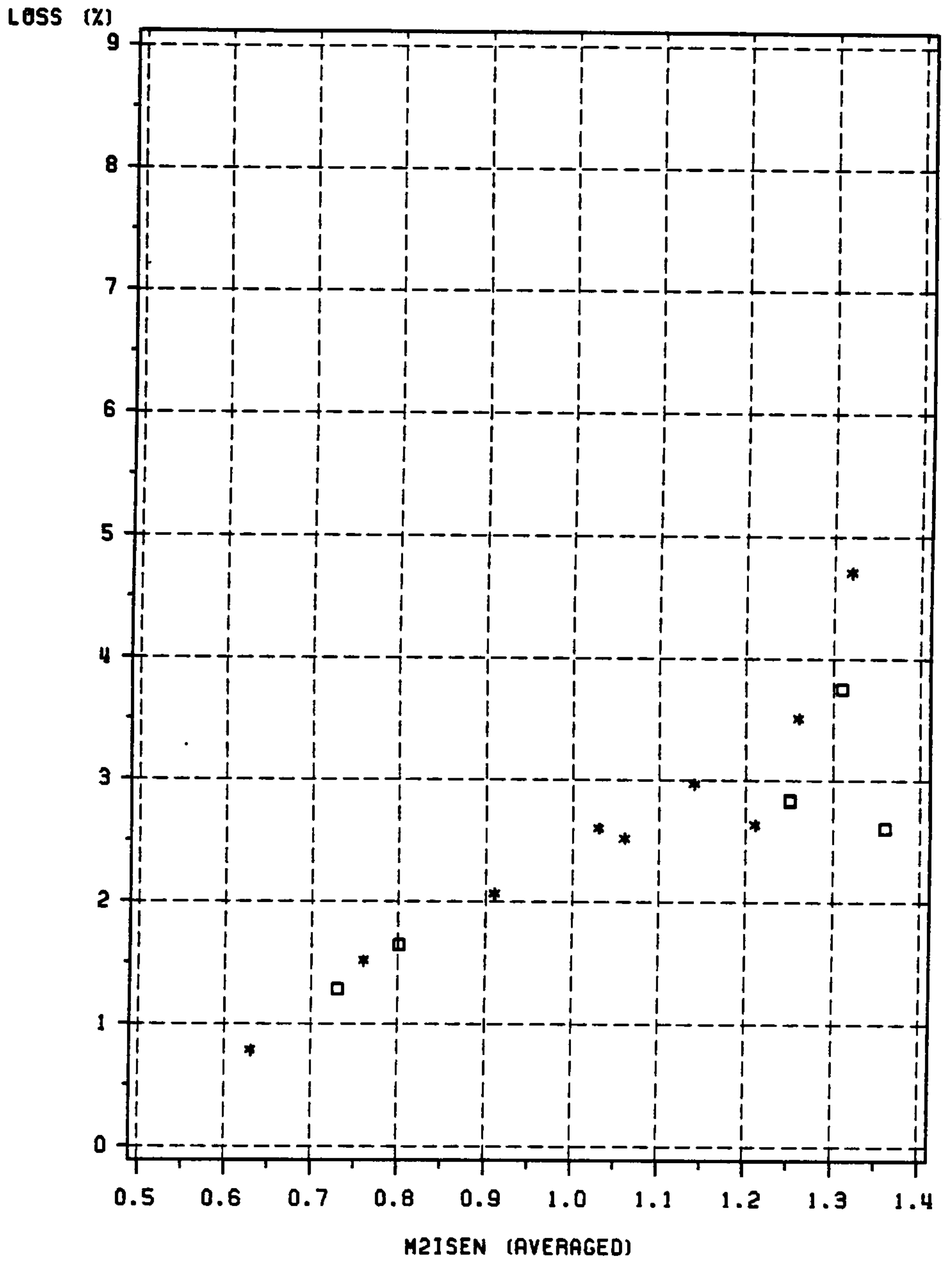

Figure 30. Loss Versus Isentropic Exit Mach Number: forward position (x/c = 1.125) - low coolant injection rate. □ - first cascade, * - second cascade.

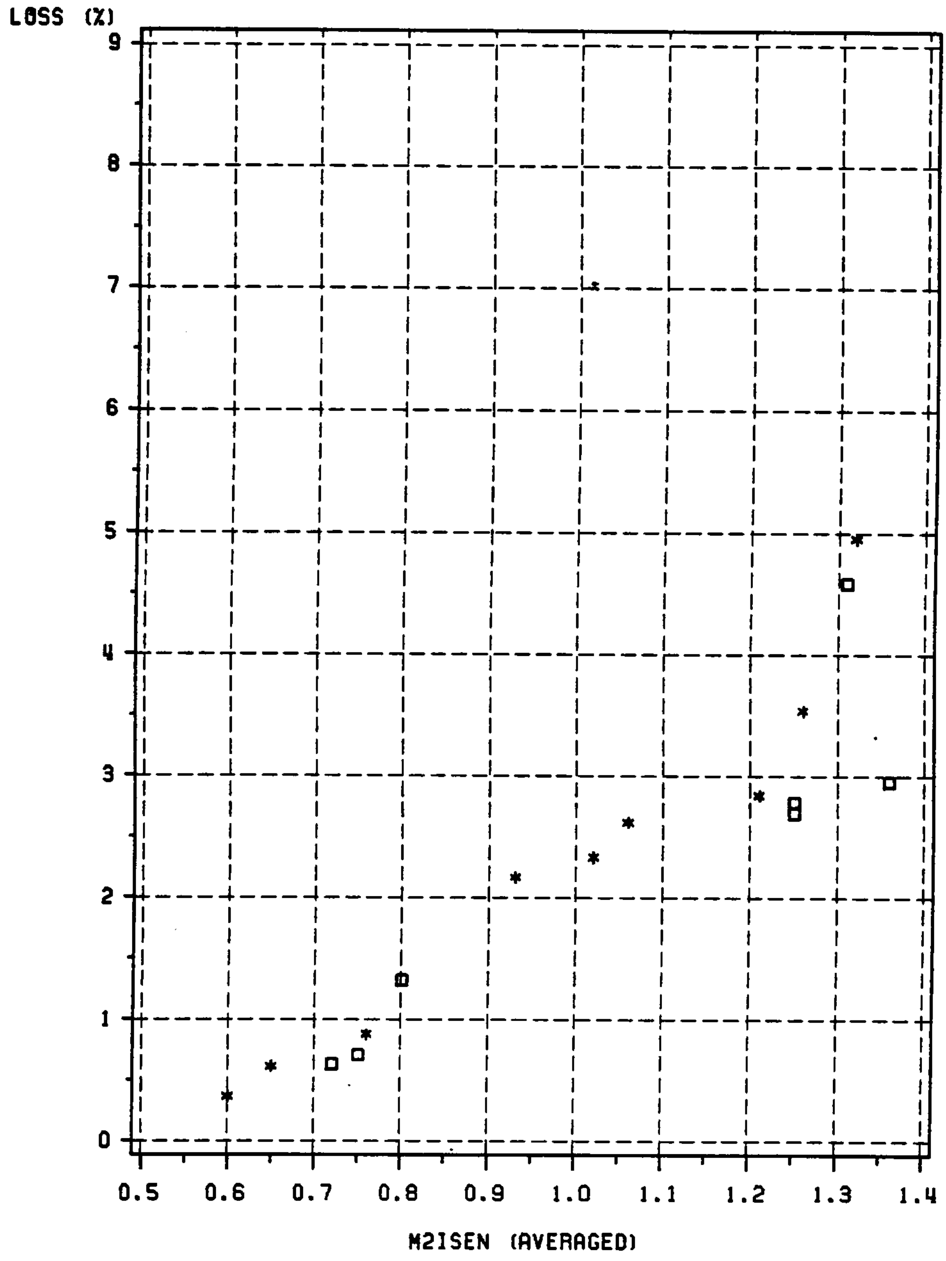

Figure 31. Loss Versus Isentropic Exit Mach Number: forward position (x/c = 1.125) - high coolant injection rate. □ - first cascade, * - second cascade.

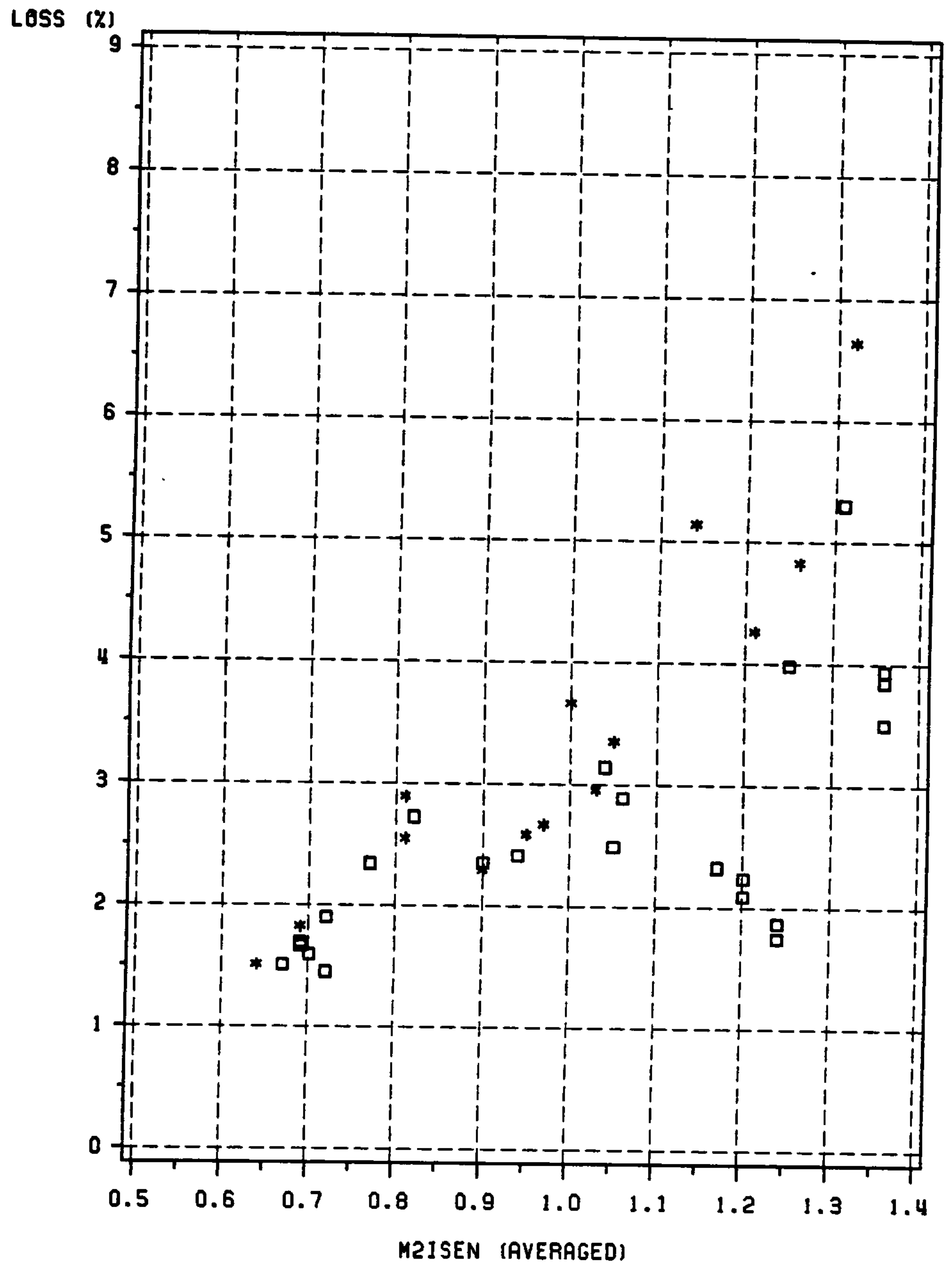

Figure 32. Loss Versus Isentropic Exit Mach Number: middle position (x/c = 1.667) - no coolant injection. □ - first cascade, * - second cascade.

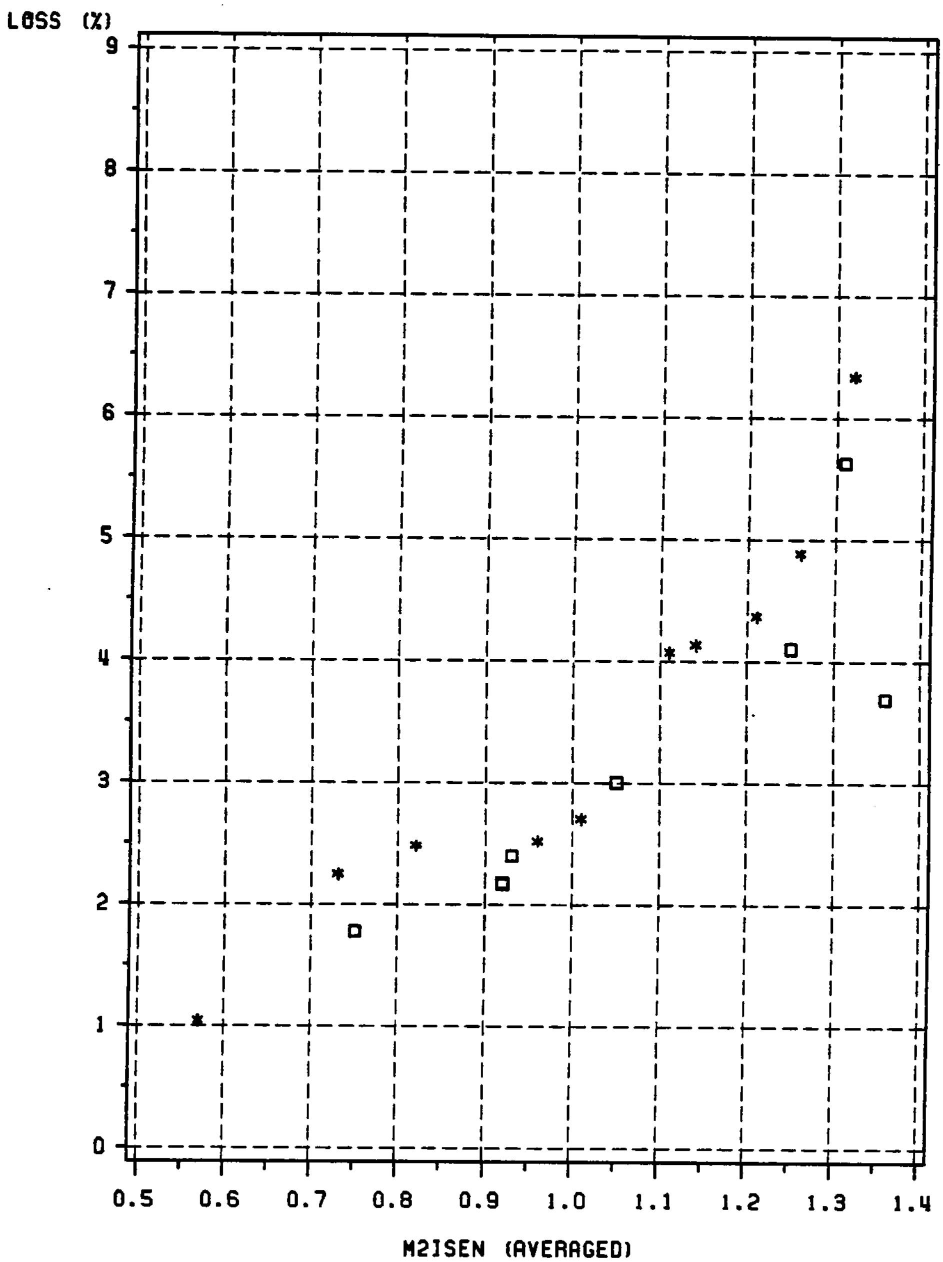

Figure 33. Loss Versus Isentropic Exit Mach Number: middle position (x/c = 1.667) - low coolant injection rate. ☐ - first cascade, * - second cascade.

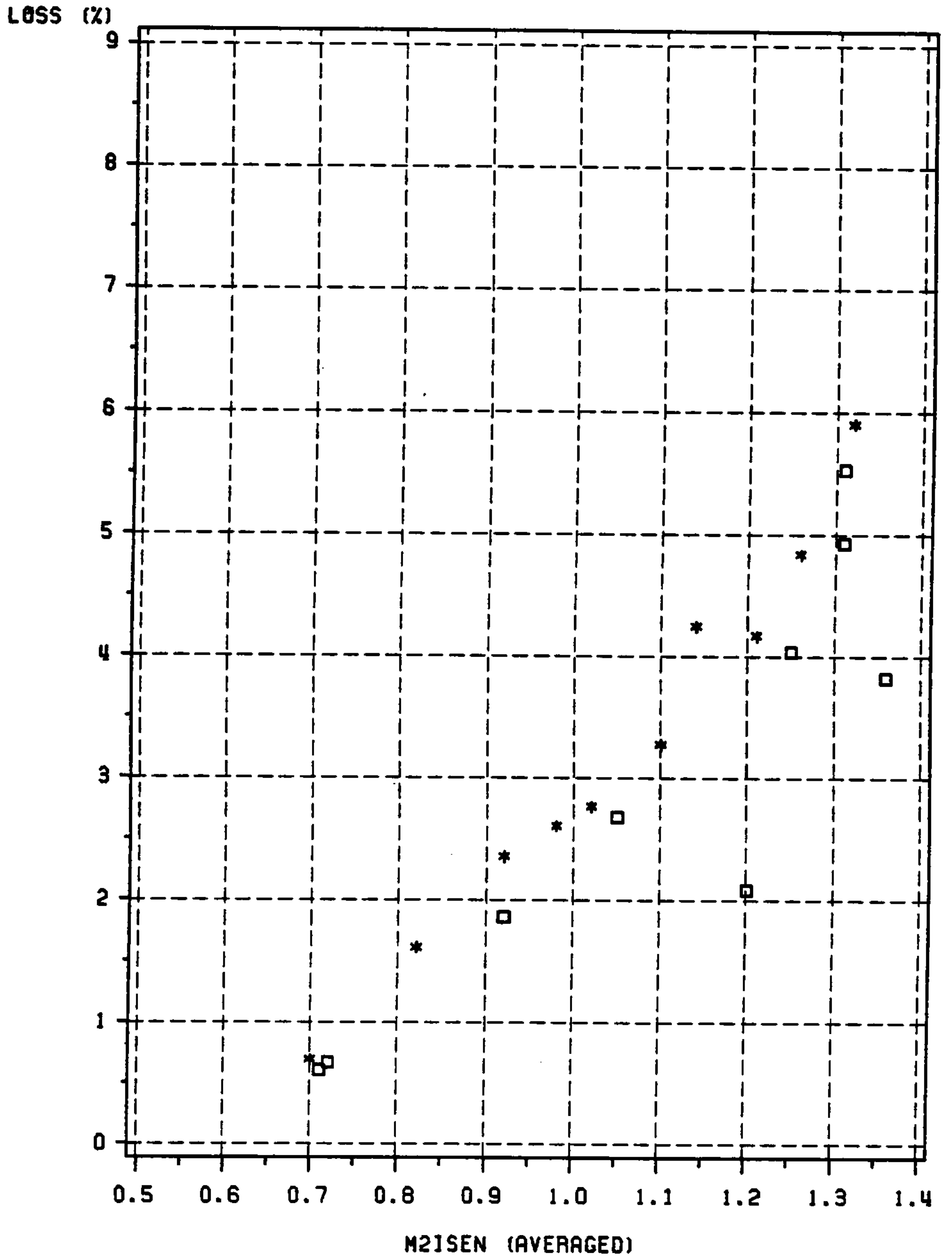

Figure 34. Loss Versus Isentropic Exit Mach Number: middle position (x/c = 1.667) - high coolant injection rate. □ - first cascade, * - second cascade.

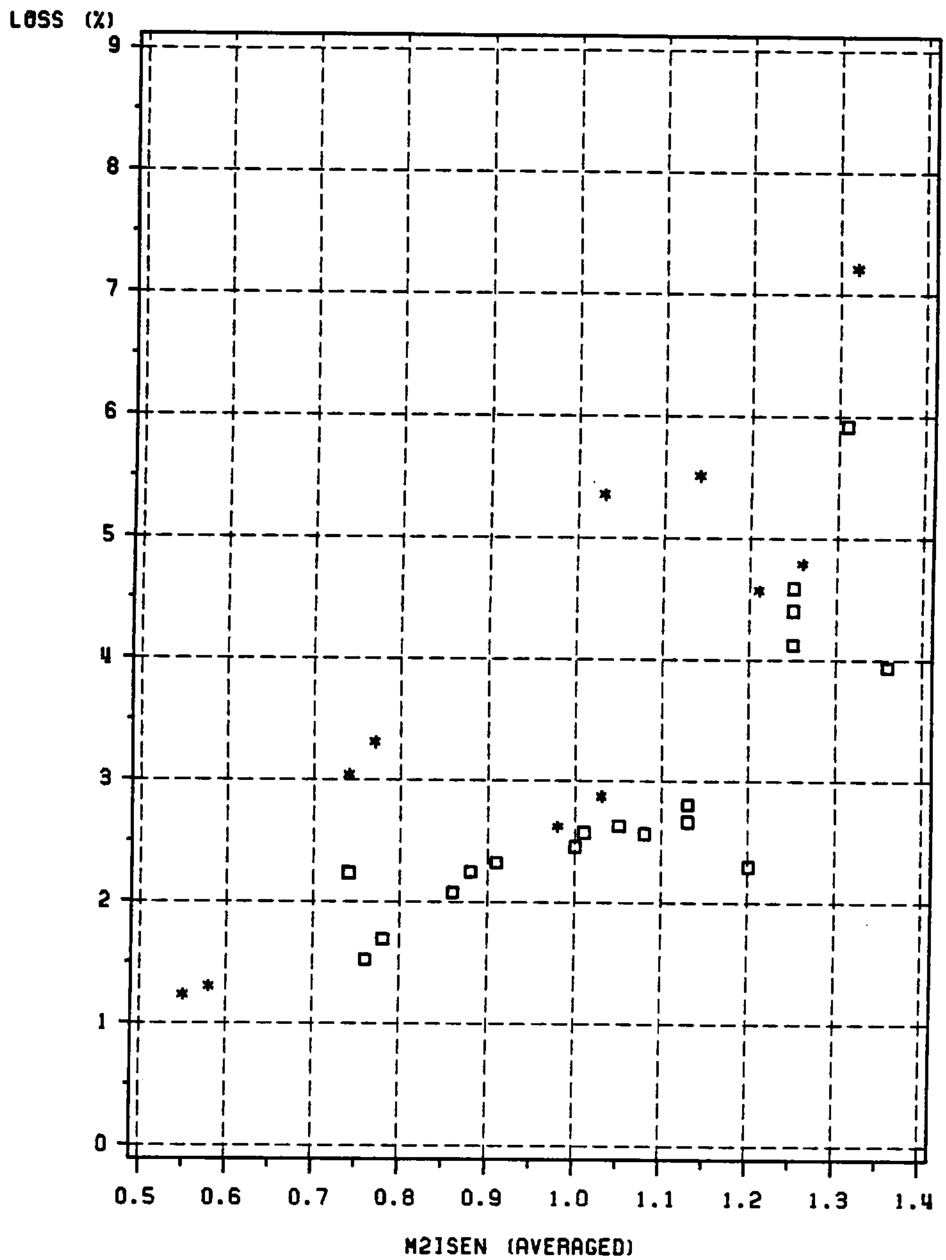

Figure 35. Loss Versus Isentropic Exit Mach Number: rear position (x/c = 3.000) - no coolant injection. □ - first cascade, * - second cascade.

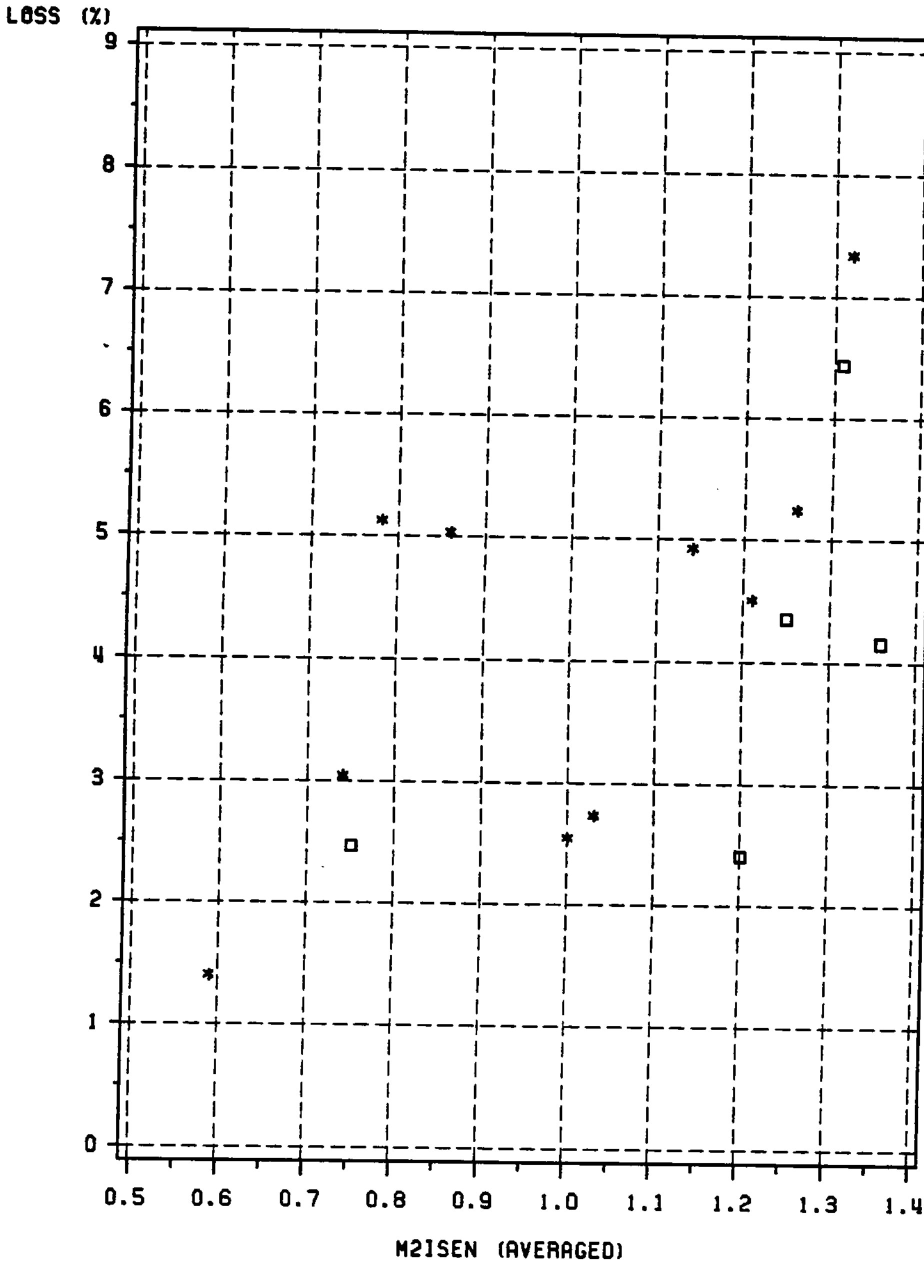

Figure 36. Loss Versus Isentropic Exit Mach Number: rear position (x/c = 3.000) - low coolant injection rate. □ - first cascade, * - second cascade.

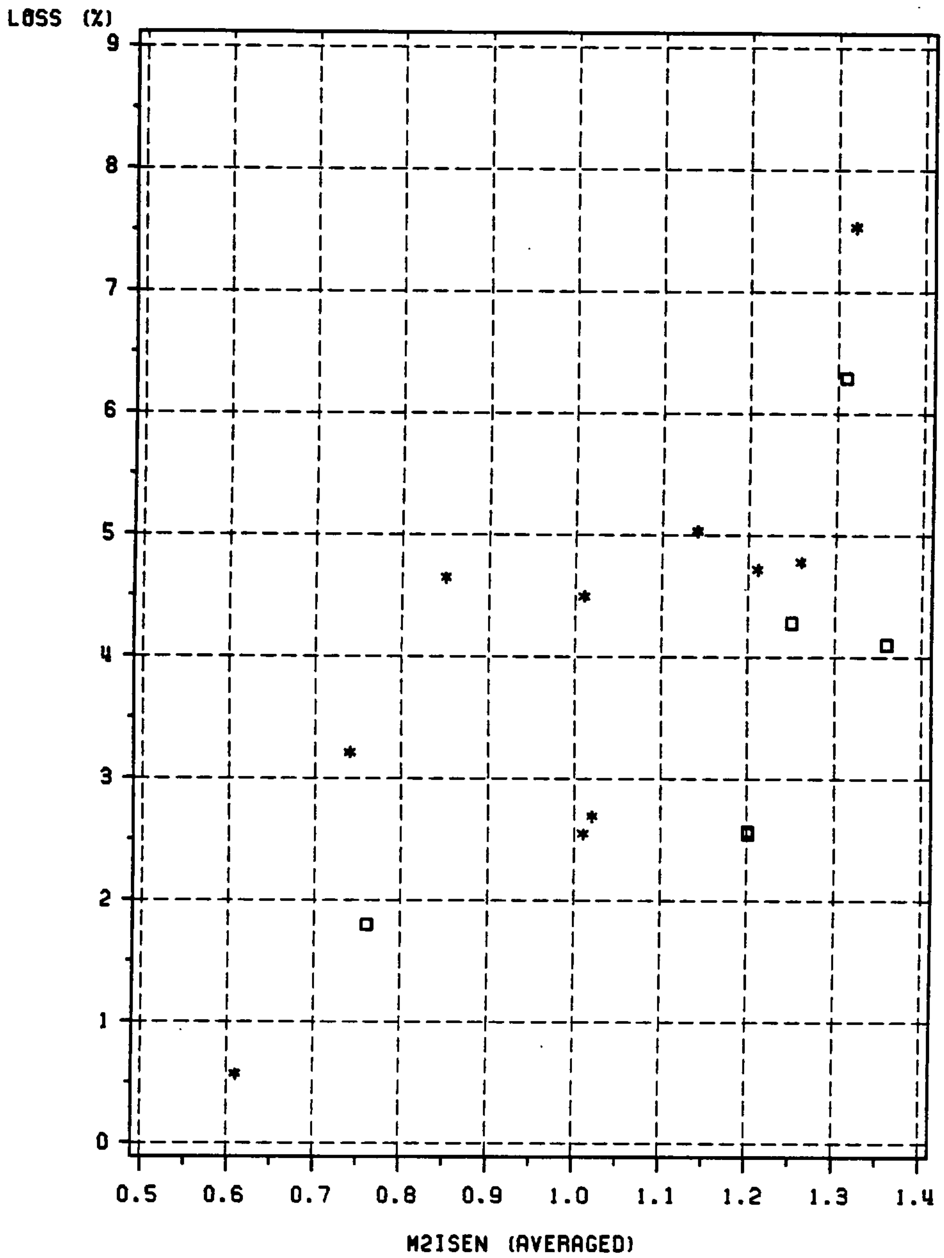

Figure 37. Loss Versus Isentropic Exit Mach Number: rear position (x/c = 3.000) - high coolant injection rate. ☐ - first cascade, * - second cascade.

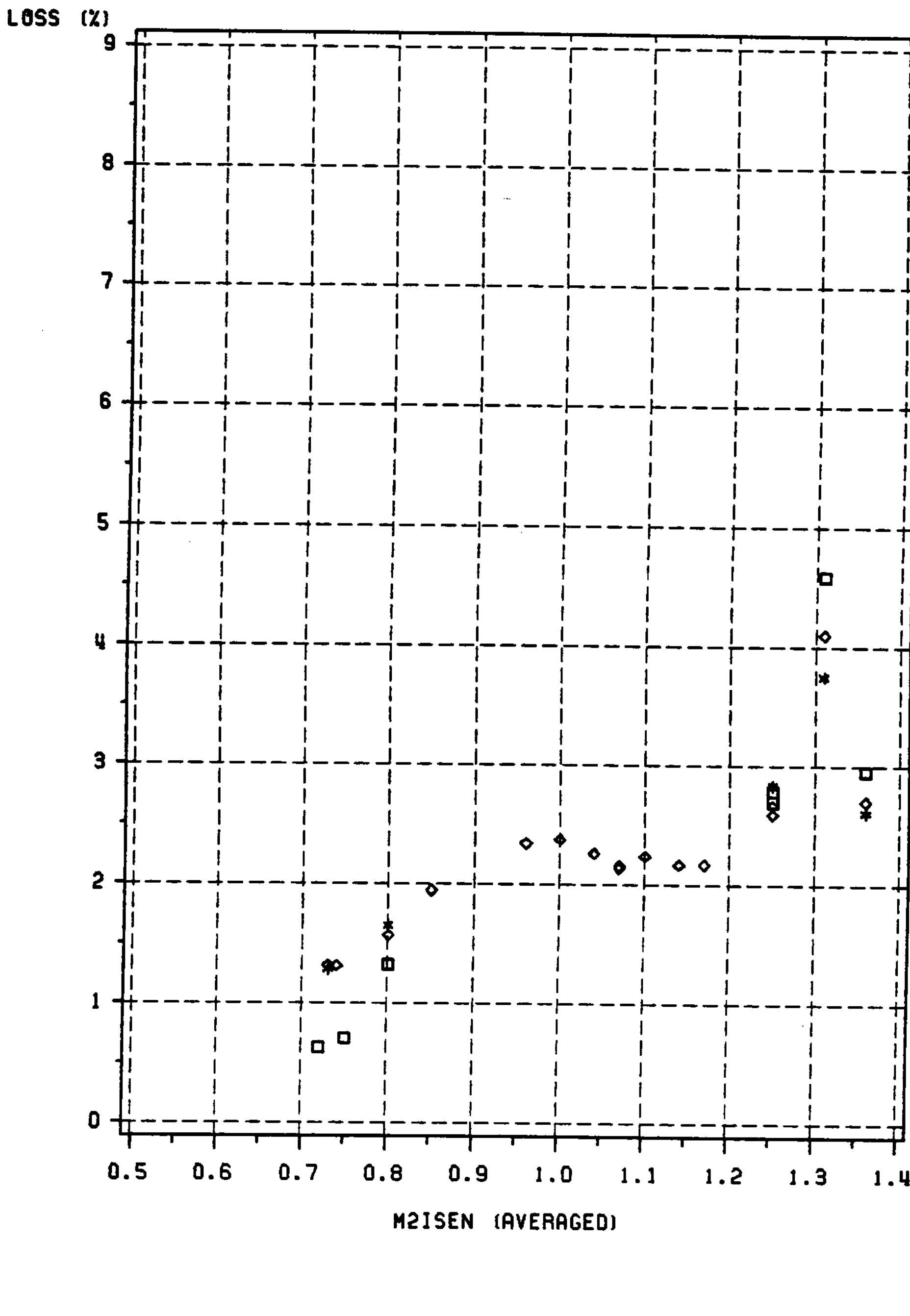

Figure 38. Loss Versus Isentropic Exit Mach Number: first cascade only - forward position (x/c = 1.125). ◇ - no injection, * - low injection, □ - high injection.

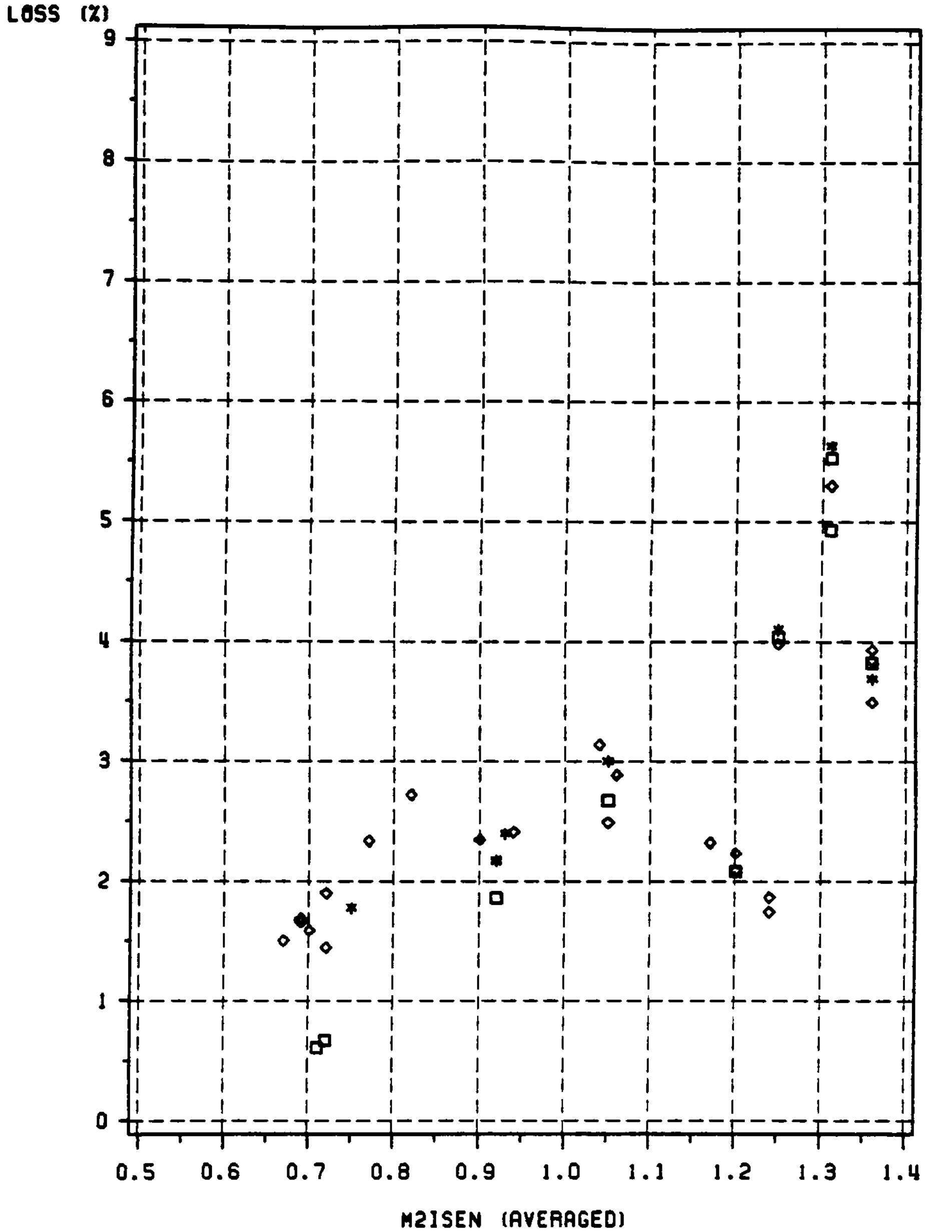

Figure 39. Loss Versus Isentropic Exit Mach Number: first cascade only - middle position (x/c = 1.667). ◇ - no injection, * - low injection, □ - high injection.

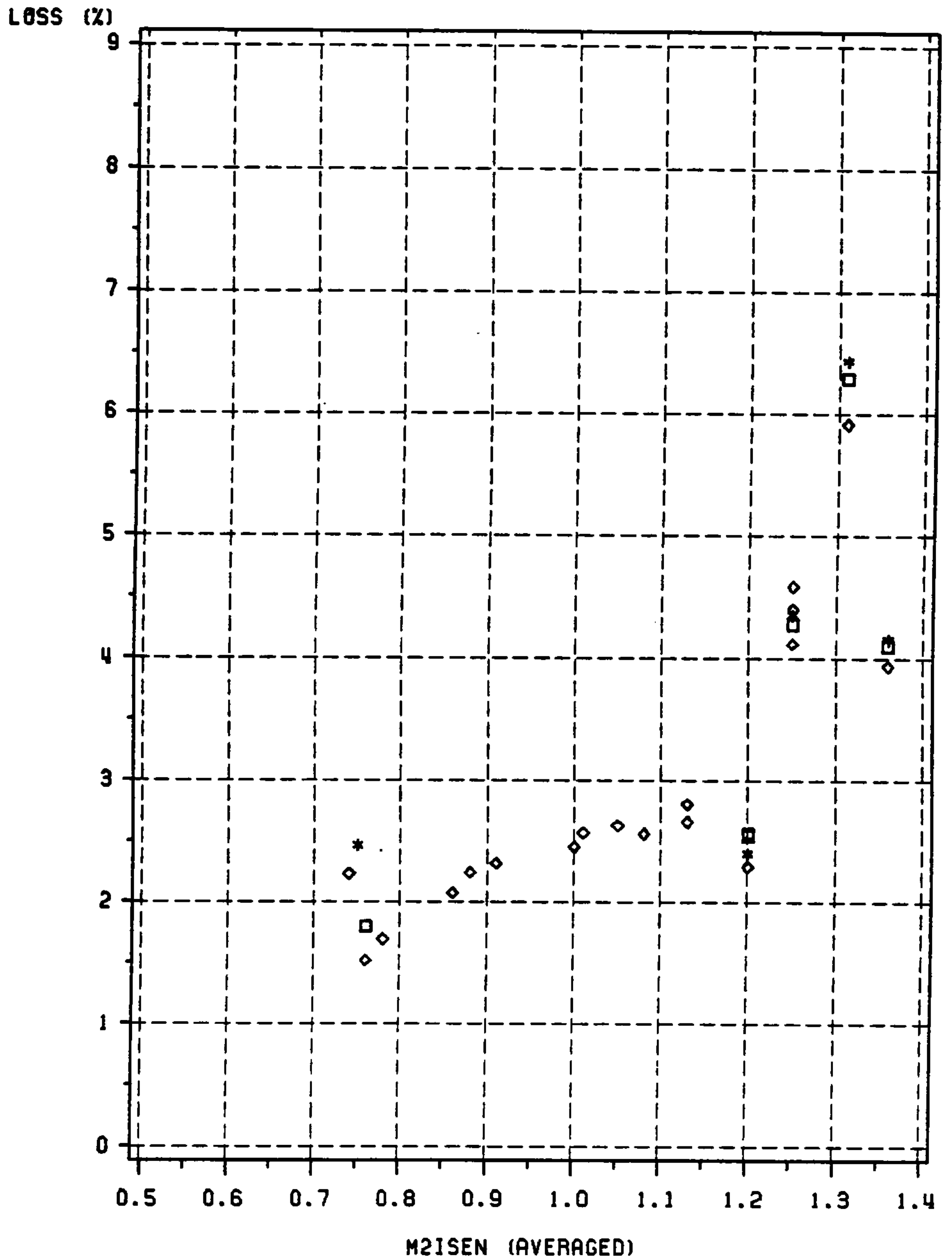

Figure 40. Loss Versus Isentropic Exit Mach Number: first cascade only - rear position (x/c = 3.000). ◇ - no injection, * - low injection, □ - high injection.

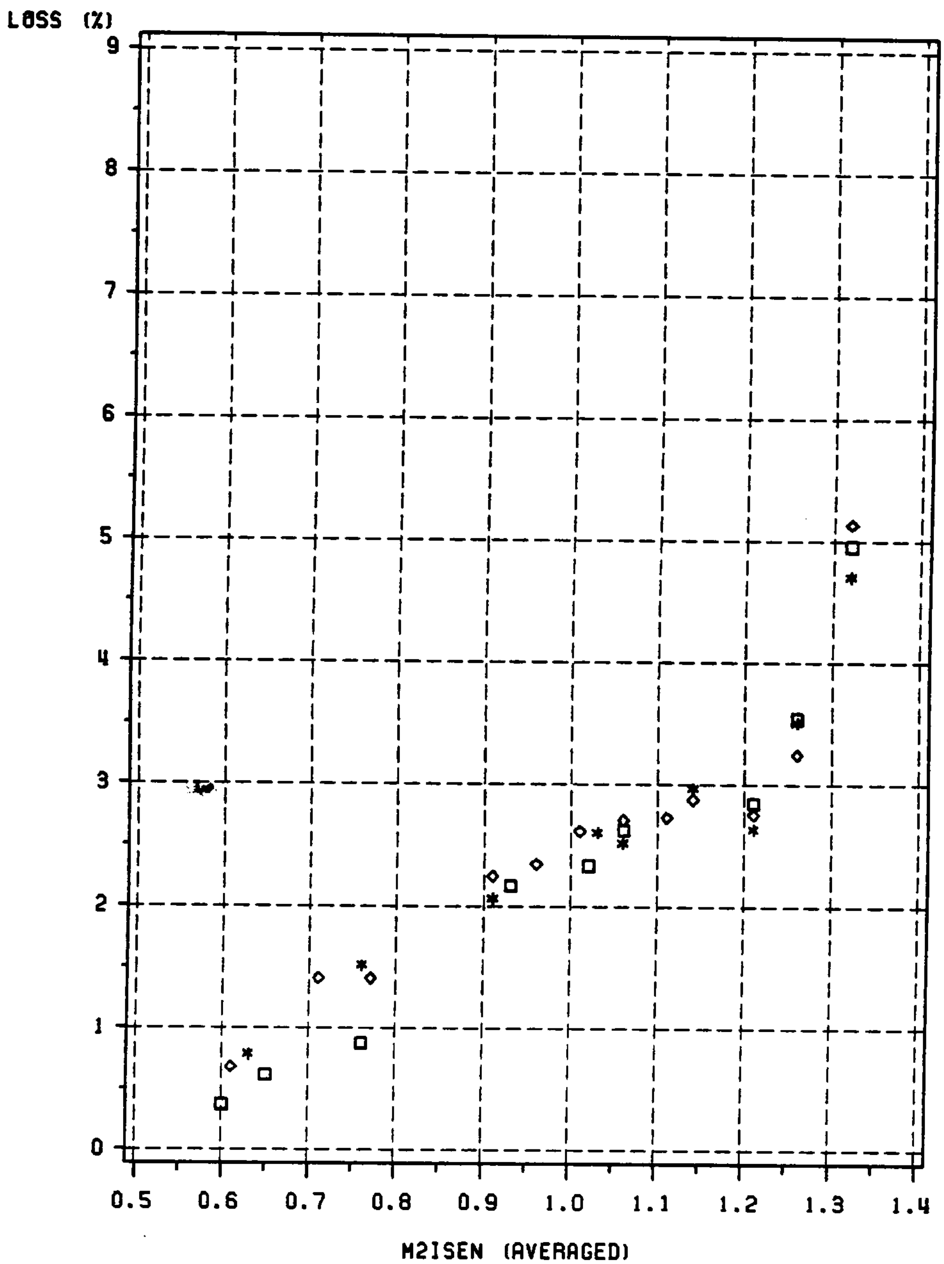

Figure 41. Loss Versus Isentropic Exit Mach Number: second cascade only - forward position (x/c = 1.125). ◇ - no injection, * - low injection, □ - high injection.

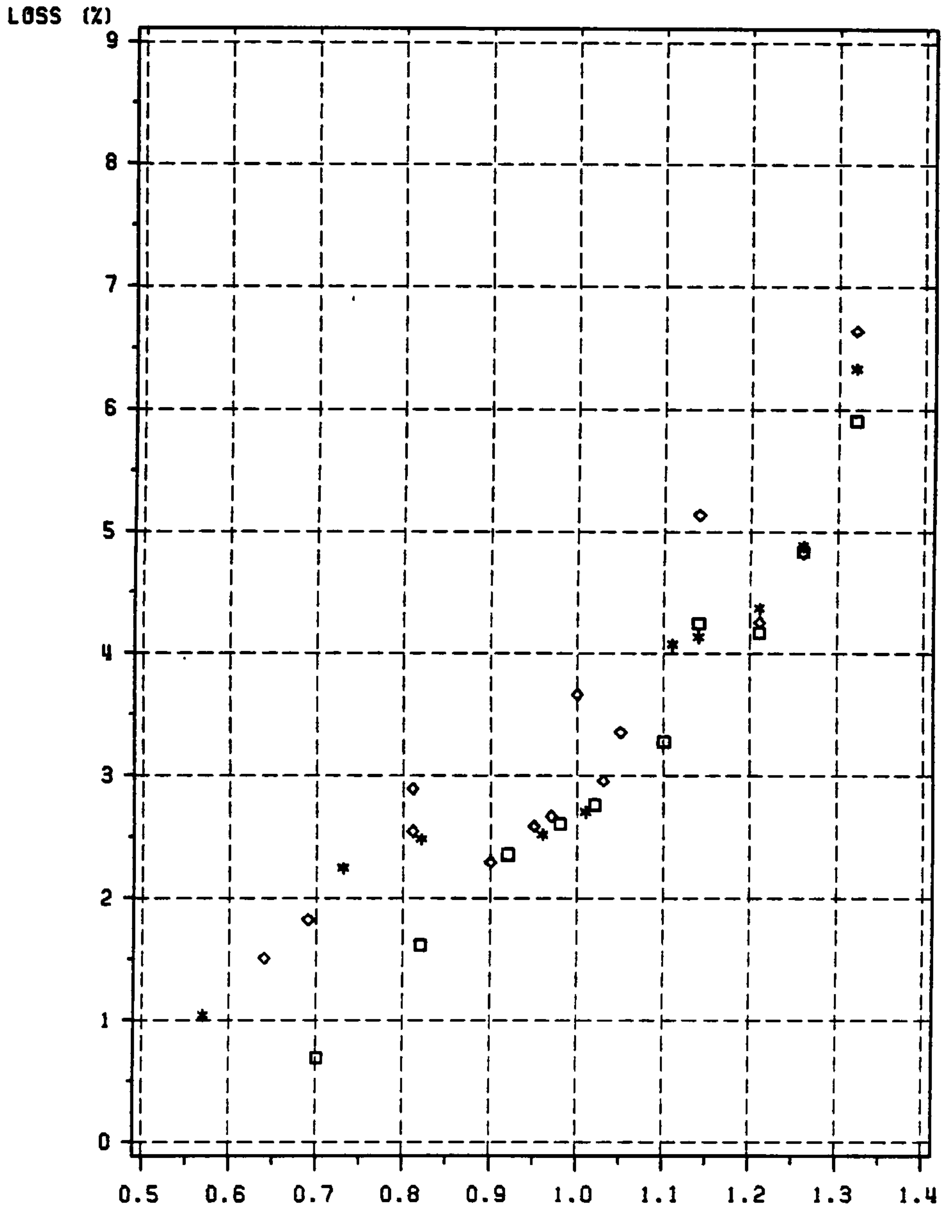

Figure 42. Loss Versus Isentropic Exit Mach Number: second cascade only - middle position (x/c = 1.667). ◇ - no injection, * - low injection, □ - high injection.

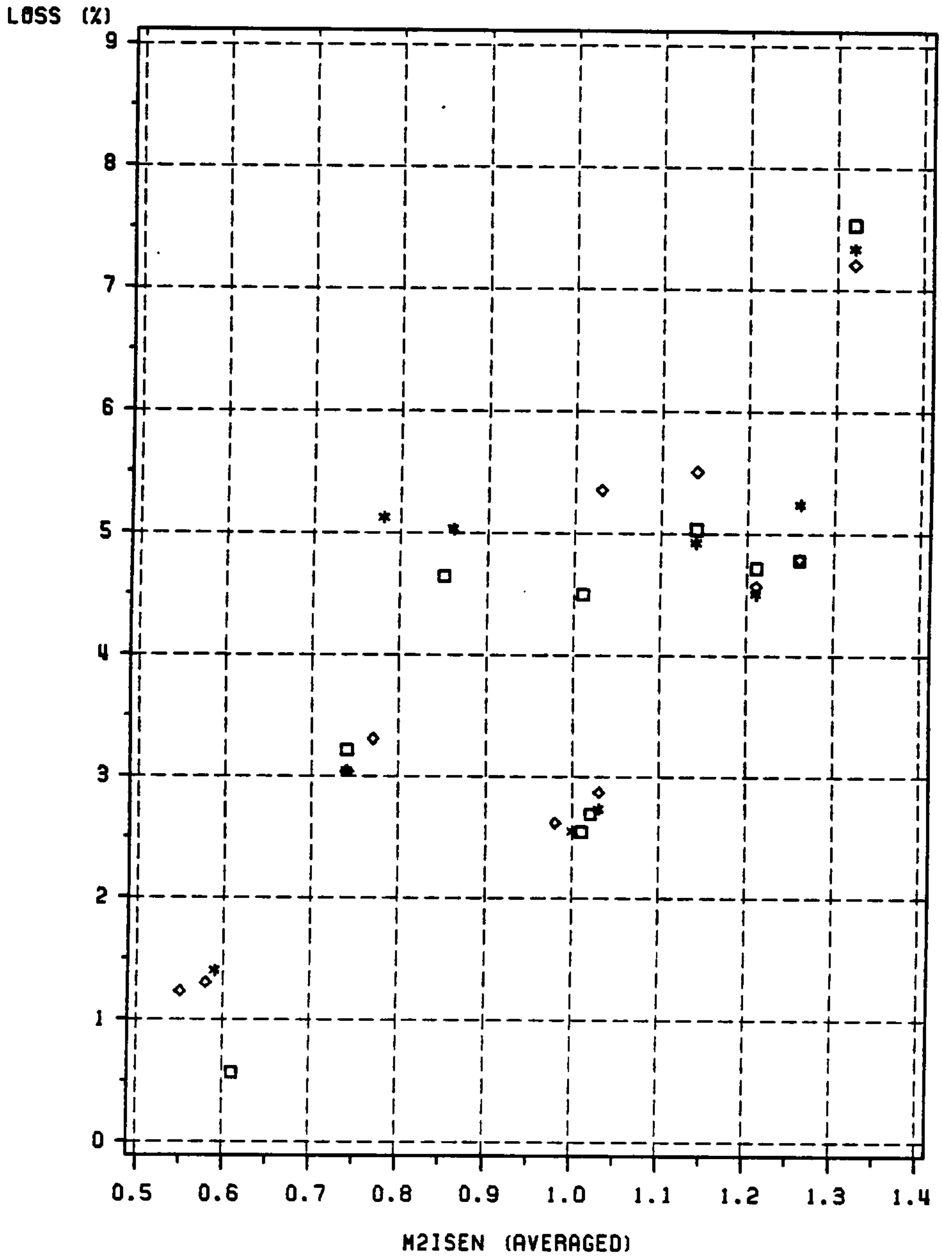

Figure 43. Loss Versus Isentropic Exit Mach Number: second cascade only - rear position (x/c = 3.000). ◇ - no injection, * - low injection, □ - high injection.

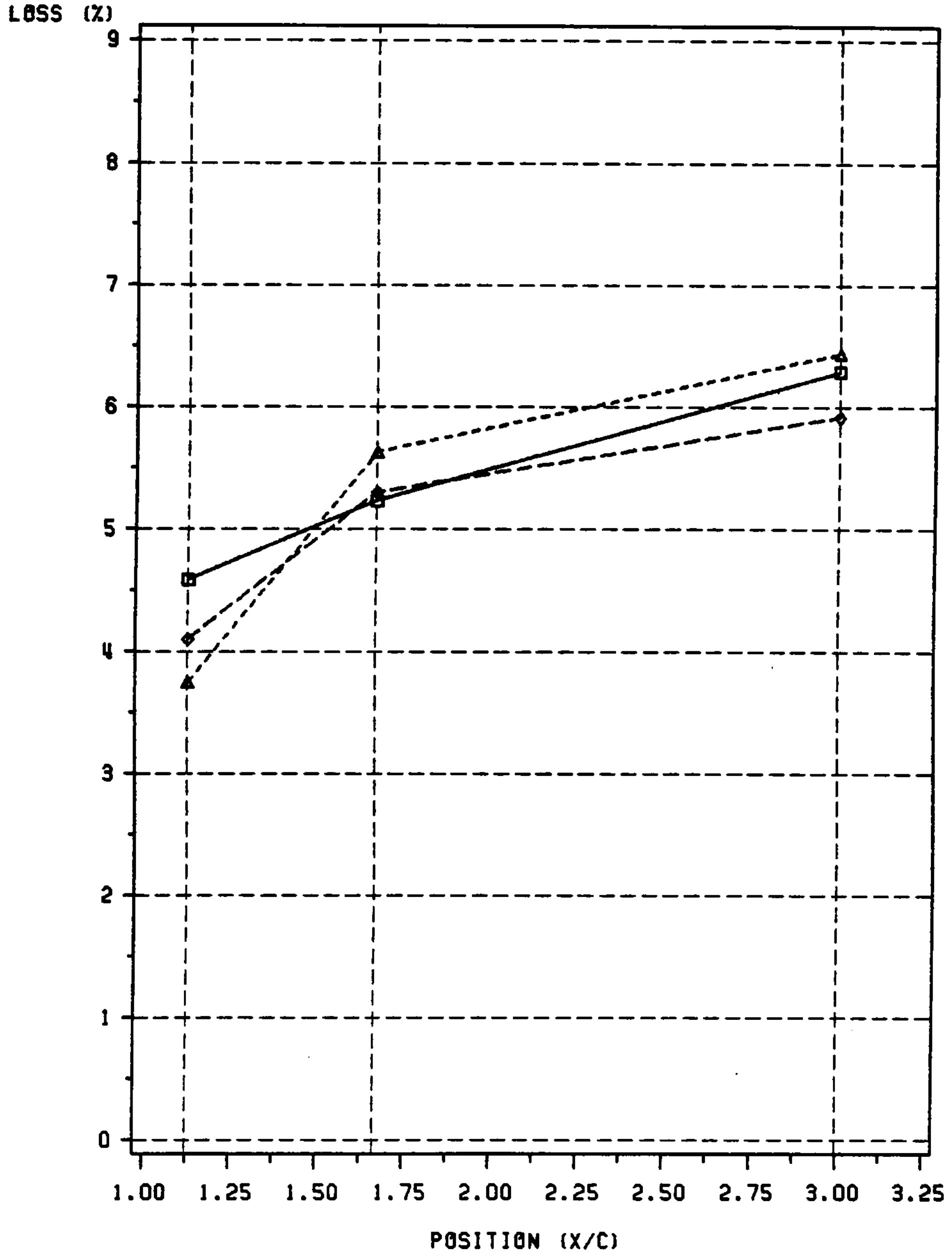

Figure 44. Loss Versus Downstream Probe Position: first cascade - $M_{2,isen}$ = 1.31. ◇ - no injection, △ - low injection, □ - high injection.

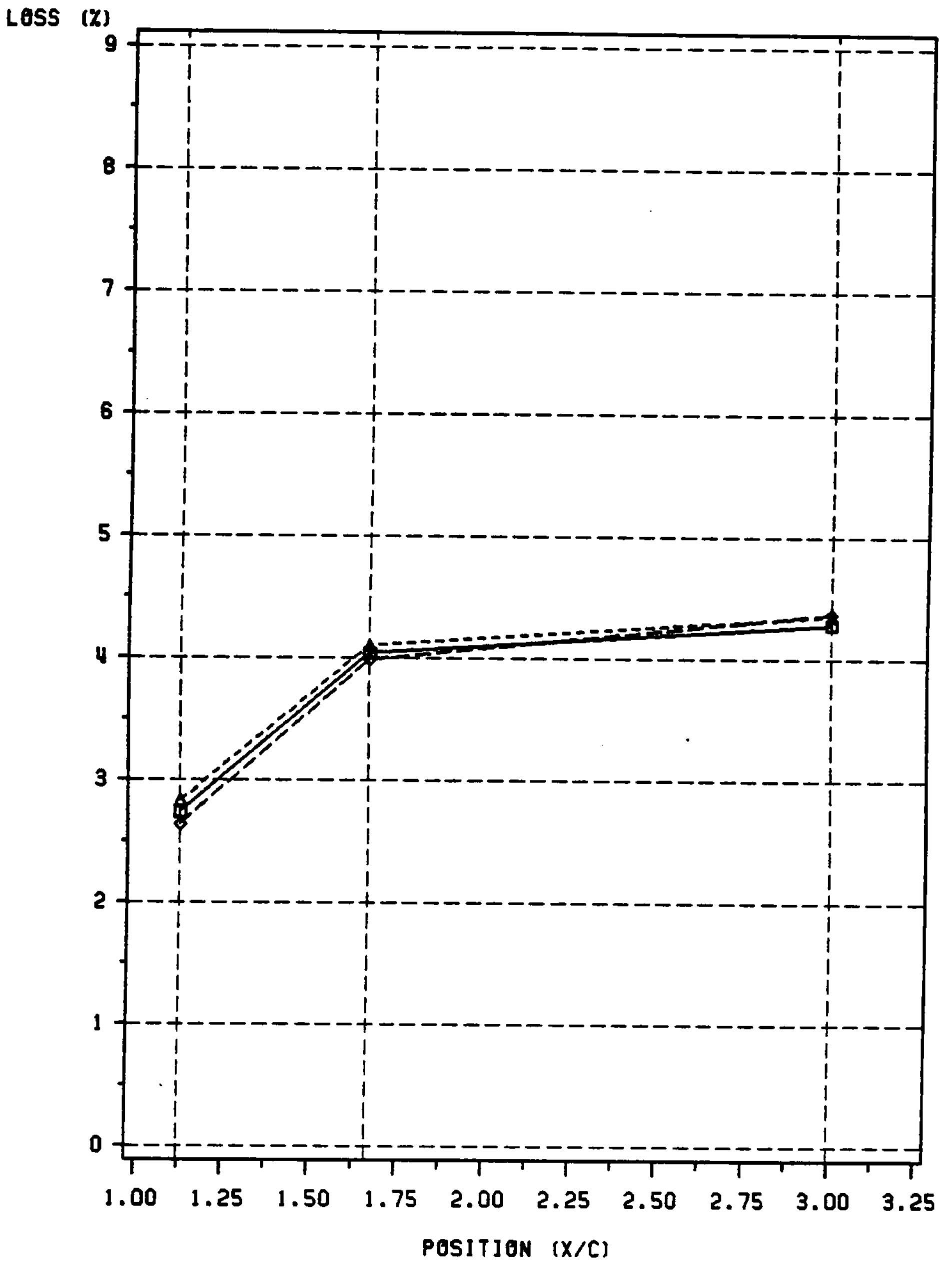

Figure 45. Loss Versus Downstream Probe Position: first cascade - $M_{2,isen}$ = 1.25. ◇ - no injection, △ - low injection, □ - high injection.

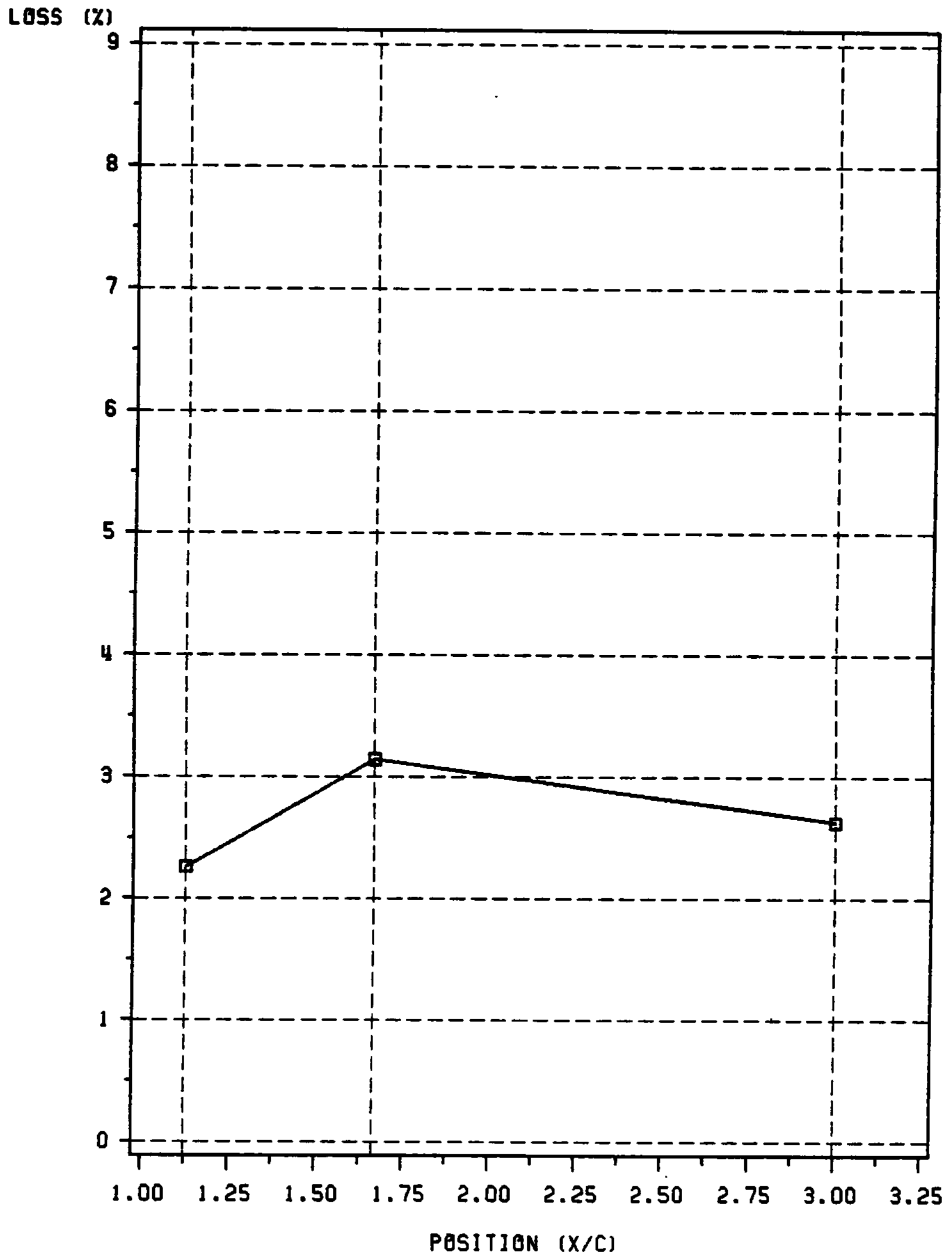

Figure 46. Loss Versus Downstream Probe Position: first cascade - $M_{2,isen}$ = 1.04. No coolant injection.

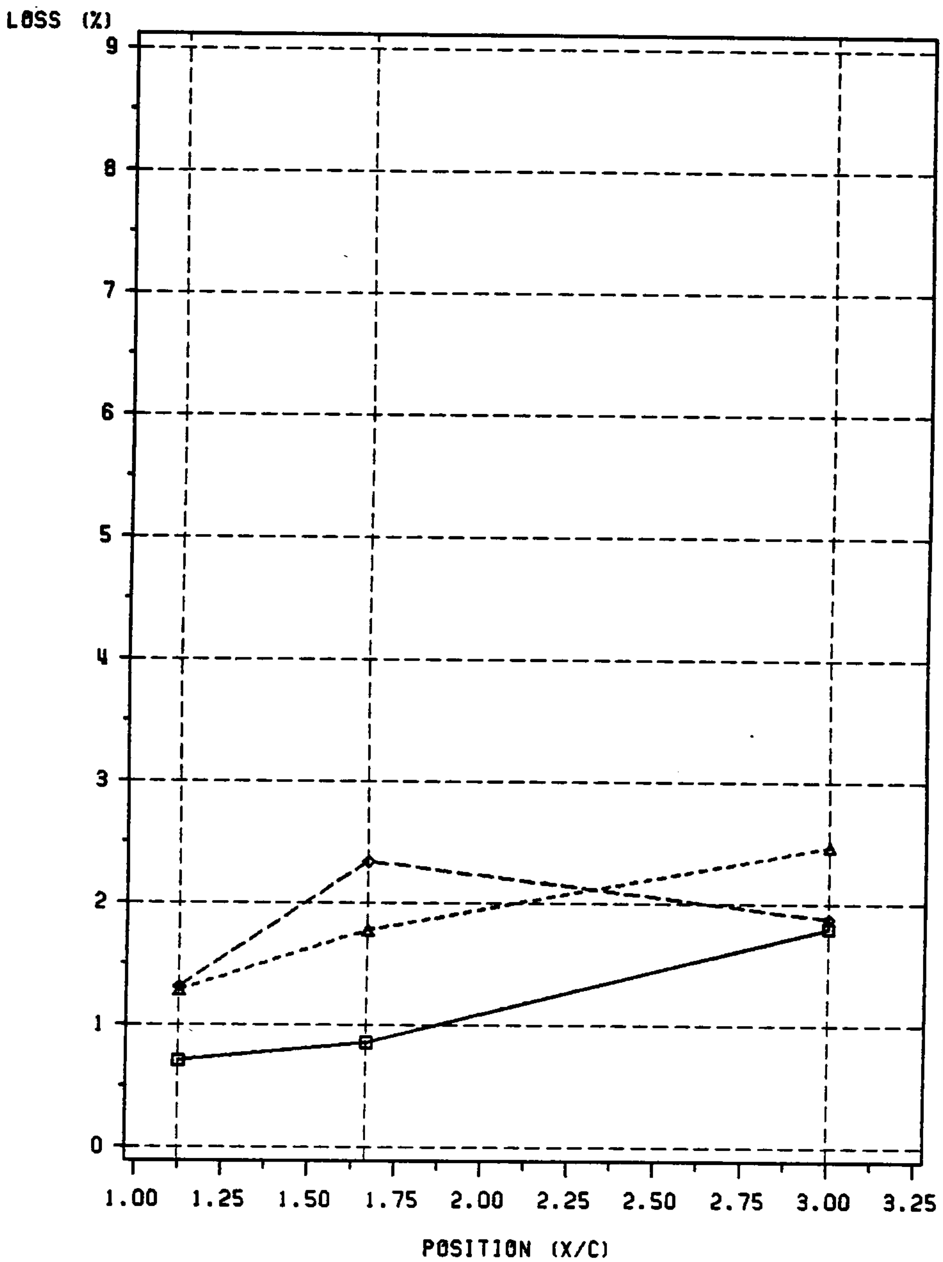

Figure 47. Loss Versus Downstream Probe Position: first cascade - $M_{2,isen}$ = 0.75. ◇ - no injection, △ - low injection, □ - high injection.

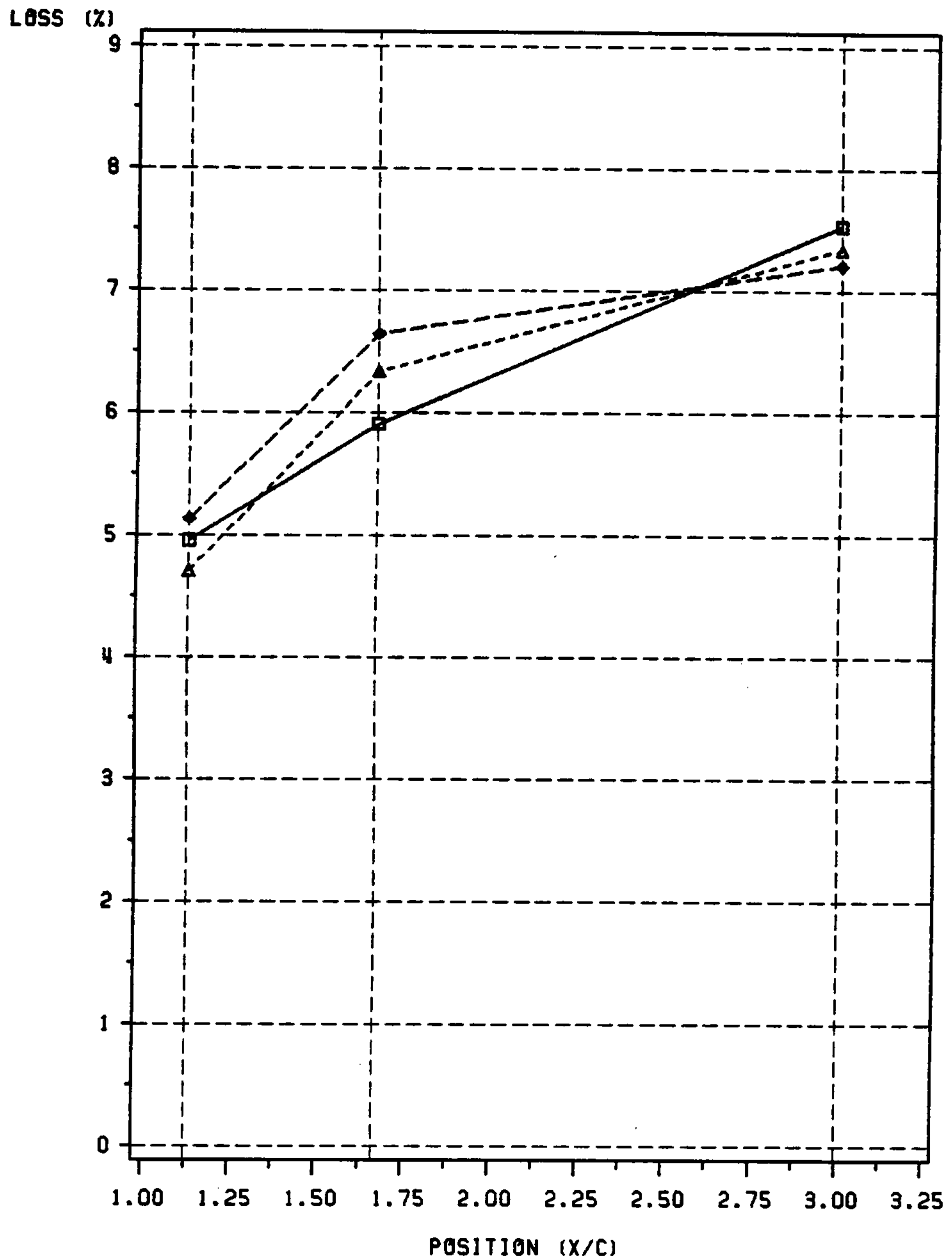

Figure 48. **Loss Versus Downstream Probe Position:** second cascade - $M_{2,isen}$ = 1.32. ◇ - no injection, △ - low injection, □ - high injection.

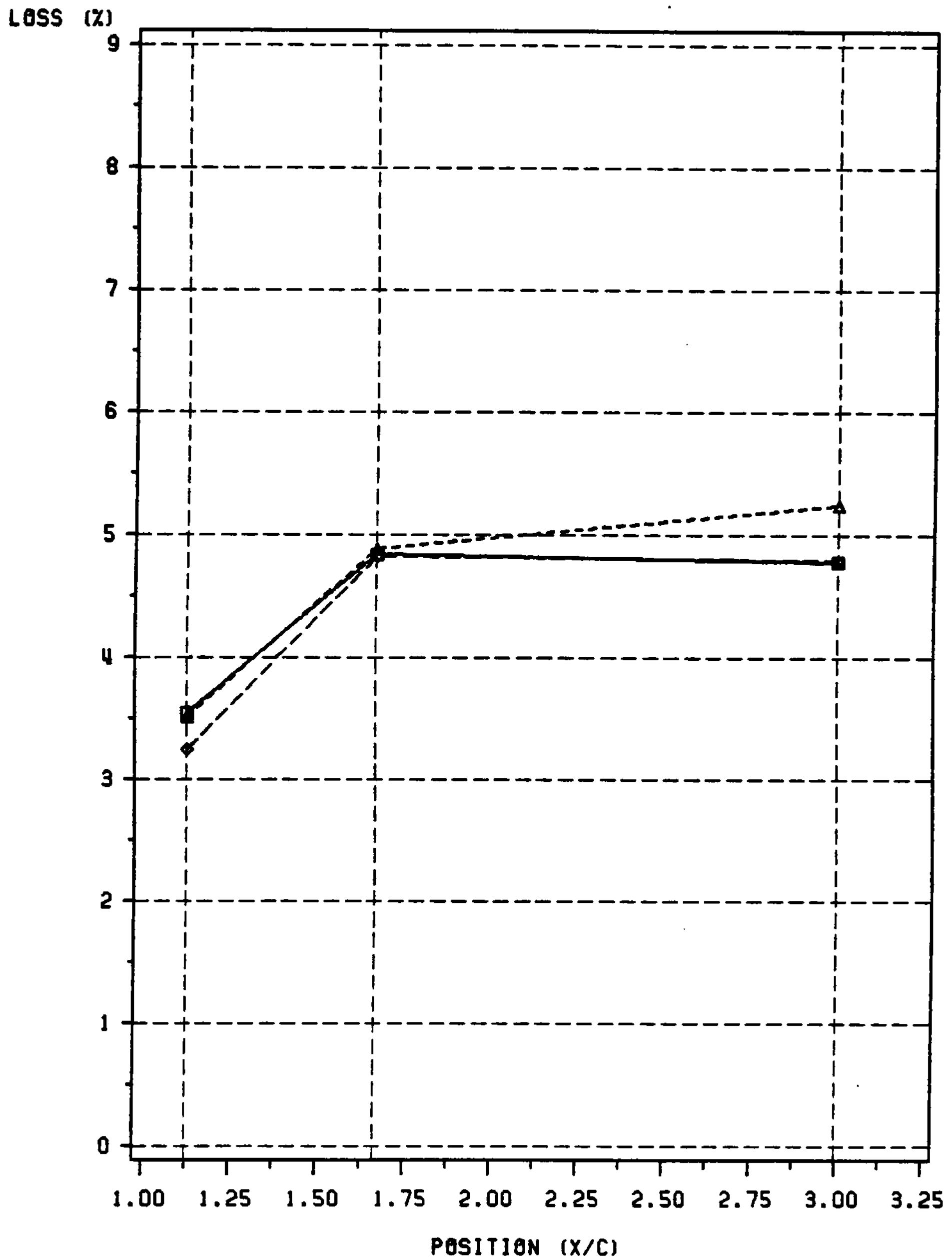

Figure 49. Loss Versus Downstream Probe Position: second cascade - $M_{2,isen}$ = 1.26. ◇ - no injection, △ - low injection, □ - high injection.

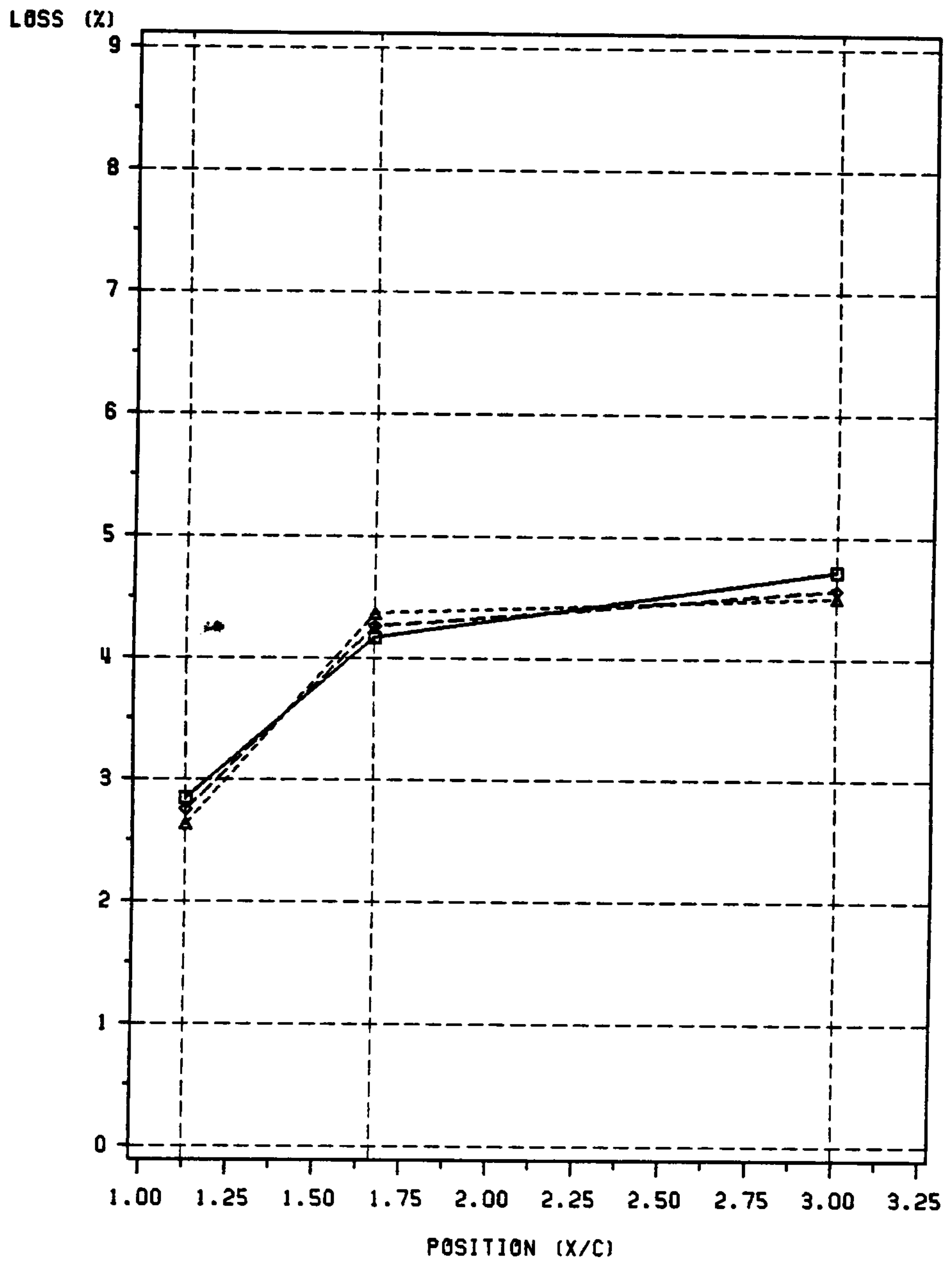

Figure 50. Loss Versus Downstream Probe Position: second cascade - $M_{2,isen}$ = 1.21. ◇ - no injection, △ - low injection, □ - high injection.

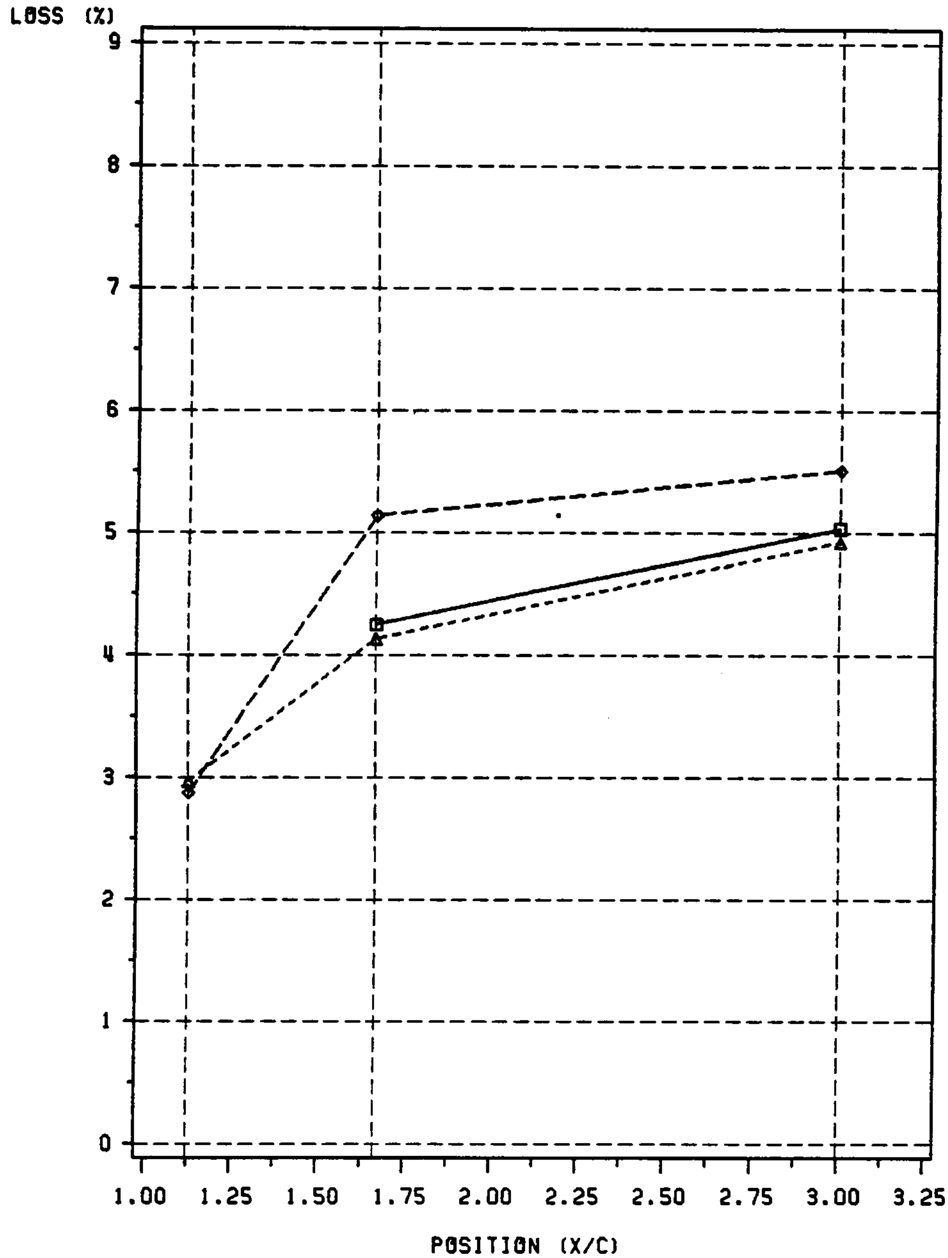

Figure 51. Loss Versus Downstream Probe Position: second cascade - $M_{2,isen}$ = 1.14. ◇ - no injection, △ - low injection, □ - high injection.

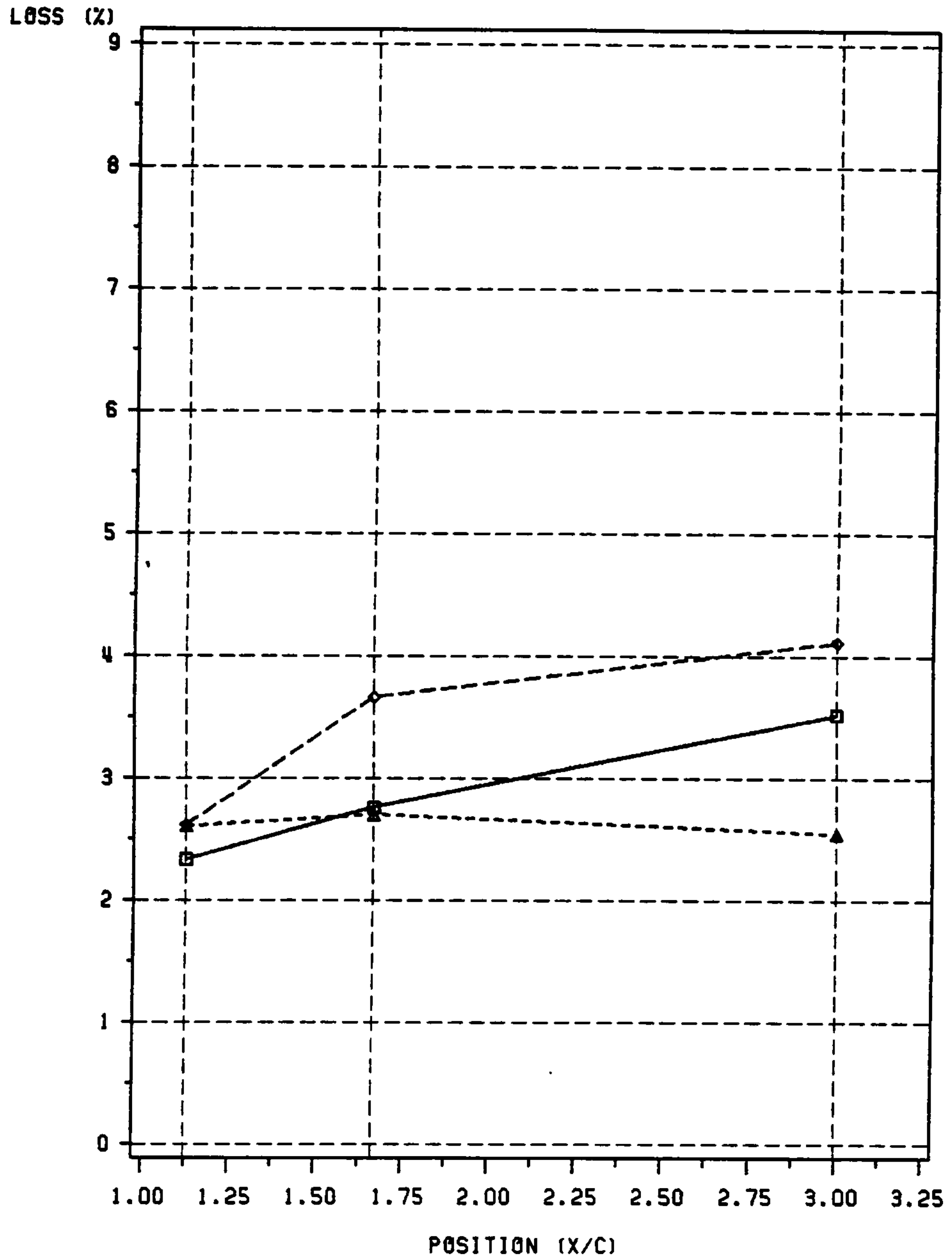

Figure 52. Loss Versus Downstream Probe Position: second cascade - $M_{2,isen}$ = 1.01. ◇ - no injection, △ - low injection, □ - high injection.

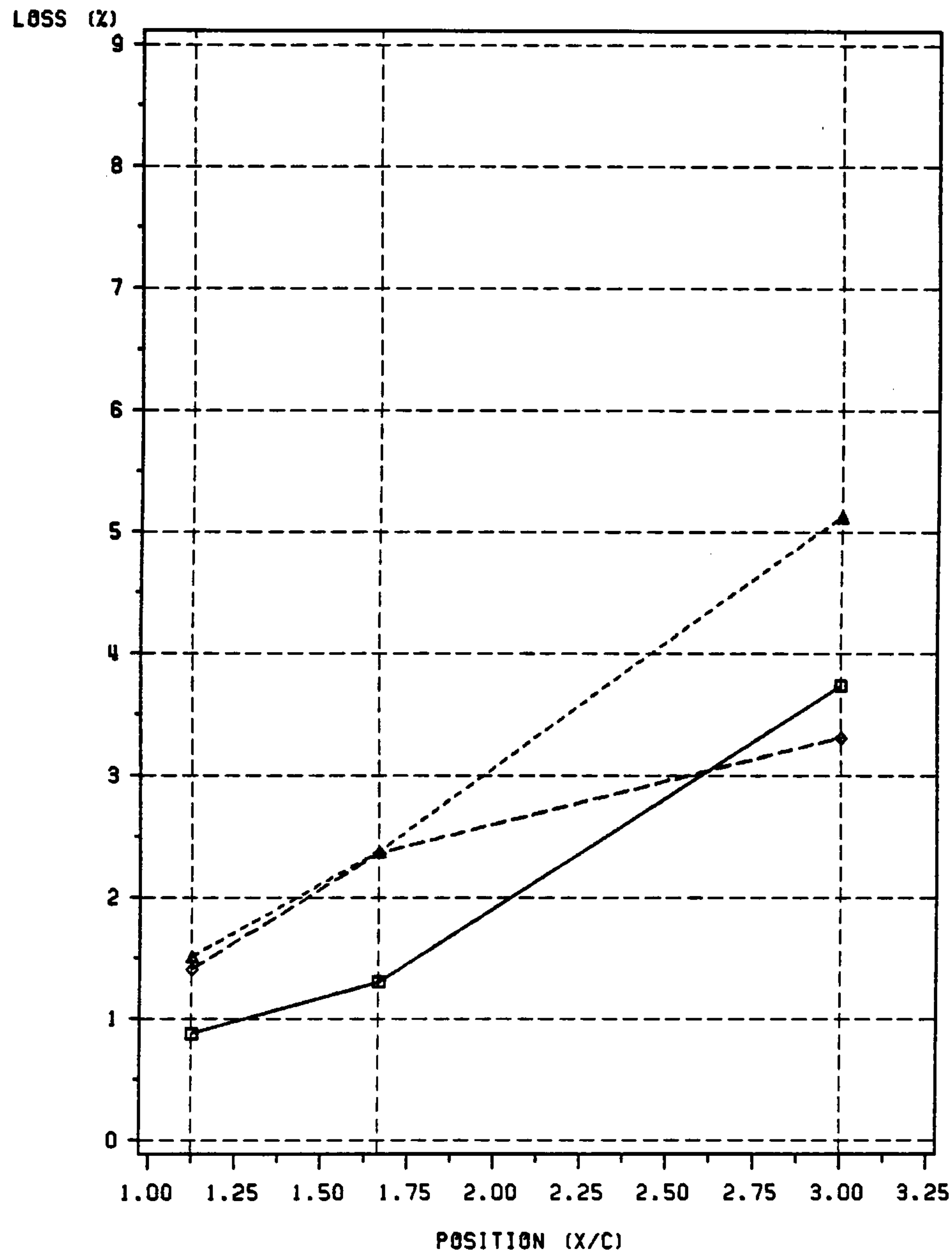

Figure 53. Loss Versus Downstream Probe Position: second cascade - $M_{2,isen}$ = 0.78. ◇ - no injection, △ - low injection, □ - high injection.

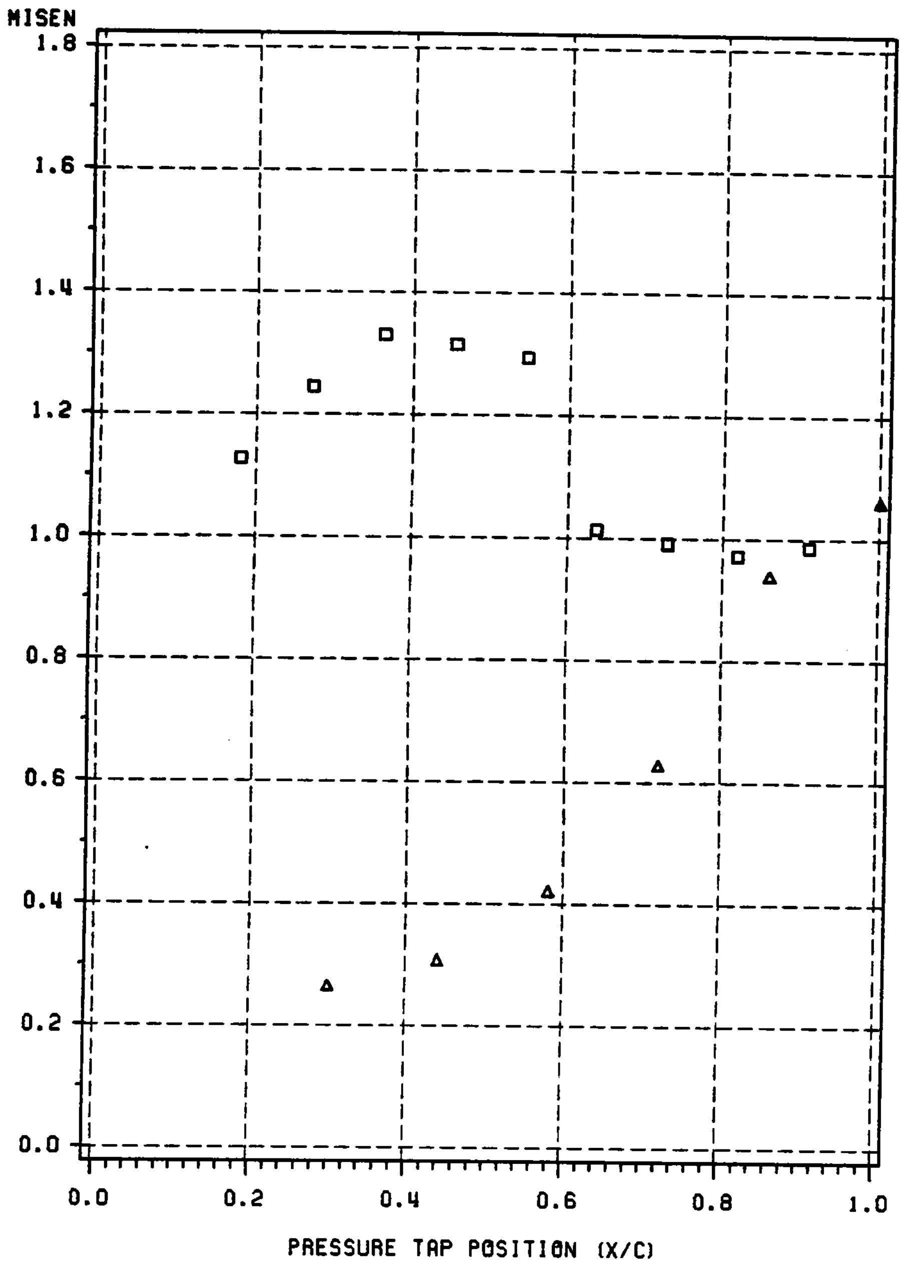

Figure 54. Blade Surface Isentropic Mach Number Distribution: a first cascade run, $M_{2,isen}$ = 0.90. △ - pressure side, □ - suction side.

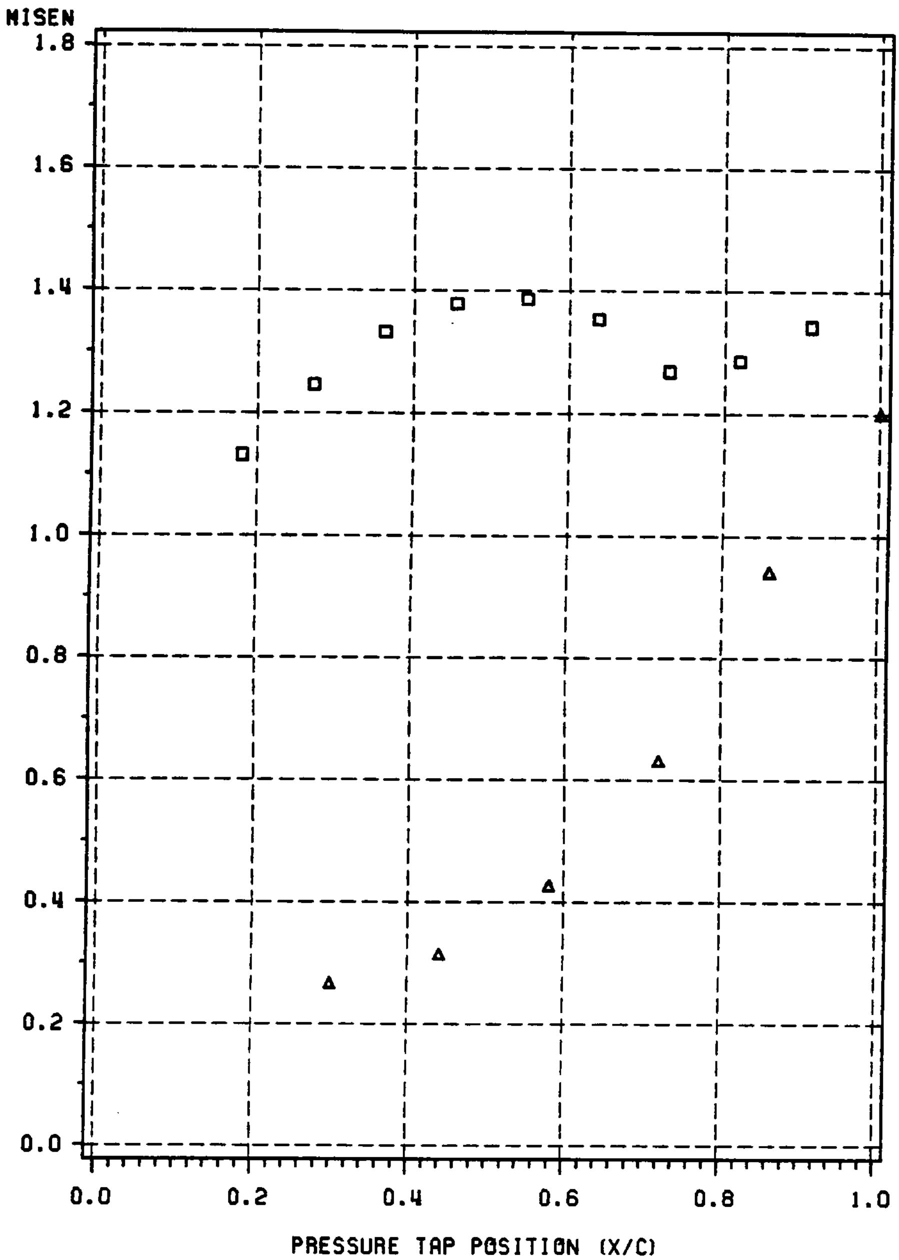

Figure 55. Blade Surface Isentropic Mach Number Distribution: a first cascade run, $M_{2,isen}$ = 1.20. △ - pressure side, □ - suction side.

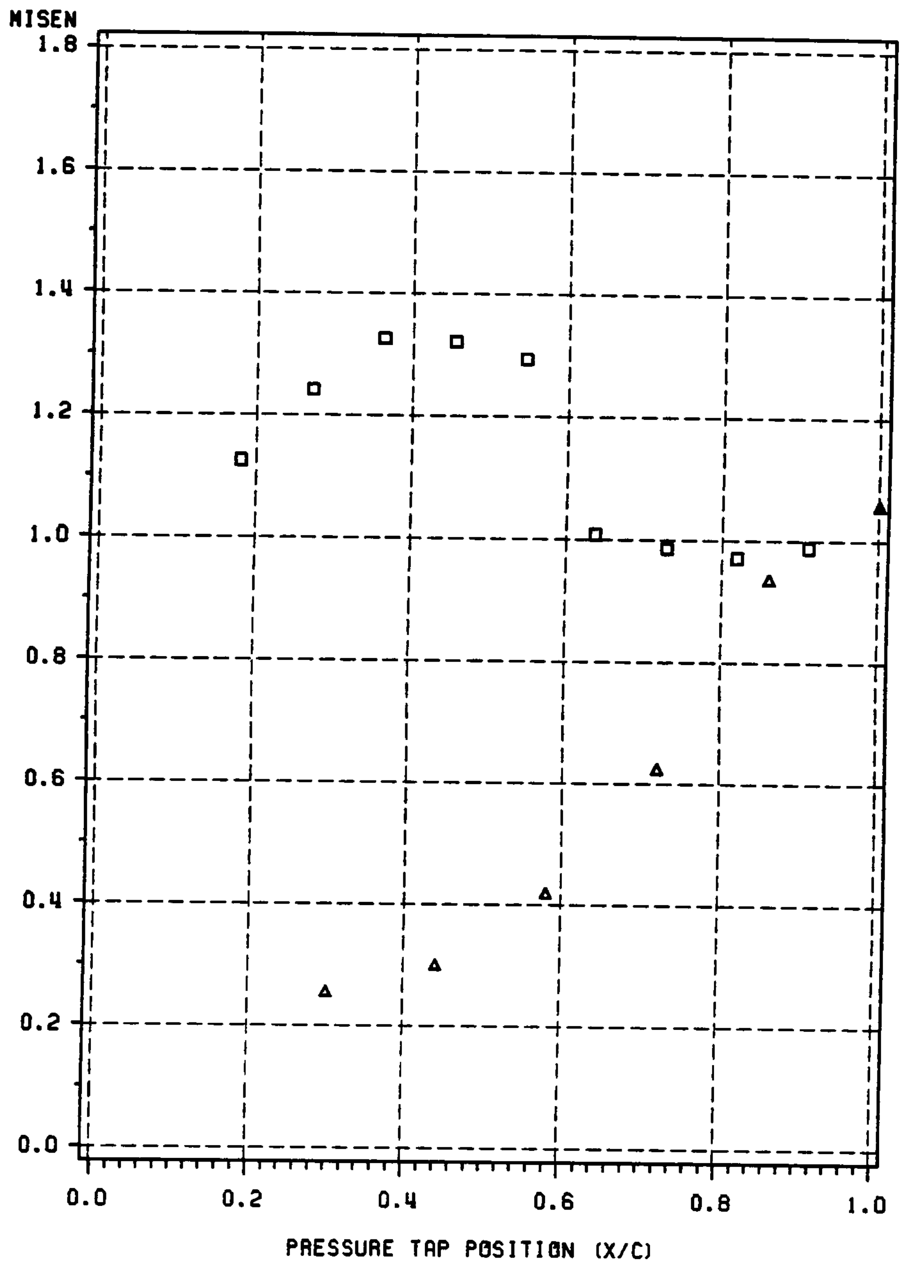

Figure 56. Blade Surface Isentropic Mach Number Distribution: a second cascade run, $M_{2,isen}$ = 0.90. △ - pressure side, □ - suction side.

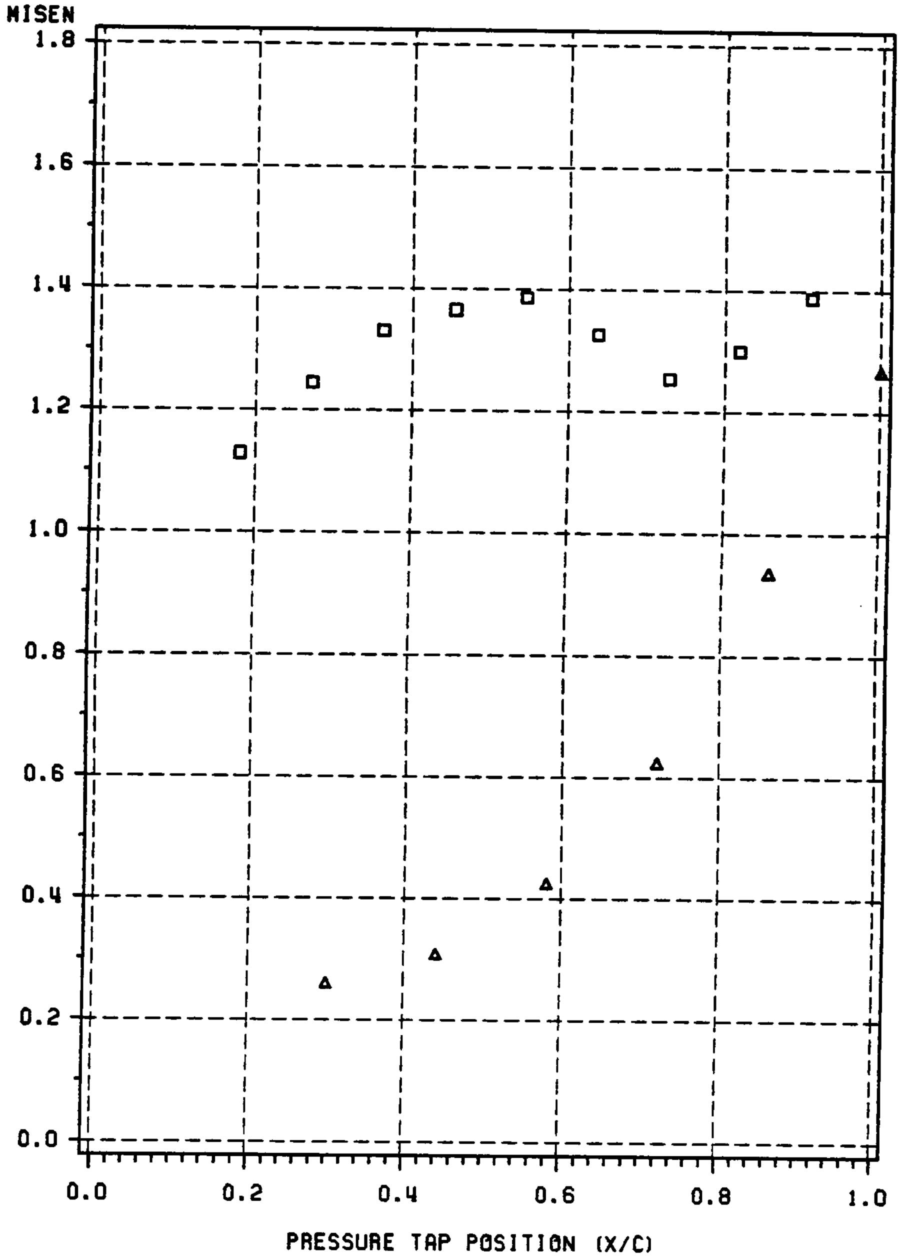

Figure 57. Blade Surface Isentropic Mach Number Distribution: a second cascade run, $M_{2,isen}$ = 1.23. △ - pressure side, □ - suction side.

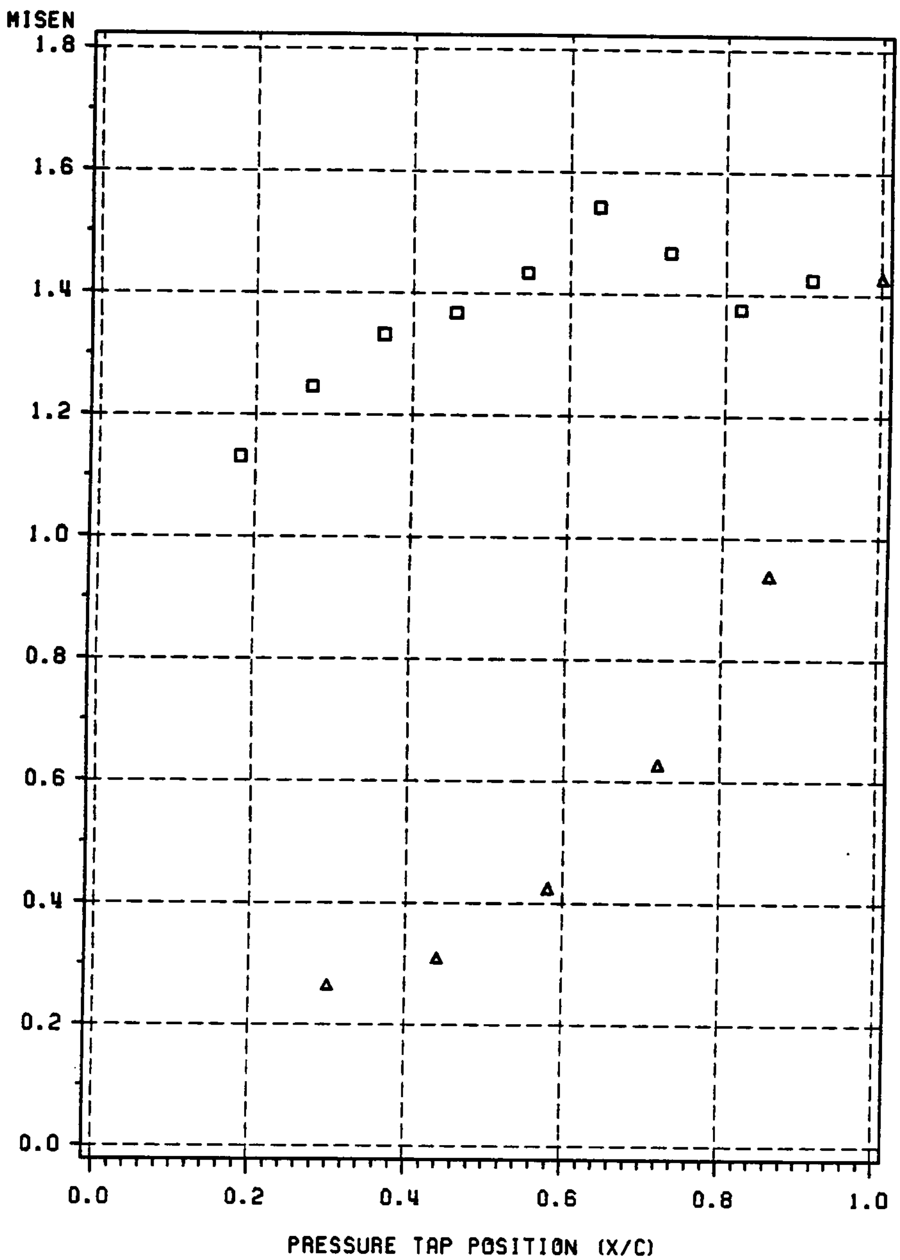

Figure 58. Blade Surface Isentropic Mach Number Distribution: a second cascade run, $M_{2,isen}$ = 1.32. △ - pressure side, □ - suction side.

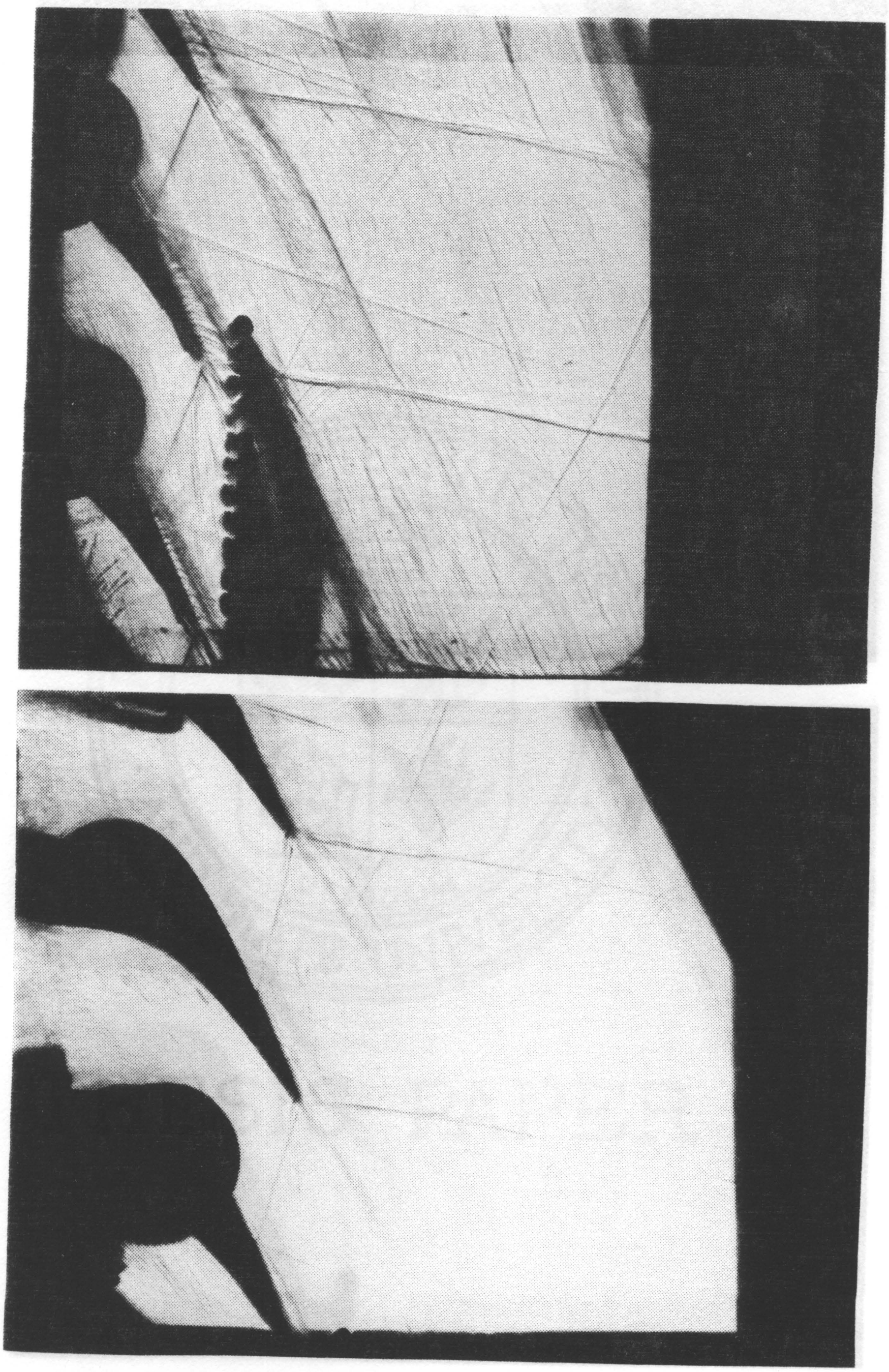

Figure 59. **Visual Data:** top - first cascade run, $M_{2,isen}$ = 1.31, bottom - second cascade run, $M_{2,isen}$ = 1.33. Both with no coolant injection and tailboard installed.

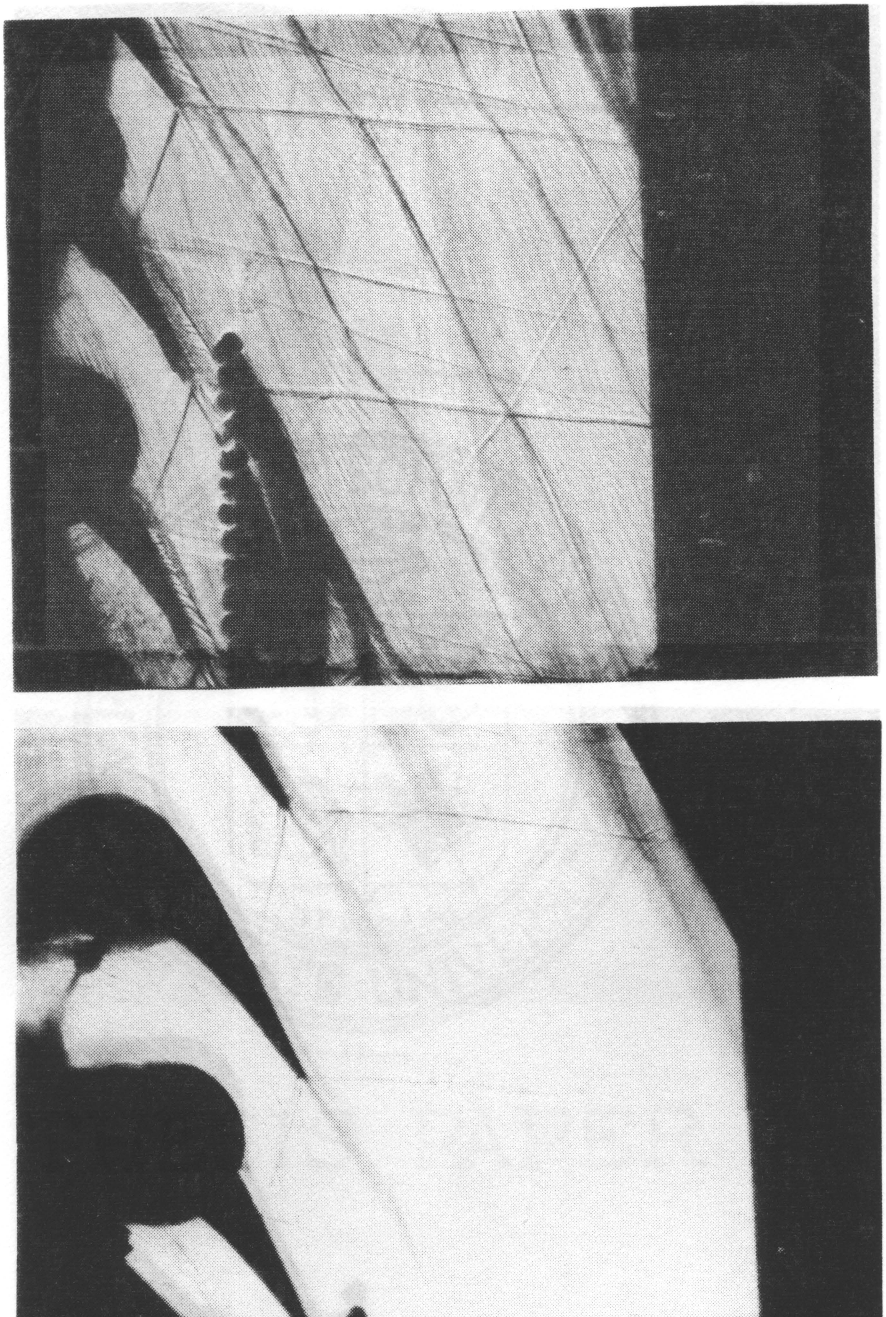

Figure 60. Visual Data: top - first cascade run, $M_{2,isen}$ = 1.25, bottom - second cascade run, $M_{2,isen}$ = 1.27. Both with no coolant injection and tailboard installed.

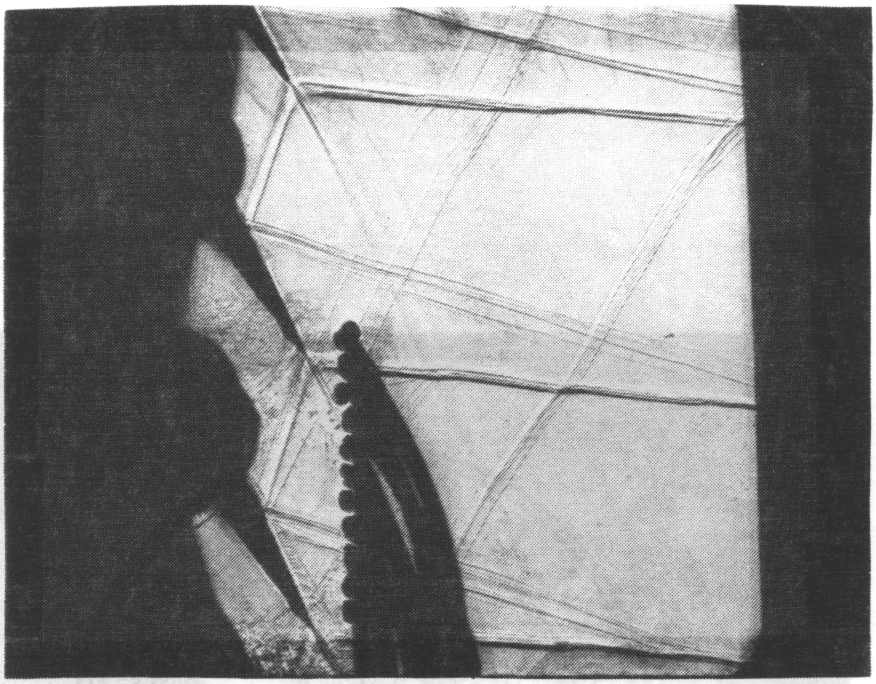

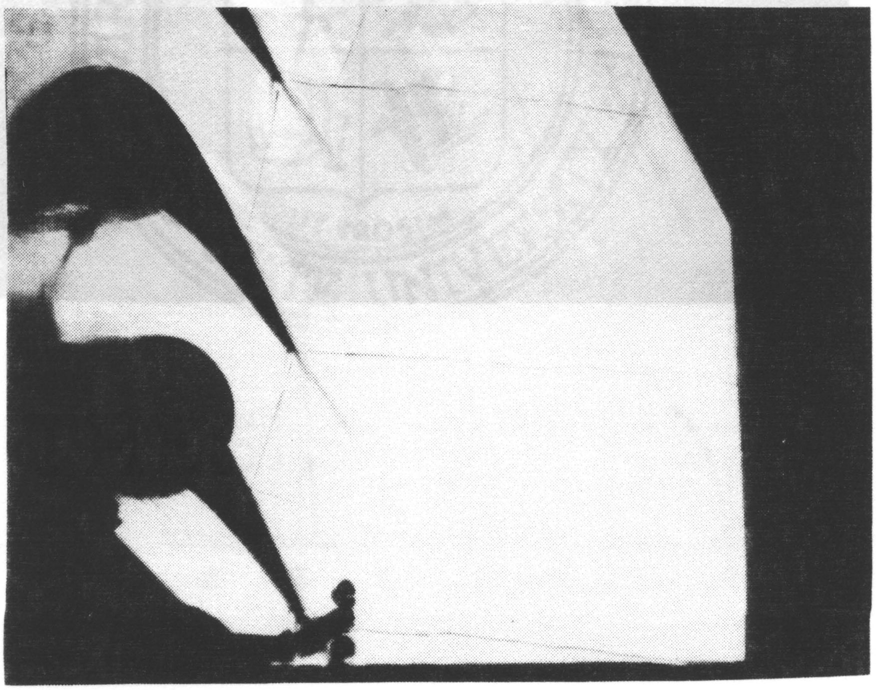

Figure 61. **Visual Data:** top - first cascade run, $M_{2,isen}$ = 1.25, bottom - second cascade run, $M_{2,isen}$ = 1.27. Both with high coolant injection rate and tailboard installed.

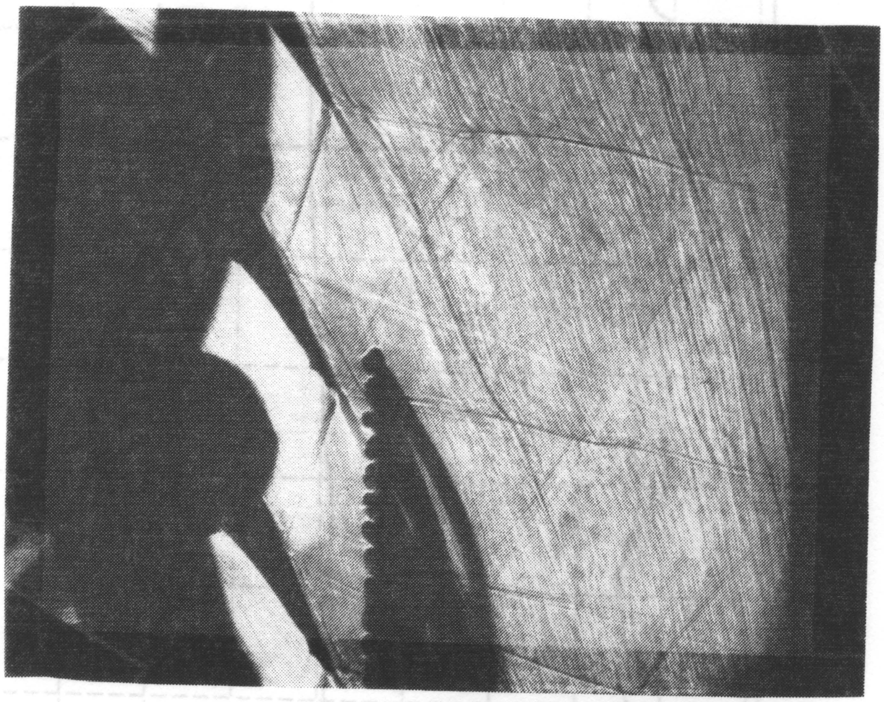

Figure 62. **Visual Data:** first cascade run, $M_{2,isen}$ = 1.24, no coolant injection and no tailboard installed.

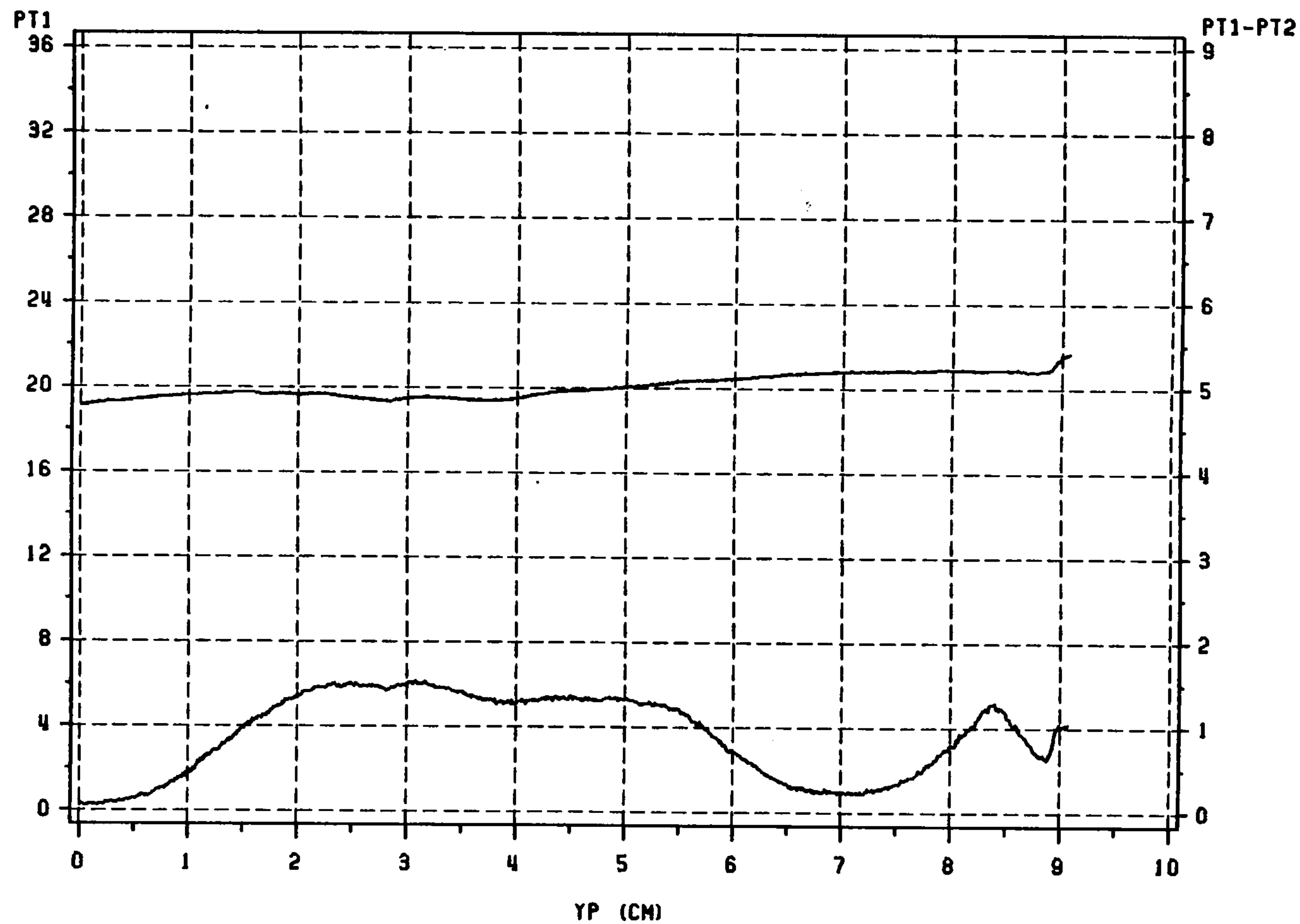

Figure 63. **Example Raw Data:** a second cascade run, rear station ($x/c = 3.000$), low coolant injection, $M_{2,isen} = 0.78$. YP is the probe's vertical position. $p_{t,1}$ is in psia. Note the merging wakes.

Appendix B. Tables

Table 1. Test Program and Results - First Cascade, Tailboard Installed

$M_{2,isen,avg}$	$M_{2,isen}$	Station	B	$\bar{L}$ (percent)
0.80	0.804	FWD	NONE	1.6
0.80	0.806	FWD	LOW	1.6
0.80	0.793	FWD	HIGH	1.3
0.92	0.936	MID	LOW	2.2
0.92	0.943	MID	LOW	2.2
0.92	0.875	MID	HIGH	1.9
1.20	1.198	MID	NONE	2.2
1.20	1.200	MID	NONE	2.1
1.20	------	MID	LOW	------
1.20	1.200	MID	HIGH	2.1
1.20	1.209	REAR	NONE	2.3
1.20	1.207	REAR	LOW	2.4
1.20	1.189	REAR	HIGH	2.6
1.20	1.185	REAR	HIGH	2.5
1.25	1.257	FWD	NONE	2.6
1.25	1.252	FWD	NONE	2.7
1.25	1.253	FWD	NONE	2.7
1.25	1.250	FWD	LOW	2.8
1.25	1.251	FWD	LOW	2.8
1.25	1.243	FWD	HIGH	2.7
1.25	1.244	FWD	HIGH	2.8
1.25	1.257	MID	NONE	4.0
1.25	1.251	MID	LOW	4.1
1.25	1.245	MID	HIGH	4.0
1.25	1.257	REAR	NONE	4.4
1.25	1.255	REAR	NONE	4.1
1.25	1.255	REAR	NONE	4.6
1.25	1.252	REAR	LOW	4.4
1.25	1.244	REAR	HIGH	4.3

FWD - x/c = 1.125, MID - x/c = 1.667, REAR - x/c = 3.000
NONE - no injection , LOW - B= 0.47 , High - B= 1.33
------ data not available

(continued...)

$M_{2,isen,avg}$	$M_{2,isen}$	Station	B	$\bar{L}$ (percent)
1.31	1.309	FWD	NONE	4.1
1.31	1.311	FWD	LOW	3.8
1.31	1.297	FWD	HIGH	4.6
1.31	1.314	MID	NONE	5.3
1.31	1.307	MID	LOW	5.6
1.31	1.307	MID	HIGH	4.9
1.31	1.301	MID	HIGH	5.5
1.31	1.312	REAR	NONE	5.9
1.31	1.312	REAR	LOW	6.4
1.31	1.299	REAR	HIGH	6.3
1.36	1.354	FWD	NONE	2.7
1.36	1.359	FWD	LOW	2.6
1.36	1.346	FWD	HIGH	3.0
1.36	1.361	MID	NONE	3.9
1.36	1.364	MID	NONE	3.8
1.36	1.364	MID	NONE	3.5
1.36	1.359	MID	LOW	3.7
1.36	1.353	MID	HIGH	3.8
1.36	1.364	REAR	NONE	3.9
1.36	1.360	REAR	LOW	4.2
1.36	1.354	REAR	HIGH	4.1

FWD - x/c = 1.125, MID - x/c = 1.667, REAR - x/c = 3.000
NONE - no injection , LOW - B= 0.47 , High - B= 1.33
------ data not available

Table 2. Test Program and Results - First Cascade, Tailboard Removed

$M_{2,isen}$	Station	B	$\bar{L}$ (percent)
0.73	FWD	NONE	1.3
0.74	FWD	NONE	1.3
0.85	FWD	NONE	1.9
0.96	FWD	NONE	2.3
1.00	FWD	NONE	2.4
1.04	FWD	NONE	2.3
1.07	FWD	NONE	2.2
1.07	FWD	NONE	2.1
1.10	FWD	NONE	2.2
1.14	FWD	NONE	2.2
1.17	FWD	NONE	2.2
0.73	FWD	LOW	1.3
0.72	FWD	HIGH	0.6
0.75	FWD	HIGH	0.7

FWD - x/c = 1.125, MID - x/c = 1.667, REAR - x/c = 3.000
NONE - no injection , LOW - B= 0.47 , High - B= 1.33
------ data not available

(continued...)

$M_{2,isen}$	Station	B	$\bar{L}$ (percent)
0.67	MID	NONE	1.5
0.69	MID	NONE	1.7
0.69	MID	NONE	1.7
0.70	MID	NONE	1.6
0.72	MID	NONE	1.9
0.72	MID	NONE	1.4
0.77	MID	NONE	2.3
0.77	MID	NONE	2.3
0.82	MID	NONE	2.7
0.90	MID	NONE	2.3
0.94	MID	NONE	2.4
1.04	MID	NONE	3.1
1.05	MID	NONE	2.5
1.06	MID	NONE	2.9
1.17	MID	NONE	2.3
1.24	MID	NONE	1.7
1.24	MID	NONE	1.9
0.75	MID	LOW	1.8
0.93	MID	LOW	2.4
1.05	MID	LOW	3.0
0.71	MID	HIGH	0.6
0.72	MID	HIGH	0.7
1.05	MID	HIGH	2.7

FWD - x/c = 1.125, MID - x/c = 1.667, REAR - x/c = 3.000
NONE - no injection , LOW - B= 0.47 , High - B= 1.33
------ data not available

(continued...)

$M_{2,isen}$	Station	B	$\bar{L}$ (percent)
0.74	REAR	NONE	2.2
0.76	REAR	NONE	1.5
0.78	REAR	NONE	1.7
0.86	REAR	NONE	2.1
0.88	REAR	NONE	2.2
0.91	REAR	NONE	2.3
1.00	REAR	NONE	2.5
1.01	REAR	NONE	2.6
1.05	REAR	NONE	2.6
1.08	REAR	NONE	2.6
1.13	REAR	NONE	2.8
1.13	REAR	NONE	2.7
0.75	REAR	LOW	2.5
0.76	REAR	HIGH	1.8

FWD - x/c = 1.125, MID - x/c = 1.667, REAR - x/c = 3.000
NONE - no injection , LOW - B= 0.47 , High - B= 1.33
------ data not available

Table 3. Test Program and Results - Second Cascade, Tailboard Installed

$M_{2,isen,avg}$	$M_{2,isen}$	Station	B	$\bar{L}$ (percent)
1.14	1.139	FWD	NONE	2.9
1.14	1.132	FWD	LOW	3.0
1.14	------	FWD	HIGH	------
1.14	1.152	MID	NONE	5.1
1.14	1.148	MID	LOW	4.1
1.14	1.138	MID	HIGH	4.2
1.14	1.144	REAR	NONE	5.5
1.14	1.140	REAR	LOW	4.9
1.14	1.130	REAR	HIGH	5.0
1.21	1.230	FWD	NONE	2.8
1.21	1.220	FWD	LOW	2.6
1.21	1.210	FWD	HIGH	2.8
1.21	1.203	MID	NONE	4.3
1.21	1.202	MID	LOW	4.4
1.21	1.219	MID	HIGH	4.2
1.21	1.204	REAR	NONE	4.6
1.21	1.208	REAR	LOW	4.5
1.21	1.193	REAR	HIGH	4.7
1.26	1.279	FWD	NONE	3.2
1.26	1.273	FWD	LOW	3.5
1.26	1.262	FWD	HIGH	3.5
1.26	1.262	MID	NONE	4.8
1.26	1.250	MID	LOW	4.9
1.26	1.246	MID	HIGH	4.8
1.26	1.261	REAR	NONE	4.8
1.26	1.253	REAR	LOW	5.2
1.26	1.251	REAR	HIGH	4.8

FWD - x/c = 1.125, MID - x/c = 1.667, REAR - x/c = 3.000
NONE - no injection , LOW - B= 0.47 , High - B= 1.33
------ data not available

(continued...)

$M_{2,isen,avg}$	$M_{2,isen}$	Station	B	$\bar{L}$ (percent)
1.32	1.331	FWD	NONE	5.1
1.32	1.332	FWD	LOW	4.7
1.32	1.320	FWD	HIGH	5.0
1.32	1.324	MID	NONE	6.6
1.32	1.324	MID	LOW	6.3
1.32	1.315	MID	HIGH	5.9
1.32	1.328	REAR	NONE	7.2
1.32	1.323	REAR	LOW	7.3
1.32	1.316	REAR	HIGH	7.5

FWD - x/c = 1.125, MID - x/c = 1.667, REAR - x/c = 3.000
NONE - no injection , LOW - B= 0.47 , High - B= 1.33
------ data not available

Table 4. Test Program and Results - Second Cascade, Tailboard Removed

$M_{2,isen}$	Station	B	$\bar{L}$ (percent)
0.61	FWD	NONE	0.7
0.71	FWD	NONE	1.4
0.77	FWD	NONE	1.4
0.91	FWD	NONE	2.2
0.96	FWD	NONE	2.3
1.01	FWD	NONE	2.6
1.06	FWD	NONE	2.7
1.11	FWD	NONE	2.7
0.63	FWD	LOW	0.8
0.76	FWD	LOW	1.5
0.91	FWD	LOW	2.1
1.03	FWD	LOW	2.6
1.06	FWD	LOW	2.5
0.60	FWD	HIGH	0.4
0.65	FWD	HIGH	0.6
0.76	FWD	HIGH	0.9
0.93	FWD	HIGH	2.2
1.02	FWD	HIGH	2.3
1.06	FWD	HIGH	2.6

FWD - x/c = 1.125, MID - x/c = 1.667, REAR - x/c = 3.000
NONE - no injection , LOW - B= 0.47 , High - B= 1.33
------ data not available

(continued...)

$M_{2,isen}$	Station	B	$\bar{L}$ (percent)
0.64	MID	NONE	1.5
0.69	MID	NONE	1.8
0.81	MID	NONE	2.5
0.81	MID	NONE	2.9
0.90	MID	NONE	2.3
0.95	MID	NONE	2.6
0.97	MID	NONE	2.7
1.00	MID	NONE	3.7
1.03	MID	NONE	3.0
1.05	MID	NONE	3.4
0.57	MID	LOW	1.0
0.73	MID	LOW	2.2
0.82	MID	LOW	2.5
0.96	MID	LOW	2.5
1.01	MID	LOW	2.7
1.11	MID	LOW	4.1
0.58	MID	HIGH	0.7
0.70	MID	HIGH	0.7
0.82	MID	HIGH	1.6
0.92	MID	HIGH	2.4
0.98	MID	HIGH	2.6
1.02	MID	HIGH	2.8
1.10	MID	HIGH	3.3

FWD - $x/c = 1.125$, MID - $x/c = 1.667$, REAR - $x/c = 3.000$
NONE - no injection , LOW - $B = 0.47$, High - $B = 1.33$
------ data not available

(continued...)

$M_{2,isen}$	Station	B	$\bar{L}$ (percent)
0.55	REAR	NONE	1.2
0.58	REAR	NONE	1.3
0.74	REAR	NONE	3.0
0.77	REAR	NONE	3.3
0.98	REAR	NONE	2.6
1.03	REAR	NONE	5.4
1.03	REAR	NONE	2.9
0.59	REAR	LOW	1.4
0.74	REAR	LOW	3.0
0.78	REAR	LOW	5.1
0.86	REAR	LOW	5.0
1.00	REAR	LOW	2.5
1.03	REAR	LOW	2.7
0.61	REAR	HIGH	0.6
0.74	REAR	HIGH	3.2
0.85	REAR	HIGH	4.6
1.01	REAR	HIGH	4.5
1.01	REAR	HIGH	2.5
1.02	REAR	HIGH	2.7

FWD - x/c = 1.125, MID - x/c = 1.667, REAR - x/c = 3.000
NONE - no injection , LOW - B= 0.47 , High - B= 1.33
------ data not available

Appendix C. Coolant Flow Rate Calculations

This appendix presents the procedure followed to approximate the two nominal values of the blowing rate, B, that are taken to quantify the two coolant injection rates used in this research. The two mass flow rates of coolant, and the mass flow rate of air at a Mach number of 1.15 are also calculated (the design Mach number of the blades is, approximately, 1.2).

Recall the definition of blowing rate:

$$B = \frac{\rho_{c,ex} V_{c,ex}}{\rho_{air} V_{air}} \qquad [3.4]$$

$V_{c,ex}$ is related to the corresponding volumetric flow rate $Q_{c,ex}$, the total exit area, A_{ex} , and the discharge coefficient, C_D , of the orifice-like discharge slots by the following familiar relationship:

$$V_{c,ex} = \frac{Q_{c,ex}}{A_{ex} C_D} \qquad [A.1]$$

The volumetric flow rate of CO_2 has been monitored by a float-type flow-meter designed for standard air, located just upstream of the distribution manifold. Naturally, the value read off the meter has to be corrected for the density discrepancy between the CO_2 and standard air. Let the subscript "m" denote conditions at the flow-meter, and $\Delta p_{c,m}$ the difference in the pressure across the flow-meter's float. The correction is carried out as follows: from the Bernoulli equation:

$$\Delta p_{c,m} = \frac{1}{2} \rho_{c,m} V_{c,m}^2 \qquad [A.2]$$

the density is taken to be invariant across the float, and $V_{c,m}$ is the velocity in the narrow clearance between the float and the tube it gets displaced in. An assumption here is that the velocity of the flow below the float is negligible compared to the velocity in the clearance. Let the area of the clearance be A_m (it varies along the tube). The volumetric flow rate is given by:

$$Q_{c,m} = A_m V_{c,m} \qquad [A.3]$$

Substituting Eqn. A.2 in Eqn. A.3:

$$Q_{c,m} = A_m \sqrt{\frac{2\Delta p_{c,m}}{\rho_{c,m}}} \qquad [A.4]$$

If the flow-meter were measuring standard air, and the float were at the same vertical position, then:

$$Q_{air,m} = A_m \sqrt{\frac{2\Delta p_{air,m}}{\rho_{air,stp}}} \qquad [A.5]$$

Since it takes the same pressure increment to lift the float,

$$\Delta p_{c,m} = \Delta p_{air,m} \qquad [A.6]$$

Using Eqn. A.6, and dividing Eqn. A.4 by Eqn. A.5:

$$\frac{Q_{c,m}}{Q_{air,m}} = \sqrt{\frac{\rho_{air,stp}}{\rho_{c,m}}} \qquad [A.7]$$

$Q_{air,m}$ is the value read off the flow-meter.

From continuity, the mass flow rate of CO_2 is the same at the flow-meter and at the exit from the blades. Therefore,

$$\rho_{c,ex} Q_{c,ex} = \rho_{c,m} Q_{c,m}$$

or,

$$Q_{c,ex} = Q_{c,m} \frac{\rho_{c,m}}{\rho_{c,ex}} \qquad [A.8]$$

Combining Eqns. A.1, A.7, A.8, and 3.4:

$$B = \frac{Q_{air,m}}{A_{ex}C_D V_{air}} \sqrt{\frac{\rho_{c,m}}{\rho_{air}} \times \frac{\rho_{air,stp}}{\rho_{air}}} \qquad [A.9]$$

It remains to evaluate V_{air}, ρ_{air}, and $\rho_{c,m}$ to get the value of B from Eqn. A.9.

Let the temperature in the air tanks be $T_{t,air}$. With the adiabatic assumption, $T_{t,air}$ is taken to be the value of the stagnation temperature throughout the flow. As the blow-down is in process, however, the tank pressure drops, and so does its temperature. To see this, consider the ideal gas equation:

$$p = \rho RT \qquad [A.10]$$

and the derived equation for a perfect gas undergoing an isentropic process:

$$p \propto \rho^{\gamma} \qquad [A.11]$$

from Eqns. A.10 and A.11:

$$T \propto p^{\frac{\gamma-1}{\gamma}} \qquad [A.12]$$

for air, $\gamma = 1.4$, and hence:

$$T \propto p^{0.286} \qquad [A.13]$$

Eqn. A.13 shows why the tank temperature decreases with tank pressure. Let the initial value of $T_{t,air}$ be $T_{t,air,i}$; also let $p_{t,air}$ denote the pressure in the tanks. Assuming isentropic flow, the tank pressure is the total pressure of the entire flow. From Eqn. A.13:

$$\frac{T_{t,air}}{T_{t,air,i}} = \left[\frac{p_{t,air}}{p_{t,air,i}} \right]^{0.286} \qquad [A.14]$$

and using run-average values from here on:

$$T_{t,air,avg} = T_{t,air,i}\left[\frac{p_{t,air,avg}}{p_{t,air,i}}\right]^{0.286} \qquad [A.15]$$

Typically, $p_{t,air,i}$ = 517.13 kPa,abs (75 psia), $p_{t,air,avg}$ = 379.22 kPa,abs (55 psia), and $T_{t,air,i}$ = 294.26 K (530 R). Eqn. A.15 gives, $T_{t,air,avg}$ = 269.28 K (485.03 R). An exit Mach number of 1.15 is used in the calculation of nominal exit flow characteristics. At M = 1.15, $\frac{T}{T_t}$ = 0.791, therefore:

$$T_{air,avg} = 0.791\ T_{t,air,avg} = 213.00K\ (383.73R)$$

V_{air} can now be calculated as follows:

$$M = \frac{V_{air}}{\sqrt{\gamma R T_{air,avg}}} = 1.15$$

where R = 287 $\frac{Nm}{kgK}$, therefore V_{air} = 336.43 m/sec (1103.82 ft/sec). The nominal density, ρ_{air}, can be found from the equation of state:

$$\frac{p_{air,avg}}{\rho_{air}} = RT_{air,avg} \qquad [A.16]$$

where $p_{air,avg}$ is estimated at 68.95 kPa,abs (10 psia) as suggested by data gathered with the wall static pressure taps downstream of the blade row. Eqn. A.16 gives ρ_{air} = 1.128 kg/m³ (0.070 lb/ft³).

Going back to Eqn. A.9, $\rho_{air,stp}$ = 1.293 kg/m³ (0.081 lb/ft³), and C_D is taken as 0.8 as recommended by the manufacturer of the blades. A_{ex} is the total area of the ejection slots in the three cooled blades; since each blade has forty 2.381 mm (0.094 in) by 0.635 mm (0.025 in) slots, A_{ex} = 181.43 mm² (0.281 in²). Substituting the known values, so far, in Eqn. A.9, the result is:

$$B = 20.64\ Q_{air,m}\sqrt{\rho_{c,m}} \qquad [A.17]$$

low injection rate: with the low coolant injection rate, the flow meter reads 0.0132 m^3/sec (28 cfm), which is the value of $Q_{air,m}$ in Eqn. A.17. A pressure gage reads the pressure in the CO_2 distribution manifold as 158.59 kPa,abs (23 psia). Moreover, the temperature of CO_2 in the flow-meter is assumed at 277.6 K (500 R). Note that the latter temperature is below room temperature since CO_2 is emptied from commercial, high pressure bottles into a low pressure tank shortly before the run is taken. With the ideal gas constant for CO_2 being R_c = 188.92 $\frac{Nm}{kgK}$, using the equation of state for an ideal gas gives:

$$\rho_{c,m} = \frac{p_{manifold}}{R_c T_{c,m}} = 3.02 \frac{kg}{m^3} \quad (0.189 \frac{lb}{ft^3})$$

Substituting in Eqn. A.17 gives:

$$B_{low} = 0.47$$

high injection rate: with the high coolant injection rate, the flow-meter reads 0.0274 m^3/sec (58 cfm), and the manifold pressure gage reads 289.58 kPa,abs (42 psia). Following the same procedure outlined above, it is found that $\rho_{c,m}$ = 5.52 kg/m^3 (0.345 lb/ft^3), and

$$B_{high} = 1.33$$

Note that the above two values for B were approximated for air flow in the wind-tunnel with an exit Mach number of 1.15. They are used in this thesis, however, to serve as nominal values for the entire Mach number range (0.60 to 1.36). By following the same calculation procedure outlined above for exit Mach numbers of 0.60 and 1.36, the following results were obtained:

for M = 0.60: $B_{low} = 0.99$, $B_{high} = 2.77$

for M = 1.36: $B_{low} = 0.38$, $B_{high} = 1.08$

this shows that the value of the blowing rate varies significantly with air velocity.

An implicit assumption in the above calculation method is that the air flow does not affect the coolant flow. This is true only in the case of coolant flow which is choked at the exit from the blades. Preliminary calculations, not shown here, have indicated that choked flow is achieved for the high injection rate, but not for the low one. The variation in the air flow has, therefore,some effect on the coolant flow, for the case of low injection rate; but this effect is neglected.

Mass flow rate of air at an exit Mach number of 1.15: for an exit Mach number of 1.15, the nominal exit velocity has been found above to be V_{air} = 336.43 m/sec (1103.82 ft/sec), and the nominal exit density ρ_{air} = 1.128 kg/m^3 (0.070 lb/ft^3). The flow angle is assumed to be 68° below the horizontal, and the vertical flow cross-section has an area of A_{exit} = 567.84 cm^2 (88.02 in^2). The mass flow rate is, therefore, given by:

$$\dot{m}_{air} = \rho_{air} A_{exit} V_{air} \cos 68 = 8.07 \text{ kg/sec } (17.80 \text{ lb/sec})$$

Mass flow rate of coolant: the total mass flow rate of CO_2 can be approximated at the flowmeter as follows:

$$\dot{m}_c = \rho_{c,m} Q_{c,m} \qquad [A.18]$$

combining Eqns. A.18 and A.7:

$$\dot{m}_c = \rho_{c,m} Q_{air,m} \sqrt{\frac{\rho_{air,stp}}{\rho_{c,m}}} \qquad [A.19]$$

all quantities in Eqn. A.19 are already known or calculated; therefore:

$\dot{m}_{c,low}$ = 0.0261 kg/sec (0.0575 lb/sec) (0.32 percent of air flow at M = 1.15)

$\dot{m}_{c,high}$ = 0.0732 kg/sec (0.161 lb/sec) (0.91 percent of air flow at M = 1.15)

Appendix D. Data Reduction Algorithm / Tailboard Installed

A small FORTRAN program is first executed to read in the raw data taken through the A/D converter.[17] This data is converted to gage pressure units, and the results stored in an output file. The program is listed below.

```
      PROGRAM MANIP
      REAL FLO(1:800) , RIESS(1:800) , DUMMY(1:800)
C*************************************************************
C THE TWO LINES BELOW ARE CALIBRATION EQNS FOR THE UPSTREAM AND
C DOWNSTREAM PRESSURE TRANSDUCERS, RESPECTIVELY
      CLBRIS(DGTL) = (DGTL/409.5) * 3.628    + 0.03647
      CLBFLO(DGTL) = (DGTL/409.5) * 3.638    - 0.005194
      NDATA = 800
C*************************************************************
C UNIT 10 IS THE RAW DATA FILE
C UNIT 20 IS THE OUTPUT FILE OF THIS PROGRAM
      OPEN (UNIT=10,STATUS='OLD')
      OPEN (UNIT=20)
      REWIND (10)
      REWIND (20)
      DO 10 I=1,NDATA
      READ (10,*)   DUMMY(I)
      READ (10,*)   RIESS(I)
      READ (10,*)   FLO(I)
      RIESS(I) = CLBRIS(RIESS(I))
      FLO(I) = CLBFLO(FLO(I))
      FLO(I) = RIESS(I) - FLO(I)
   10 CONTINUE
      DO 20 I=1,NDATA
C THE OUTPUT IS, IN THIS ORDER, AN INDEX NUMBER, A DUMMY
C (NOT USED) NUMBER, THE UPSTREAM TOTAL PRESSURE IN PSIG,
C AND THE TOTAL PRESSURE DROP IN PSI.
      WRITE (20,30)  I , DUMMY(I) , RIESS(I) , FLO(I)
   30 FORMAT (I4,3F20.10)
   20 CONTINUE
      STOP
      END
```

The FORTRAN program listed below reads in the results generated by the previous program and the data taken through the self-calibrating pressure measurement system. The user has to input from the terminal the two regions of integration, the atmospheric pressure, the blowing rate (high, low, or none), and the position of station 2 (forward, middle, or aft). The program gives the isentropic, exit Mach number, $M_{2,isen}$, the run-averaged exit Mach number as generated by the procedure that corrects for the bow shock effect, and the mass-averaged total pressure loss coefficient, $\bar{L}$, with and without correction for the bow shock effect.

[17] A slight alteration is required in the listed program for use with the first cascade's data, where a differential transducer was used to measure the total pressure drop across the blade row.

```
      PROGRAM MAIN
C
      CHARACTER  CASCADE*1 , INJECTION*1 ,NAME*8
      REAL  FLO(1:800) , RIESS(1:800) , FORSTC(1:11) ,
     $      AFTSTC(1:3) , PTY(1:800) ,  MX(1:800) , TX(1:800) ,
     $      RHO(1:800) , U(1:800) , PTX(1:800) , PX(1:800),
     $      LOSS(1:2), MACHIS , MXAVG(1:2) , FLOSS(1:2) , MACHAVG
C
C CASCADE= '1' -ORIGINAL CASCADE
C CASCADE= '2' -CUT FIRST TIME
C CASCADE= '3' -CUT SECOND TIME
C*****************************************************************
      NDATA = 800
      HERTZ = 40.
      CASCADE = '2'
C*****************************************************************
C
      WRITE (1,*) 'INPUT FIRST DATA PT. OF FIRST INTERVAL:'
      READ (1,*) IONE
      WRITE (1,*) 'INPUT LAST DATA PT. OF SECOND INTERVAL:'
      READ (1,*) ITWO
      WRITE (1,*) 'INPUT RUN NAME:'
      READ (1,'(A)') NAME
      WRITE (1,*) 'INPUT ATMOSPHERIC PRESSURE IN PSI:'
      READ (1,*) PATM
C
C INJECTION RATE BELOW. N-NONE , L-LOW , H-HIGH
C
      WRITE (1,*) 'INPUT INJECTION RATE (N ,L ,OR H):'
      READ (1,'(A)') INJECTION
      WRITE (1,17)   'ENTER (1) , (2) , OR (3) :' ,
     $  '    (1) FORWARD PROBE POSITION' ,
     $  '    (2) MID PROBE POSITION' ,
     $  '    (3) AFT PROBE POSITION'
   17 FORMAT (A/,A/,A/,A)
      READ (1,*) IPOS
C
C UNIT 11 IS THE OUTPUT FILE OF THE PREVIOUS PROGRAM, UNIT 12 IS
C THE RAW DATA FILE FROM THE SELF-CALIBRATING PRESSURE MEASUREMENT,
C SYSTEM AND UNIT 20 IS THIS PROGRAM'S OUTPUT FILE.
C
      OPEN (UNIT=11 , FILE='RAW' , STATUS='OLD')
      OPEN (UNIT=12 , FILE='PRS' , STATUS='OLD')
      OPEN (UNIT=20 , FILE='RES' , STATUS='OLD')
      REWIND (11)
      REWIND (12)
C
C RIESS: UPSTREAM TOTAL PRESSURE IN PSIG
```

```
C FLO: DIFFERENTIAL TOTAL PRESSURE IN PSI
C
      READ (11,*)  (IDUMMY , DUMMY , RIESS(I) , FLO(I) , I=1,NDATA)
      READ (12,*)  (DUMMY , I=1,15) , (FORSTC(I) , I=11,1,-1) ,
     $             (AFTSTC(I) , I=3,1,-1) , UPTTL
C
C DY IS METERS BETWEEN DATA PTS. - TTL IN KELVIN
C
      PI = ACOS(-1.)
      G = 1.4
      R = 287.
      DY = 50. * 0.003573 / HERTZ
      NPITCH = NINT (1.467/DY)
      DY = DY / 2.54 / 100.
      TTL = 283.
C
C BELOW GIVES FLO IN PASCAL , RIESS IN PASCAL ABSOLUTE
C
      DO 10 I=1,NDATA
      FLO(I) = FLO(I) * 6894.757
      RIESS(I) = ( RIESS(I) + PATM ) * 6894.757
   10 CONTINUE
C
C BELOW AVERAGES FORSTC & AFTSTC AND CONVERTS THEM TO PASCAL
C ABSOLUTE AND GIVES UPTTL IN PASCAL ABSOLUTE
C
      FORAVG = 0.
      DO 20 I=1,11
      FORAVG = FORAVG + FORSTC(I)
   20 CONTINUE
      FORAVG = (FORAVG / 11. + PATM) * 6894.757
      AFTAVG = ((AFTSTC(1) + AFTSTC(2) + AFTSTC(3)) / 3. + PATM)
     $         * 6894.757
      UPTTL = (UPTTL + PATM) * 6894.757
C
      MACHIS = (2./(G-1.) * ((UPTTL/FORAVG)**((G-1.)/G) - 1.))**0.5
C
      IF (IPOS .EQ. 1) THEN
         STATIC = FORAVG
      ELSE IF (IPOS. EQ. 2) THEN
         STATIC = FORAVG - (13./45.)*(FORAVG - AFTAVG)
      ELSE IF (IPOS .EQ. 3) THEN
         STATIC = AFTAVG
      END IF
C
      RATIO = STATIC / UPTTL
C
C INTEGRATION
C
```

```
      DO 810 IBAW = 1,2
C
      DO 631 KK=1,2
      IF (KK .EQ. 1) THEN
         IBEGIN = IONE
         IEND = IONE + NPITCH
      END IF
      IF (KK .EQ. 2) THEN
         IBEGIN = ITWO - NPITCH
         IEND = ITWO
      END IF
      MXAVG(KK) = 0.
      DO 30 K=IBEGIN,IEND
      PTY(K) = RIESS(K) - FLO(K)
      PX(K) = RATIO * RIESS(K)
C
      IF ((PX(K)/PTY(K)) .GT. 0.528 .OR. IBAW .EQ. 1) THEN
         GOTO 909
      ELSE
         GOTO 707
      END IF
  909    PTX(K) = PTY(K)
         MX(K) = (2./(G-1.)*((PTX(K)/PX(K))**((G-1.)/G)-1.))**0.5
         GOTO 444
C
C SOLVING FOR MX BY BISECTION METHOD
C
  707 A = 1.0
      B = 1.7
      DO 50 ITER = 1,14
      C = (A + B) / 2.
      FA = -PTY(K)/PX(K) + ((G+1.)/2.*A**2)**(G/(G-1.))
     $     * (1./(2.*G/(G+1.)*A**2 - (G-1.)/(G+1.)))**(1./(G-1.))
      FC = -PTY(K)/PX(K) + ((G+1.)/2.*C**2)**(G/(G-1.))
     $     * (1./(2.*G/(G+1.)*C**2 - (G-1.)/(G+1.)))**(1./(G-1.))
      IF ((FA * FC) .LE. 0.) THEN
         B = C
      ELSE
         A = C
      END IF
   50 CONTINUE
      MX(K) = C
      A = MX(K)
      TERM = ((G+1.)/2.*A**2 / (1.+(G-1.)/2.*A**2))**(G/(G-1.))
     $     * (1./(2.*G/(G+1.)*A**2 - (G-1.)/(G+1.)))**(1./(G-1.))
      PTX(K) = PTY(K) / TERM
  444 MXAVG(KK) = MXAVG(KK) + MX(K)
      TX(K) = TTL / (1. + (G-1.)/2.*MX(K)**2)
      RHO(K) = PX(K) / R / TX(K)
      U(K) = MX(K) * ((G * R * TX(K)) ** 0.5) * COS(68./180.*PI)
```

```
   30 CONTINUE
      MXAVG(KK) = MXAVG(KK) / (NPITCH + 1)
      SNUM = 0.
      SDEN = 0.
      N = IBEGIN
      TERM1 = RHO(N) * U(N) * (RIESS(N) - PTX(N)) / RIESS(N)
      TERM3 = RHO(N) * U(N)
      DO 60 I=IBEGIN,IEND - 1
      J = I + 1
      TERM2 = RHO(J) * U(J) * (RIESS(J) - PTX(J)) / RIESS(J)
      TERM4 = RHO(J) * U(J)
      SNUM = SNUM + (TERM1 + TERM2)/2. * DY
      SDEN = SDEN + (TERM3 + TERM4)/2. * DY
      TERM1 = TERM2
      TERM3 = TERM4
   60 CONTINUE
      LOSS(KK) = SNUM / SDEN
  631 CONTINUE
C
      FLOSS(IBAW) = (LOSS(1) + LOSS(2)) / 2. * 100.
  810 CONTINUE

C
  504 MACHAVG = (MXAVG(1) + MXAVG(2)) / 2.
      WRITE (1,*) 'MACHIS=' , MACHIS
      WRITE (1,*) 'AVERAGED MACH#=' , MACHAVG
      WRITE (1,*) 'LOSS%(NO BOW CORR)=' , FLOSS(1)
      WRITE (1,*) 'LOSS%(BOW CORR)=' , FLOSS(2)
C
      WRITE (20,306) NAME , CASCADE , IPOS , INJECTION ,
     $               MACHIS , MACHAVG , FLOSS(1) , FLOSS(2)
  306 FORMAT (T1,A,T11,A,T15,I1,T19,A,T22,F7.5,T30,F7.5,
     $        T38,F9.6,T49,F9.6)
      STOP
C
      END
```

Appendix E. Data Reduction Algorithm / Tailboard not Installed

The same program listed at the beginning of Appendix C is used in this case also. It converts the raw data taken through the A/D converter into gage pressure units.

The FORTRAN program listed below requires the same input and gives, essentially, the same output as the similar program in Appendix C (refer to Appendix C for a full description). The only difference is that the reported value for $M_{2,isen}$ is the run average of the values calculated from the empirical equation. Moreover, the latter value is one and the same with the run-averaged exit Mach number.

```
      PROGRAM MAIN
C
      CHARACTER  CASCADE*1 , INJECTION*1 , NAME*8
      REAL  FLO(1:800) , RIESS(1:800) ,
     $      PTY(1:800) ,  MX(1:800) , TX(1:800) , LOSS(1:2),
     $      RHO(1:800) , U(1:800) , PTX(1:800) , PX(1:800) ,
     $      MACHIS , MXAVG(1:2) , FLOSS(1:2) , MACHAVG , MVSPT
C
C BELOW FUNCTION GIVES MACH # AS A FUNCTION OF UPSTREAM TOTAL
C PRESSURE IN PASCAL ABSOLUTE
C
      MVSPT (X) = 0.082301466 * X / 6894.757 - 0.8444566
C
C CASCADE='1'- UNCUT CASCADE
C CASCADE='2'- CUT-BACK ONCE
C CASCADE='3'- CUT-BACK TWICE
C*****************************************************************
      NDATA = 800
      HERTZ = 40.
      CASCADE = '2'
C*****************************************************************
C
      WRITE (1,*) 'INPUT FIRST DATA PT. OF FIRST INTERVAL:'
      READ (1,*) IONE
      WRITE (1,*) 'INPUT LAST DATA PT. OF SECOND INTERVAL:'
      READ (1,*) ITWO
      WRITE (1,*) 'INPUT RUN NAME:'
      READ (1,'(A)') NAME
      WRITE (1,*) 'INPUT ATMOSPHERIC PRESSURE IN PSI:'
      READ (1,*) PATM
      WRITE (1,*) 'INPUT INJECTION RATE (N ,L ,OR H):'
      READ (1,'(A)') INJECTION
      WRITE (1,17)   'ENTER (1) , (2) , OR (3) :' ,
     $  '   (1) FORWARD PROBE POSITION' ,
     $  '   (2) MID PROBE POSITION' ,
     $  '   (3) AFT PROBE POSITION'
   17 FORMAT (A/,A/,A/,A)
      READ (1,*) IPOS
C
C UNIT 11 IS THE OUTPUT FILE OF THE PREVIOUS PROGRAM
C UNIT 20 IS THE OUTPUT FILE OF THIS PROGRAM
C
```

```
      OPEN (UNIT=11 , FILE='RAW' , STATUS='OLD')
      OPEN (UNIT=20 , FILE='RES' , STATUS='OLD')
      REWIND (11)
C
      READ (11,*)  (IDUMMY , DUMMY , RIESS(I) , FLO(I) , I=1,NDATA)
C
C DY IS METERS BETWEEN DATA PTS. TTL IN KELVIN
C
      PI = ACOS(-1.)
      G = 1.4
      R = 287.
      DY = 50. * 0.003573 / HERTZ
      NPITCH = NINT (1.467/DY)
      DY = DY / 2.54 / 100.
      TTL = 283.
C
C BELOW GIVES FLO IN PASCAL, RIESS IN PASCAL ABSOLUTE,
C
      DO 10 I=1,NDATA
      FLO(I) =   FLO(I) * 6894.757
      RIESS(I) = ( RIESS(I) + PATM ) * 6894.757
   10 CONTINUE
C
C INTEGRATION
C
      DO 810 IBAW = 1,2
C
      DO 631 KK=1,2
      IF (KK .EQ. 1) THEN
         IBEGIN = IONE
         IEND = IONE + NPITCH
      END IF
      IF (KK .EQ. 2) THEN
         IBEGIN = ITWO - NPITCH
         IEND = ITWO
      END IF
      MXAVG(KK) = 0.
      DO 30 K=IBEGIN,IEND
      MX(K) = MVSPT (RIESS(K))
      PTY(K) = RIESS(K) - FLO(K)
C
      IF (MX(K) .LT. 1. .OR. IBAW .EQ. 1) THEN
         GOTO 909
      ELSE
         GOTO 707
      END IF
  909 PTX(K) = PTY(K)
      FA2 = (1. + (G-1.)/2.*A**2) ** (G/(G-1.))
      PX(K) = PTX(K) / FA2
```

```
      GOTO 444
C
  707 A = MX(K)
      FA1 = ((G+1.)/2.*A**2)**(G/(G-1.))
     $      * (1./(2.*G/(G+1.)*A**2 - (G-1.)/(G+1.)))**(1./(G-1.))
      FA2 = (1. + (G-1.)/2.*A**2) ** (G/(G-1.))
      PTX(K) = FA2 / FA1 * PTY(K)
      PX(K) = PTX(K) / FA2
C
  444 MXAVG(KK) = MXAVG(KK) + MX(K)
      TX(K) = TTL / (1. + (G-1.)/2.*MX(K)**2)
      RHO(K) = PX(K) / R / TX(K)
      U(K) = MX(K) * ((G * R * TX(K)) ** 0.5) * COS(68./180.*PI)
   30 CONTINUE
      MXAVG(KK) = MXAVG(KK) / (NPITCH + 1)
      SNUM = 0.
      SDEN = 0.
      N = IBEGIN
      TERM1 = RHO(N) * U(N) * (RIESS(N) - PTX(N)) / RIESS(N)
      TERM3 = RHO(N) * U(N)
      DO 60 I=IBEGIN,IEND - 1
      J = I + 1
      TERM2 = RHO(J) * U(J) * (RIESS(J) - PTX(J)) / RIESS(J)
      TERM4 = RHO(J) * U(J)
      SNUM = SNUM + (TERM1 + TERM2)/2. * DY
      SDEN = SDEN + (TERM3 + TERM4)/2. * DY
      TERM1 = TERM2
      TERM3 = TERM4
   60 CONTINUE
      LOSS(KK) = SNUM / SDEN
  631 CONTINUE
C
      FLOSS(IBAW) = (LOSS(1) + LOSS(2)) / 2. * 100.
  810 CONTINUE
C
  504 MACHAVG = (MXAVG(1) + MXAVG(2)) / 2.
      MACHIS = MACHAVG
      WRITE (1,*) 'AVERAGED MACH#=' , MACHAVG
      WRITE (1,*) 'LOSS%(NO BOW CORR)=' , FLOSS(1)
      WRITE (1,*) 'LOSS%(BOW CORR)=' , FLOSS(2)
C
      WRITE (20,306) NAME , CASCADE , IPOS , INJECTION ,
     $               MACHIS , MACHAVG , FLOSS(1) , FLOSS(2)
  306 FORMAT (T1,A,T11,A,T15,I1,T19,A,T22,F7.5,T30,F7.5,
     $        T39,F9.6,T50,F9.6)
      STOP
C
      END
```

The vita has been removed from the scanned document